DIRECT MEASUREMENT OF PARALLEL PLATE

HEAT SINK BYPASS FLOW

By

DEAN D. CROCKETT

A thesis submitted in partial fulfillment of the requirements for the degree of

MASTER OF SCIENCE IN MECHANICAL ENGINEERING

WASHINGTON STATE UNIVERSITY
School of Mechanical and Materials Engineering

DECEMBER 2006

To the Faculty of Washington State University:

       The members of the Committee appointed to examine the thesis of
DEAN D. CROCKETT find it satisfactory and recommend that it be accepted.

_____

Chair

_____

_____

ACKNOWLEDGMENT

First and foremost I would like to thank the chairman of my thesis committee, Prof. Russell Westphal, for his guidance throughout this research and also for his friendship. I would also like to acknowledge the contributions made by Donald Frame in the design and development of the thermistor anemometer, Steve Jordan in the construction of the *xy*-traverse, and Mark Bleazard in providing his expertise in LABVIEW. The author would like to give credit to Dustin and Jamie Crockett for the wonderful illustrations of the test setup presented within the pages of this document. Last, but not least, I extend my gratitude to Lisa Crockett for the time and effort she put into editing this manuscript. Thank you for the superb job.

On a more personal note, I would like to thank my Lord and Savior Jesus Christ for His loving grace and the unlimited mercy he has bestowed upon me throughout the years. I know that I most desperately need it. I would like to also thank my parents, Donna and Dana Crockett for their support and for always believing in me. Finally I would like to thank my understanding and loving wife, Tracy, and daughters, Hannah, Emily, and Leah for giving up their husband and daddy so that he could finish this research. I couldn't have done it without you.

DIRECT MEASUREMENT OF PARALLEL PLATE

HEAT SINK BYPASS FLOW

Abstract

by Dean D. Crockett, M.S.
Washington State University
December 2006

Chair: Russell V. Westphal

If not fully shrouded, forced air cooling flow has the propensity to bypass a highly restrictive flow channel such as those provided by the heat sinks frequently used in thermal management applications for electronic packages. While it is recognized that bypass decreases the cooling effectiveness of an extended surface, little effort has been made to directly measure the flow around an array to characterize bypass. For the current research, wind tunnel tests were performed where discrete spatial velocity measurements of the flow downstream of a densely-finned parallel plate heat sink were made with a constant temperature anemometer that utilized a miniature thermistor probe. The process of taking velocity measurements was automated by employing a probe positioning xy-traverse with computerized control and data acquisition. These measurements provided a high resolution velocity survey downstream of the array. Tests were performed with an approach velocity of 4.5 m/s and the thermistor anemometer located 2 mm and 25 mm downstream of the heat sink.

Upon inspection of the velocity surveys, flow mixing was evident in the 25 mm results while a clear "footprint" of the array was apparent in the 2 mm survey. The velocity measurements were reduced further by numerical integration to determine the average flow velocity exiting the array. The flow measurements from the 2 mm test

iv

provided an average velocity exiting the array of 1.6 *m/sec* while the 25 *mm* test produced an average velocity of 2.6 *m/sec*. The bypass ratio was determined to be 64 % for the 2 *mm* test and 42 % for the 25 *mm* test. In comparison, a two-branch model, commonly used in industry, provided a bypass ratio of 69 %. This further demonstrated flow mixing at the 25 *mm* location. The results of the 2 *mm* test and the model compared well. However the velocity measurements at this location may have been influenced by the combination of the probe sensitivity to multi-directional flow and flow separation directly downstream of the array.

TABLE OF CONTENTS

APPENDIX

LIST OF TABLES

LIST OF FIGURES

NOMENCLATURE

A_{array} frontal area array including the channels between the fins (m^2)

A_{by} cross-sectional area of the bypass channel region (m^2)

A_{duct} cross-sectional area of wind tunnel (m^2)

BR bypass ratio

AF array flow ratio

CL clearance ratio $[(A_{duct}/A_{array})-1]$

DR diversion ratio

H fin height (mm)

H_b height of the array base (mm)

L length of the heat sink (mm)

L_{US} length from the upstream side of the heat sink prior to onset of diversion (mm)

LR leakage ratio

$\dot{m}_{end}$ mass flow rate exiting the heat sink (kg/s)

$\dot{m}_{app}$ approach mass flow rate (kg/s)

$\dot{m}_{by}$ bypass mass flow rate (kg/s)

$\dot{m}_{div}$ diversion mass flow rate (kg/s)

$\dot{m}_H$ leakage mass flow rate (kg/s)

Re_L Reynolds number based on the approach velocity and the length of the heat sink

t fin thickness (mm)

u mean velocity in the finned section (m/s)

u_{app} approach velocity (m/s)

u_{end} coolant velocity exiting the heat sink (m/s)

u_0 coolant velocity entering the heat sink (m/s)

W width of the array (mm)

DEDICATION

To my beautiful wife Tracy and my three princesses,

Hannah, Emily, and Leah. I love you.

CHAPTER ONE

INTRODUCTION

The primary means of heat transfer in electronic packages has been through forced convection. Electronic components that generate heat typically possess a dedicated heat sink to increase the surface area for convection. Air supplied by a system fan is used as the coolant that is forced through these heat sinks. This setup for thermal management of electronic packages has proven to be cost effective and reliable. However, as performance and speed in electronics has increased, so has the need for heat removal from these devices. As a result, optimizing heat sink designs has become an essential practice in the thermal management of electronic components. Existing convection heat transfer data in the literature for extended surfaces require the coolant velocity contiguous to the surface be known. However, in determining the thermal performance of a heat sink located in a partially confined configuration, as is characteristic of electronic components, one of the unknown and difficult-to-determine parameters is the actual coolant velocity through the heat sink.

If the heat sink does not occupy the whole cross-sectional area of the flow path then some of the coolant will bypass the heat sink. To illustrate bypass, an open system is selected with a control volume containing the entire heat sink and an arbitrary volume upstream of the array (figure 1.1). The approaching coolant flow ($\dot{m}_{app}$) enters the control volume upstream of the heat sink at a uniform velocity. As the air flow enters the control volume and approaches the upstream face of the heat sink, a portion of the flow is diverted around the array and leaves the control volume through the top and both sides of the control surfaces; this is referred to as "diversion" flow, or $\dot{m}_{div}$. The flow that is left in the control volume enters the finned array at a reduced velocity through the upstream face. A portion of the flow that enters the finned array leaves the control volume through the top of the array due to static pressure imbalances between the heat sink and the

clearance region in the flow duct above the heat sink; this is referred to as "leakage," or $\dot{m}_H$. The sum of diversion and leakage is referred to as the total bypass flow or simply bypass ($\dot{m}_{by}$). The flow that is left passes through the heat sink at a further-reduced velocity. This flow exits the array at the downstream face, consequently leaving the control volume; this is referred to as the array flow ($\dot{m}_{end}$).

The continuity equation for the control volume provided in figure 1.1 can be written as follows:

$$\dot{m}_{app} = \dot{m}_{div} + \dot{m}_H + \dot{m}_{end} \tag{1.1}$$

If equation (1.1) is divided by $\dot{m}_{app}$ and rearranged, then the continuity equation can be rewritten in non-dimensional terms as follows:

$$DR + LR + AF = 1 \tag{1.2}$$

where *DR, LR* and *AF* are the diversion, leakage and array flow ratios respectively. Assuming incompressible flow, the definitions of *DR* and *AF* are expressed by equations (1.3) and (1.4) as,

$$DR = \frac{u_{app} - u_0}{u_{app}} \tag{1.3}$$

$$AF = \frac{u_{end}}{u_{app}} \tag{1.4}$$

where u_0 and u_{end} are the velocities entering and leaving the heat sink respectively and u_{app} is the mean approach velocity entering the control volume upstream of the finned array. By definition, the diversion ratio is the ratio of the diversion mass flow rate ($\dot{m}_{div}$) to the approaching mass flow rate ($\dot{m}_{app}$) (see figure 1.1). Likewise, the leakage ratio is the ratio of the leakage mass flow rate ($\dot{m}_H$) to the approaching mass flow rate ($\dot{m}_{app}$). The overall bypass ratio (*BR*) is defined in terms of diversion ratio (*DR*) and leakage ratio (*LR*):

$$BR = DR + LR \tag{1.5}$$

Given that bypass either evades the heat sink in its entirety, as is the case with diversion (figure 1.2), or only provides coolant to part of the array in the form of leakage (figure 1.3), the contribution of bypass in cooling the extended surface is minimal. It is this ineffectiveness of bypass in cooling along with the difficulty in quantifying the actual amount of bypass, and subsequently the velocity of the coolant that travels through the array, that is of most significance. For this reason, considerable attention has been given to the measurement and modeling of the bypass phenomenon in anticipation of coming up with a method to accurately determine the velocity of the coolant that comes into contact with the extended surface and to ultimately predict the thermal performance of the heat sink.

Literature Review

The literature for heat sinks used in thermal management of electronic packages is extensive. It is not the intent of the author to provide an exhaustive review of the literature, but rather to provide a synopsis of the more significant studies as it pertains to bypass for parallel plate heat sinks. Of special interest to the current research are the studies that deal with bypass for large clearance ratios (ratio of the area of the bypass region to the area of the heat sink), since this is typical of heat sink configurations in electronic packages.

Wirtz et al. (1994) investigated the effect of bypass flow on the thermal performance of parallel plate heat sinks at large clearance ratios through a series of thermal experiments. From the experimental data they formulated a correlation for the bypass ratio and the parallel plate Nusselt number. The bypass ratio was not directly measured but rather its value was inferred from heat transfer measurements. Simultaneous solution of these correlations along with the thermal resistance of the array for a given fin thickness and approach flow rates give the results shown in figure 1.4. The figure illustrates variation of the thermal resistance with fin density for fin plates

3

having a thickness of $t = 1.5$ *mm* and footprint length of $L = 50$ *mm*. The results are depicted for a heat sink with a fin plate height of 40 *mm* and approach flow rate with Reynolds number of 3,000. The results illustrate the trade-off in performance which occurs when the fin density is varied. Figure 1.4 demonstrates as the fin density increase, the thermal resistance decreases until a point of "optimum" fin density is achieved. As the fin density increases from this optimum point, the effect of bypass manifests itself through increasing thermal resistance.

Lee (1995) determined this bypass ratio implicitly by performing a mass and momentum balance. The analytical procedure he proposed was an iterative one through which an assumed initial value for the array velocity is used to determine its corresponding pressure drop across the heat sink from correlations or data tables presented in the literature. This pressure drop value, in addition to the geometry of the duct and heat sink and approach velocity, are used in the mass and momentum balance to calculate the array velocity. Figure 1.5 provides a comparison of the variation of bypass with Reynolds number for heat sinks of various fin densities as calculated by this model against the experimental results reported by Wirtz et al. (1994). The Reynolds number (Re_L) provided in figure 1.5 is based on the approach velocity (u_{app}) and length of the heat sink (L) as shown in figure 1.1:

$$Re_L = \frac{u_{app} \cdot L}{\nu} \tag{1.6}$$

where ν is the kinematic viscosity of the air. As can be seen from figure 1.5, the model developed by Lee (1995) is in excellent agreement with the experimental data presented by Wirtz et al. (1994). Simons et al. (1997) expounded on this analytical model by developing a non-iterative model consisting of a quadratic equation to calculate the approach velocity from a predetermined array velocity and corresponding heat sink pressure drop, as well as the geometry of the duct and finned array.

Muzychka et al. (1998) developed friction factor solutions to hydrodynamically developing flow in circular and non-circular ducts. It was shown the apparent friction factor based on the square root of the cross-sectional area is a weak function the shape of the geometry, provided an appropriate aspect ratio is defined. The proposed model was developed by combining the developing and fully developed flow asymptotes and was shown to be valid for many duct configurations. The model coincided well with the data for rectangular channels with low aspect ratios thus having applications to parallel plate heat sinks.

Culham et al. (2001) offered a procedure that allows the simultaneous optimization of heat sink design parameters based on a minimization of the entropy generation associated with heat transfer and fluid resistance. The relevant parameters used in the model for a parallel plate heat sink include the geometric parameters, heat dissipation, material properties, and flow conditions. The model discerns a heat sink that minimizes entropy generation, which results in a minimum operating temperature. The model assumes the flow duct is shrouded, therefore eliminating bypass flow. The velocity through the array is determined from the pressure drop across the heat sink. This pressure drop is calculated as outlined in Kays et al. (1984) by taking into account the pressure drop due to form losses (contraction at the inlet of the heat sink and expansion at the exit) along with the friction factor of the channel walls of the heat sink. The friction factor used for the model is the same one derived in the study by Muzychka et al. (1998).

Simons (2004) proposed that, by using the heat sink pressure drop equation presented by Culham et al. (2001) for a fully confined duct in conjunction with the fan curve for the system fan supplying the air flow, the velocity of the coolant through the array, and subsequently the bypass ratio, can be determined for a parallel plate heat sink. This method involves first developing the system curve for the heat sink without bypass using the pressure drop equation developed by Culham et al. (2001). Next, a system curve is developed for the heat sink with bypass flow using the method outlined by

Simons et al. (1997) utilizing estimated values for the air velocity through the array. From the two system curves (with and without bypass) and the fan curve, the bypass ratio can be determined. However, as with previous methods, this only provides an estimate of the bypass ratio. This type of model is referred to as a "two-branch" model since it is assumed the flow directly upstream of the array branches into either the bypass region or the finned array. The model does not take leakage into account.

Recent experimental research has included pressure loss measurements for heat sinks with fin tip clearance in wind tunnel tests, such as those performed by Ortega Gutierrez et al. (2005) and Ortega (2003). However, during these experiments, the actual bypass flow was not measured directly. In the research performed by Ortega Gutierrez et al. (2005), wind tunnel tests for heat sinks with three different finned densities were conducted. Overall heat sink thermal resistance was measured and, along with pressure measurements, compared to a non-iterative two-branch model. The results obtained showed for all three fin pitches, as the top clearance ratio increased, the pressure drop across the heat sink decreased and the overall thermal resistance increased (see figure 1.6 and figure 1.7). The measured pressure drop was compared to results predicted by numerical models that included bypass. As illustrated in figure 1.6, the overall pressure drop becomes comparatively small as the top clearance ratio and, consequently, the bypass ratio increase. In figure 1.7, the model demonstrates agreement with the experimental results at the small clearance ratios. However, as the top clearance increases for all fin pitch cases, the model under predicts the experimental values. This could be attributed to increased leakage at the higher clearance ratios which the two-branch model does not take into account.

Dogruoz et al. (2006) developed a "leakage" model that is similar to the "two-branch" bypass model but with the physics of leakage taken into account. The leakage mechanisms were modeled by introducing momentum equations in the flow normal direction in both the heat sink and the bypass region with ad hoc assumptions about the

6

static pressure distribution in that direction. However, as is the case with the aforementioned studies, bypass is implicitly derived. To establish a base case, the model was developed for a pin fin heat sink and the results compared to experimental pressure drop and heat transfer data. It was shown that leakage effects are important in setting the overall pressure drop for sparsely pitched pin arrays.

Research Objectives

Based on the results from the literature review, the means of determining bypass has been through physics-based numerical models or by deriving bypass implicitly from the experimental data. The two methods of determining bypass from the experimental results have been based on implicitly deriving the bypass from the pressure drop or thermal resistance measurements of the heat sink. As illustrated in figure 1.5, the bypass results derived from the thermal resistance measurements for heat sinks with large clearance ratios reported by Wirtz et al. (1994) and respective numerical modeling results provided by Lee (1995) were in excellent agreement. However, for the strictly hydraulic experiments such as those performed by Ortega Gutierrez et al. (2005), while producing excellent results at lower clearance ratios, produced bypass results at higher clearance ratios that deviated from the experimental results. Hence, it is proposed that direct flow measurements be used to characterize bypass with larger clearance ratios.

The objective of the current work is to directly measure the flow that exits a parallel plate heat sink and, ultimately, determine the bypass flow. The approach taken utilizes thermal anemometry to map the flow field near the downstream face of a parallel plate heat sink in a small, low-speed wind tunnel with large clearance ratios.
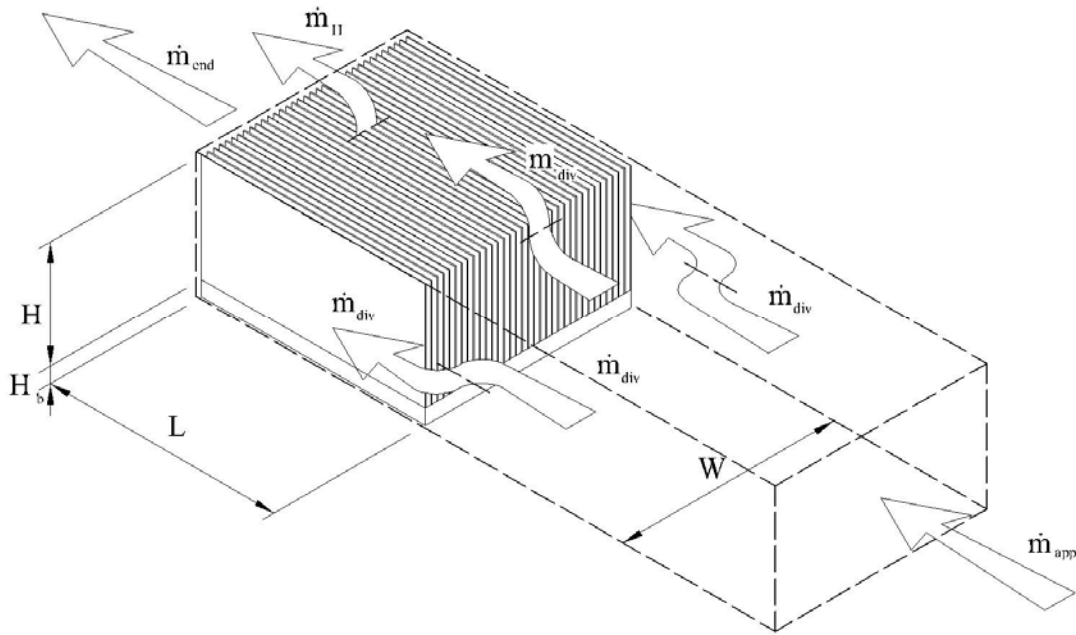
Figure 1.1 Control Volume of the Parallel Plate Heat Sink
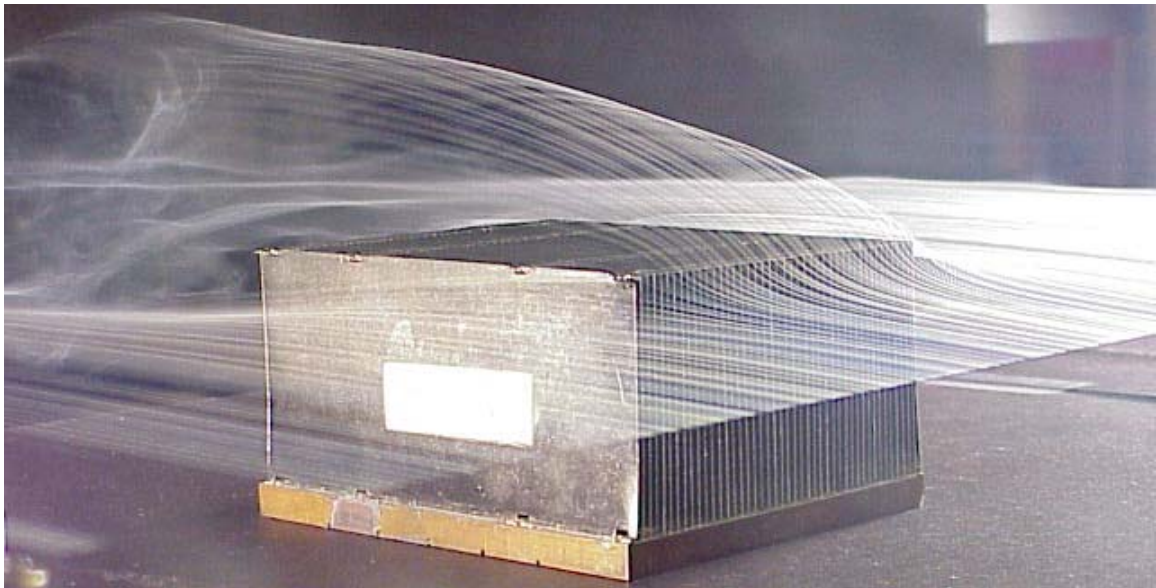
Figure 1.2 Top and Side Diversion Shown in a Smoke Wire Flow Visualization Test
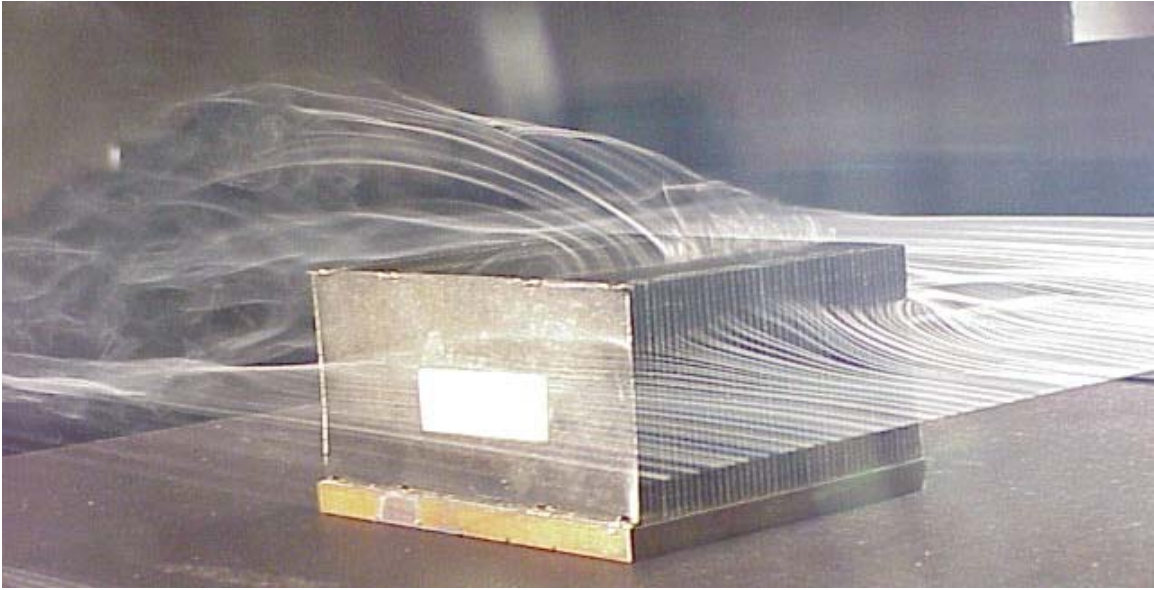
Figure 1.3 Leakage Shown in a Smoke Wire Flow Visualization Test
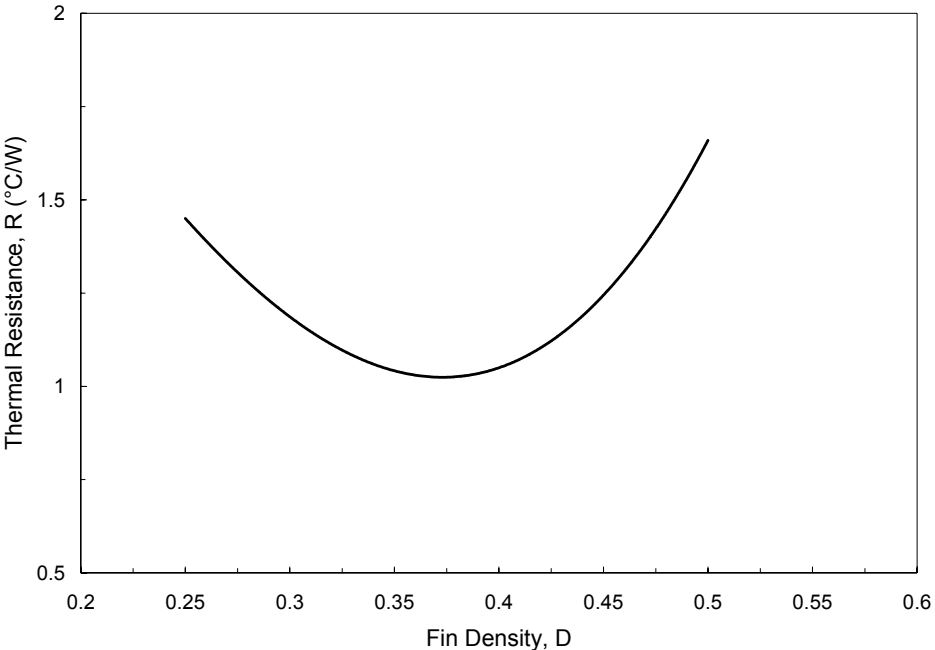
Figure 1.4 Calculated Heat Sink Thermal Resistance for a Parallel Fin Heat Sink, Source: Wirtz et al. (1994)
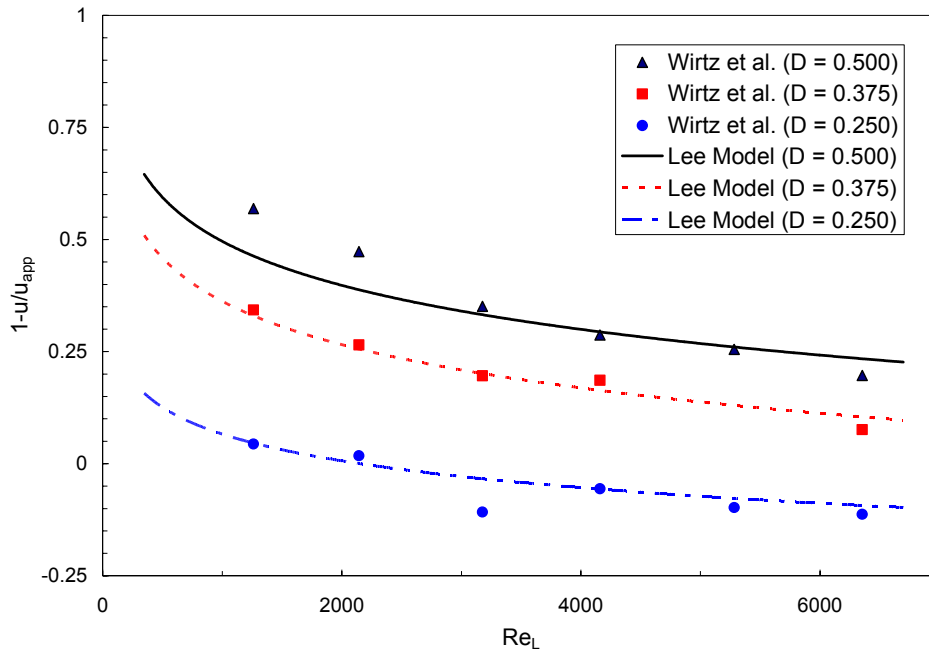
Figure 1.5 Comparison of Bypass Determined Experimentally Versus Analytically, Source: Wirtz et al. (1994) and Lee (1995)
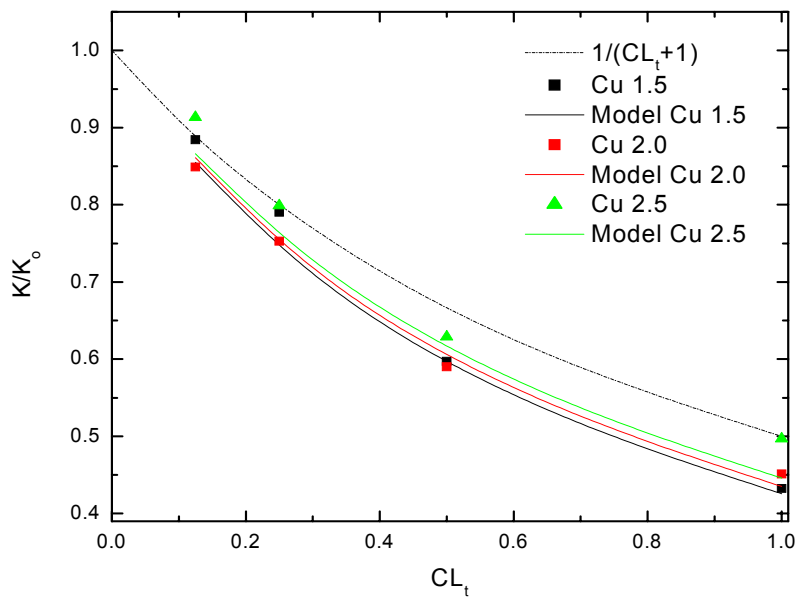
Figure 1.6 Dimensionless Pressure Drop Ratio Versus Top Clearance Ratio (u_a=5 m/s), Source: Ortega Gutierrez et al. (2005)
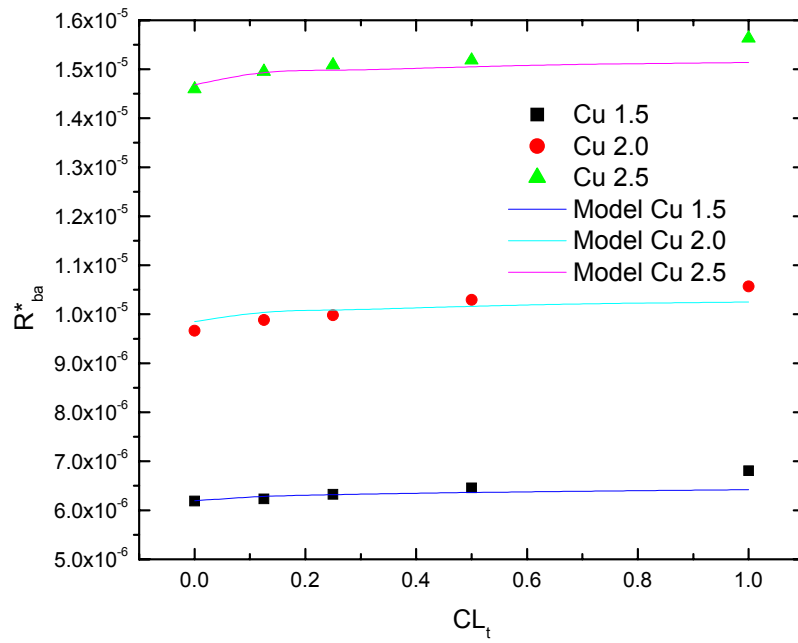
Figure 1.7 Thermal Resistance Versus Top Clearance Ratio (u_a=6.0 m/s) Source: Ortega Gutierrez et al. (2005)

CHAPTER TWO

EXPERIMENTAL DESCRIPTION AND METHODOLOGY

Heat Sink

The heat sink used for this study was a high-density parallel plate finned array that consisted of a copper base with soldered copper fins (figure 2.1). The heat sink was the "Cu 2.0" heat sink which was developed for and used in the experiments conducted by Ortega Gutierrez et al. (2005). The dimensions of the heat sink are provided in figure 2.2.

Wind Tunnel

The Electronic Cooling Wind Tunnel in the Fluid Dynamics Lab at Washington State University Tri-Cities was used to perform the bypass flow experiments (figures 2.3 and 2.4). The wind tunnel was an indraft-type consisting of an inlet, test section, and exit plenum with a bank of variable speed axial fans. The inlet did not include a flow nozzle; however, it provided flow conditioning by means of a 1.5 *in* thick aluminum honeycomb core having ¼ inch cells. The inlet section was followed by the test section. This segment of the wind tunnel was a 0.610 *m* long rectangular duct constructed of ¼ inch Plexiglas. The test section had cross-sectional dimensions 0.155 *m* in height and 0.408 *m* in width as shown in figure 2.4. The large cross-sectional area of the duct with respect to the cross-sectional area of the heat sink provided a large clearance ratio. The clearance ratio is defined as follows:

$$CL = \frac{A_{by}}{A_{array}} = \frac{A_{duct} - A_{array}}{A_{array}} = \frac{A_{duct}}{A_{array}} - 1 \qquad (2.1)$$

where A_{by}, A_{duct}, and A_{array} are the bypass channel, wind tunnel, and heat sink cross-sectional areas, respectively. The cross-sectional areas of the wind tunnel test section (A_{duct}) and the heat sink (A_{array}) are given by:

$$A_{duct} = H_{duct}W_{duct} \tag{2.2}$$

and

$$A_{array} = (H + H_b)W \tag{2.3}$$

Substituting equations (2.2) and (2.3) into equation (2.1) and using the dimension values provided in figure 2.2 and figure 2.4, it is shown the clearance ratio of the test setup was approximately $CL \approx 15$. The configuration shown in figure 2.4 allowed for not only flow diversion over the top of the heat sink but also around the sides of the finned array. The combination of the large clearance ratio (CL) and full diversion provided for flow channel characteristics similar to those found in electronic packages.

A brush-sealed slot spanning the width of the ceiling of the wind tunnel was located in the test section to exit plenum transition piece to accommodate instrumentation access. Three Comair-Rotron Maltese 24 VDC, five-blade axial fans were mounted in parallel at the end of the exit plenum to draw air through the wind tunnel. These fans had a rated air flow of 300 *CFM* at a system pressure drop of 0.790 inches of water. The fan bank was driven by a variable DC power supply to allow test section air speed to vary between 3 *m/sec* and 5 *m/sec*.

Experimental Method

As stated in Chapter One, the objective of the research was to directly measure the flow that exits a parallel plate heat sink and, ultimately, determine the bypass flow. To measure the flow exiting the heat sink, discrete spatial point velocity measurements were made using a thermistor anemometer. This type of velocity probe works by electrically heating the thermistor with it placed in the flow stream. The thermistor anemometer had a constant temperature arrangement. This was achieved through a feedback control circuit that varied the current so the temperature of the thermistor remained steady. The heat dissipated from the thermistor through convective heat

13

transfer is measured experimentally and, using calibration curves, is reduced to a velocity value. A detailed circuit diagram, along with a full description of the thermistor anemometer, is provided in Appendix A.

The discrete spatial point velocity measurements were made across the cross-sectional area of the wind tunnel at a distance of Δz downstream of the heat sink (figure 2.5a). An automated, stepper motor driven xy-traverse was built for this research. This system allowed control of the incremental movement of the anemometer with a maximum resolution per step of 0.42 *mm* in the *x*-direction and 0.02 *mm* in the *y*-direction (refer to figure 2.5a for axis direction). The typical path that the thermistor velocity probe traveled during a test is provided in figure 2.5b where Δx is the incremental movement in the *x*-direction, Δy is the incremental movement in the *y*-direction, and *m* is the number of incremental steps made in the *y*-direction. The maximum distances the *xy*-traverse could travel was approximately 100 *mm* in the *y*-direction and 390 *mm* in the *x*-direction. The *y*-directional component of the traverse could be adjusted manually so any 100 *mm* swathe between the floor of the test section up to 6 *mm* below the ceiling of the wind tunnel could be spanned. The *x*-directional component of the traverse could cover the span of the wind tunnel up to 9 *mm* to either wall. The *xy*-traverse system is illustrated in figure 2.6.

A typical test was split into two subsets: a high resolution flow survey and a low resolution survey. The high resolution survey was conducted with the anemometer starting at a distance y_i from the wind tunnel floor and a distance x_i from the test section wall, as illustrated in figure 2.7a and at a distance of Δz downstream of the array, as shown in figure 2.5a. The *xy*-traverse began by controlling the movement of the velocity probe in the positive *y*-direction, stopping in increments of $\Delta y = 0.8$ *mm* to allow for a velocity measurement to be made. This continued until the traverse moved the anemometer *m* increments in the *y*-direction (Δy), as shown in figure 2.5b. At this point, the velocity probe was located at a distance of $y_f = m\Delta y$ above the wind tunnel floor

(figure 2.7a). After a measurement was made at this position (y_f), the traverse moved the anemometer in the x-direction at an increment of $\Delta x = 0.42 \, mm$ and took a velocity measurement before proceeding in the negative y-direction. As the anemometer traveled along the negative y-direction path, as shown in figure 2.5b, it stopped at increments of $\Delta y = 0.8 \, mm$ to allow for velocity measurements to be made. This continued until the traverse moved the velocity probe m increments of Δy to a spatial position located at the original y-directional distance of y_i and new x-directional distance of $x_i + \Delta x$, as illustrated in figure 2.5b. After a measurement was made at this location, the traverse moved the anemometer in the x-direction one increment $\Delta x = 0.42 \, mm$ and made another velocity measurement, thus completing the first "cycle." After traveling several of these velocity measurement "cycles," the high resolution survey concluded with the anemometer finishing at the y_i and x_f location (figure 2.7a). The purpose of the high resolution survey was to provide a detailed map of the air flow exiting the heat sink.

The low resolution survey was conducted in a similar manner as the high resolution survey with two exceptions: 1) velocity measurements were made over the entire cross-sectional area of the wind tunnel and 2) the Δx and Δy increments were increased to 6 mm to accommodate the larger survey region. Upstream flow conditions and the location of the probe (Δz) downstream of the heat sink were held constant to the corresponding high resolution survey. The purpose of the low resolution survey was to collect velocity measurements of the whole wind tunnel cross-sectional area for a final mass balance calculation. As previously mentioned, the xy-traverse could not travel the whole span of the wind tunnel in the y-direction. Therefore, the low resolution survey of the entire wind tunnel cross-sectional area was split into two separate subsets: one providing a survey of the lower portion of the wind-tunnel (see figure 2.7b) and a second providing a survey of the upper portion (see figure 2.7c). As with the high resolution survey, the low resolution survey started with the velocity probe at the spatial location of

15

x_i and y_i, making velocity measurements along the velocity probe path shown in figure 2.5b with the test concluding at point x_f and y_i (see figures 2.7b and 2.7c).

During these tests, a separate velocity measurement was made upstream of the heat sink using a Pitot-tube. The Pitot-tube remained stationary near the inlet of the wind tunnel and was used as a reference measurement. This upstream velocity measurement was made every time a discrete spatial velocity measurement was made downstream of the finned array. This measurement was used as a reference between the high and low resolution tests performed at the same upstream velocity to ensure continuity between tests. This was accomplished by normalizing each of the upstream velocity measurements to the average upstream velocities measured during the first subset test. These normalized upstream values then were multiplied by the corresponding downstream thermistor anemometer velocity measurement to obtain the normalized downstream velocity at the discrete location xy:

$$u_{ds,xy,norm} = \left(u_{us,xy} / \overline{u}_{us,xy} \right) u_{ds,xy} \tag{2.4}$$

where $u_{ds,xy}$ and $u_{us,xy}$ are the measured downstream and upstream velocities, taken at the time the anemometer probe was located at the spatial location xy. These values were normalized against the average value of the upstream velocities instead of a single point velocity measurement to ensure a possible statistical outlier did not set the normalization.

Instrumentation and Data Acquisition System (DAS)

To measure the barometric pressure (p_∞), a SMI SM5812 pressure sensor was utilized with a 0.5 *VDC* to 4.5 *VDC* output signal range and having a 15 *psia* full-scale pressure span. The pressure sensor was located outside the wind tunnel near the inlet. A Type-K thermocouple located inside the wind tunnel was used to measure the ambient temperature (T_∞).

As previously discussed, the upstream reference velocity was measured utilizing a

Pitot-tube. The Pitot-tube total pressure was measured by a Setra 239 pressure transducer having high accuracy for low pressure applications. The pressure transducer had a measurement range of 0.0 to 0.5 inches of water with a linearly corresponding output signal range of 0 to 5 *VDC*.

The thermistor used in the anemometer was a BetaTHERM 10K3MCD1 micro-BetaCHIP thermistor probe. The probe was cylindrical in shape with a length of 3.18 *mm* and a 0.457 *mm* diameter. The small size of the probe allowed for good spatial resolution for the previously mentioned velocity surveys. The output signals given by the thermistor anemometer unit were two 0 to 10 *VDC* outputs. One signal was used to determine the current supplied to the thermistor and the other was used to calculate the thermistor resistance and, ultimately, the temperature of the heated thermistor.

All analog measurements were sampled and converted to a digital output by a NI-6036E DAQ card with a 16-bit resolution. The DAQ card, in conjunction with the stepper motor controller, provided the automation for the *xy*-traverse. Figure 2.8 provides a block diagram of the instrumentation, data acquisition, and control used in this research.

Uncertainty

The uncertainty analysis was carried out using the methods outlined by Coleman et al. (1999). The data collected during the experiments was reduced to two quantities: the upstream velocity determined by the Pitot-tube total pressure measurements and convective heat transfer coefficients of the thermistor anemometer. Ultimately, the convective heat transfer coefficients were used to calculate air velocity via calibration regression curves.

To calculate the velocity from the Pitot-tube total pressure measurements, the following data reduction equation was used:

$$u = \sqrt{\frac{2\Delta p}{\rho}}$$

(2.5)

where Δp is the difference between total stagnation and static pressures measured by the Pitot-tube and ρ is the density of the air. The air density in equation (2.5) was determined from the ideal-gas equation of state:

$$\rho = \frac{p}{R(T + 459.67)}$$

(2.6)

where R is the gas constant, p is the static pressure measurement, and T is the temperature of the air. Substituting equation (2.6) into equation (2.5) provides the following relation between the air velocity and the measured quantities:

$$u = \sqrt{\frac{2\Delta pR(T + 459.67)}{p}}$$

(2.7)

and the corresponding uncertainty is given by:

$$\delta u = \sqrt{\left(\frac{\partial u}{\partial \Delta p}\delta\Delta p\right)^2 + \left(\frac{\partial u}{\partial T}\delta T\right)^2 + \left(\frac{\partial u}{\partial p}\delta p\right)^2}$$

(2.8)

$$\delta u = \sqrt{\left(\frac{u\delta\Delta p}{2\Delta p}\right)^2 + \left(\frac{u\delta T}{2(T + 459.67)}\right)^2 + \left(\frac{-u\delta p}{2p}\right)^2}$$

where $\delta\Delta p$, δT, and δp are the uncertainties in the experimental measurements of total pressure, temperature, and barometric pressure, respectively. The systematic and random uncertainties for the instrumentation and data acquisition system (DAS) are provided in table 2.1. As stated in the previous section, the SMI pressure transducer was used to measure the barometric pressure and the NI 6036E 16-bit DAQ board was used to convert the analog measurement to a digital signal output. Taking into account the uncertainties in the transducer and data acquisition chain, as provided in table 2.1, the overall uncertainty of the barometric pressure in equation (2.8) as measured by the SMI pressure transducer is given by:

$$\delta p = \sqrt{\left(\frac{\partial p}{\partial V}(0.00756\ VDC)\right)^2 + \left(\frac{\partial p}{\partial V}(0.08\ VDC)\right)^2 + \ldots \atop \ldots + \left(\frac{\partial p}{\partial V}(0.02\ VDC)\right)^2 + \left(\frac{\partial p}{\partial V}(0.004\ VDC)\right)^2}$$

(2.9)

where p is the equation used to reduce the raw pressure data into engineering units as follows:

$$p = [V + 0.5\ VDC]\cdot\left(\frac{15\ psia}{4\ VDC}\right)$$

(2.10)

Solving for equation (2.9), the following uncertainty is derived for the pressure measured by the SMI pressure transducer

$$\delta p = \left[\sqrt{(0.00756\ VDC)^2 + (0.08\ VDC)^2 \atop + (0.02\ VDC)^2 + (0.004\ VDC)^2}\right]\left(\frac{15\ psia}{4\ VDC}\right)$$

(2.11)

$$\delta p = \pm\ 0.311\ psia$$

In a similar manner the Setra 239 differential pressure transducer measurement uncertainty is provided below:

$$\delta \Delta p = \sqrt{\left(\frac{\partial \Delta p}{\partial V}(0.005\ VDC)\right)^2 + \left(\frac{\partial \Delta p}{\partial V}(0.001\ VDC)\right)^2 \atop + \left(\frac{\partial \Delta p}{\partial V}(0.005\ VDC)\right) + \left(\frac{\partial \Delta p}{\partial V_0}(0.005\ VDC)\right)^2 \atop + \left(\frac{\partial \Delta p}{\partial V_0}(0.001\ VDC)\right)^2 + \left(\frac{\partial \Delta p}{\partial V_0}(0.005\ VDC)\right)^2 \atop + \left[2\left(\frac{\partial \Delta p}{\partial V}\right)\left(\frac{\partial \Delta p}{\partial V_0}\right)\sqrt{(0.005\ VDC)^2 + (0.005\ VDC)^2}\right]}$$

(2.12)

where Δp is

$$\Delta p = (V - V_0)\left(\frac{0.5''\ H_2O}{5\ VDC - V_0}\right)$$

(2.13)

The variables V and V_0 in equations (2.12) and (2.13) are the voltage output signals from the differential pressure transducer and the zero voltage reading. The seventh term on the RHS of equation (2.2) is the correlated bias uncertainty as prescribed by Coleman et al. (1999) and is a result of the V and V_0 measurements sharing the same systematic uncertainty. Equation (2.12) is reduced further as shown:

$$\delta \Delta p = \left(\frac{0.5'' H_2O}{(5\,VDC - V_0)^2} \right) \sqrt{ \begin{array}{l} 0.00051\,VDC^2(V^2 + V_0^2) - 0.00385\,VDC^2(V_0 + V) \\ -0.00025\,VDC^2(V_0 V) + 0.01925\,VDC^2 \end{array} } \tag{2.14}$$

Assuming an output signal of $V = 0.38\,VDC$ from the differential pressure transducer with a zero measurement reading of $V_0 = 0.04\,VDC$, equations (2.13) and (2.14) provide a differential pressure measurement of $\Delta p = 0.0343'' H_2O$, having an uncertainty of $\delta \Delta p = \pm 0.0027'' H_2O$, or 7.9 % of the measured value.

The temperature measurement used in equation (2.7) was performed using a Type-K thermocouple with an uncertainty value of $\pm 1\,°C$ (table 2.1). Therefore with a $\Delta p = 0.0343 \pm 0.0027'' H_2O$, $p = 14.696 \pm 0.311\,psia$, and $T = 22.5 \pm 1\,°C$ $(72.5 \pm 1.8\,°F)$, equations (2.7) and (2.8) give, respectively:

$$u = \sqrt{ \frac{2(0.0343'' H_2O)\left(5.197\,\dfrac{psf}{'' H_2O}\right)\left(53.35\,\dfrac{ft - lbf}{lbm\,°R}\right)[(72.5) + 459.67]\,°R}{(14.696\,psia)\left(144\,\dfrac{psf}{psia}\right)\left(\dfrac{1}{32.127}\,\dfrac{lbf\;sec^2}{lbm\;\;ft}\right)} } \tag{2.15}$$

$$u = 12.396\,\frac{ft}{sec}\;\left(3.778\,\frac{m}{sec} \right)$$

$$\delta u = \sqrt{ \left(3.778\,\frac{m}{sec} \right)^2 \left[\begin{array}{l} \left(\dfrac{0.0027'' H_2O}{2(0.0343'' H_2O)} \right)^2 + \left(\dfrac{1.8\,°R}{2(72.5 + 459.67)\,°R} \right)^2 + \ldots \\[2mm] \ldots + \left(\dfrac{-0.311\,psia}{2(14.696\,psia)} \right)^2 \end{array} \right] } \tag{2.16}$$

$$\delta u = 0.507 \frac{ft}{sec} \left(0.155 \frac{m}{sec} \right)$$

At the conditions prescribed in the aforementioned equations, the accuracy of the velocity measurement provided by the Pitot-tube is ± 4.1 %.

The second quantity determined from the experimental measurements was the convective heat transfer coefficient of the themistor anemometer. This value was used to determine the air velocity downstream of the heat sink by using regression curves obtained from calibration. The equation for the thermistor convective heat transfer coefficient is given by:

$$h_{therm} = \frac{Q_{therm}}{T_{therm} - T_{air}} \tag{2.17}$$

where Q_{therm} is the heat dissipated by the thermistor anemometer, T_{therm} is the temperature of the thermistor, and T_∞ is the temperature of the free-stream flow. Assuming the uncertainty in the heat dissipation measurement is small relative to the uncertainty in the temperature measurement and neglecting the random uncertainty of the temperature measurement, the uncertainty of the thermistor heat transfer coefficient is given by:

$$\delta h_{therm} = \sqrt{\left(\frac{\partial h_{therm}}{\partial T_{therm}} (0.2\,°C) \right)^2 + \left(\frac{\partial h_{therm}}{\partial T_\infty} (1\,°C) \right)^2} \tag{2.18}$$

$$\delta h_{therm} = \left(\frac{h_{therm}}{T_{therm} - T_\infty} \right) \sqrt{((-1)(0.2\,°C))^2 + ((1\,°C))^2}$$

For nominal test conditions of $T_{therm} = 60\,°C$ and $T_{t\infty} = 22.5\,°C$ the normalized uncertainty of the heat transfer measurement would be $\delta h_{therm} / h_{therm} = \pm 2.7$ %. Upon observation of equation (2.18), it was determined the dominant contributor to the heat transfer coefficient uncertainty was the thermocouple measurement of the ambient conditions.

To determine the velocity measured by the thermistor anemometer, a regression

curve is needed to convert the heat transfer coefficient to a velocity value. The following regression curve was obtained from a previous calibration

$$u_{therm} = 23.102 h_{therm}^2 - 25.112 h_{therm} + 6.824 \qquad (2.19)$$

where u_{therm} and h_{therm} are in units of m/s and $mW/°C$. Neglecting the uncertainty contribution by the calibration curve, the uncertainty associated with u_{therm} is given by:

$$\delta u_{therm} = \sqrt{\left(\frac{\partial u_{therm}}{\partial h_{therm}} \delta h_{therm} \right)^2} \qquad (2.20)$$

$$\delta u_{therm} = \sqrt{\left(\left(46.204 \, h_{therm} - 25.112 \right) \delta h_{therm} \right)^2}$$

At nominal test conditions ($T_{therm} = 60 °C$ and $T_\infty = 22.5 °C$) and with a thermistor anemometer heat dissipation of $h_{therm} = 0.9595 \, mW/°C$, equations (2.19) and (2.20) provide a thermistor velocity of $u_{therm} = 4.00 \, m/s$ with an uncertainty of $\delta u_{therm} = \pm 0.50 \, m/s$ or $\pm 12.5 \%$. This level of uncertainty in the thermistor anemometer was deemed unacceptable by the author therefore, a system calibration was warranted.

The overriding influence in the calculated uncertainty of the thermistor anemometer velocity was traced back to the contribution of the uncertainty in the ambient temperature measurement by the Type-K thermocouple in equation (2.18). To reduce this uncertainty, a system calibration was performed for the Type-K thermocouple using an ice bath and boiling water bath. Then, the calibrated Type-K thermocouple was used in a system calibration of the anemometer, which was performed in the wind tunnel. The specifics of these calibrations are provided in Appendix B. However, the new calibration curve and corresponding uncertainty equation used to determine the thermistor anemometer velocity are provided as follows:

$$u_{therm} = \left(8.810 \, h_{therm} - 7.905 \sqrt{h_{therm}} + 1.247 \right)^2 \qquad (2.21)$$

and

$$\delta u_{therm} = \left[\begin{array}{l} \left(-3.520 \times 10^2 \right) h_{therm}^6 + \left(2.469 \times 10^3 \right) h_{therm}^5 - \left(6.679 \times 10^3 \right) h_{therm}^4 \\ + \left(9.188 \times 10^3 \right) h_{therm}^3 - \left(6.885 \times 10^3 \right) h_{therm}^2 + \left(2.689 \times 10^3 \right) h_{therm} \\ - 429.840 \end{array} \right] \qquad (2.22)$$

At nominal test conditions ($T_{therm} = 60\,°C$ and $T_\infty = 22.5\,°C$) and with a thermistor anemometer heat dissipation of $h_{therm} = 0.9595\,mW/°C$, equations (2.21) and (2.22) provide a thermistor anemometer velocity of $u_{therm} = 3.83\,m/s$ with an uncertainty of $\delta u_{therm} = \pm\,0.18\,m/s$ or $\pm\,4.7\,\%$. This was almost a three-fold reduction in the thermistor anemometer velocity measurement uncertainty.

Table 2.1 Systematic and Random Uncertainties of Instrumentation and Data Acquisition System (DAS)

Source	Value	Description
NI 6036E 16bit DAQ Accuracy	±7.560mV	±10V span
Bourdon Tube Barometer Bias	±0.1cmHg	±0.1%FS
Bourdon Tube Barometer Precision	±0.025cmHg	±1/2 of the least division of the meter
SMI Pressure Transducer SM5812 Bias	±0.08V	4V span, 15psi span
SMI Pressure Transducer SM5812 Precision	±0.02V	±0.5%FS
SMI Pressure Transducer SM5812 Hysteresis	±4mV	±0.1%FS
Type K Thermocouple	±1.0°C	
Setra 239 Pressure Transducer Bias	±0.005V	±0.1%FS
Setra 239 Pressure Transducer Precision	±0.001V	±0.02%FS
Setra 239 Pressure Transducer Hysteresis	±0.005V	±0.1%FS
BetaTHERM micro-thermister Bias	±0.2°C	@ 25°C'

Figure 2.1 High-Density Parallel Plate Heat Sink
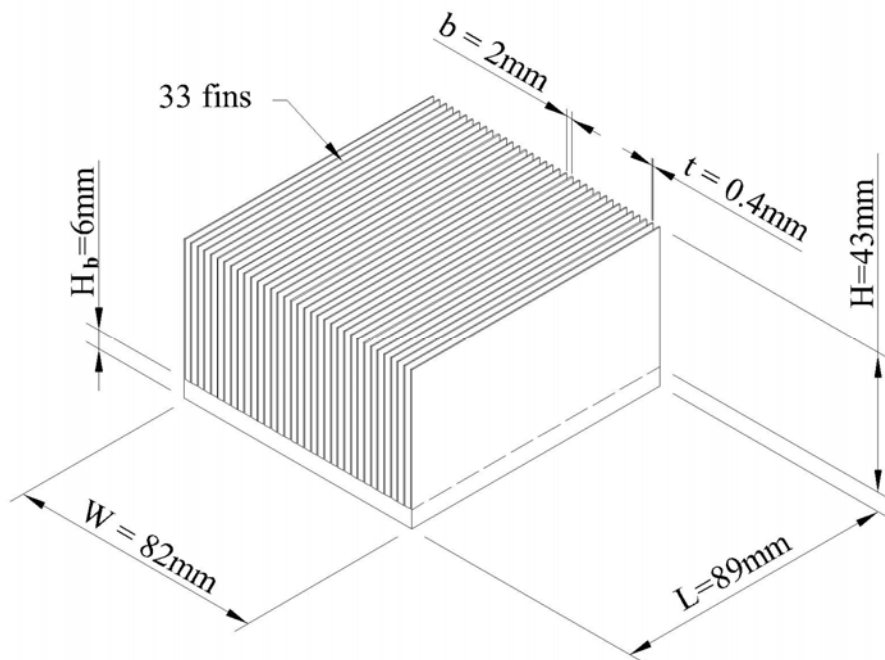
Figure 2.2 Dimensions of the Optimum High-Density Parallel Plate Heat Sink
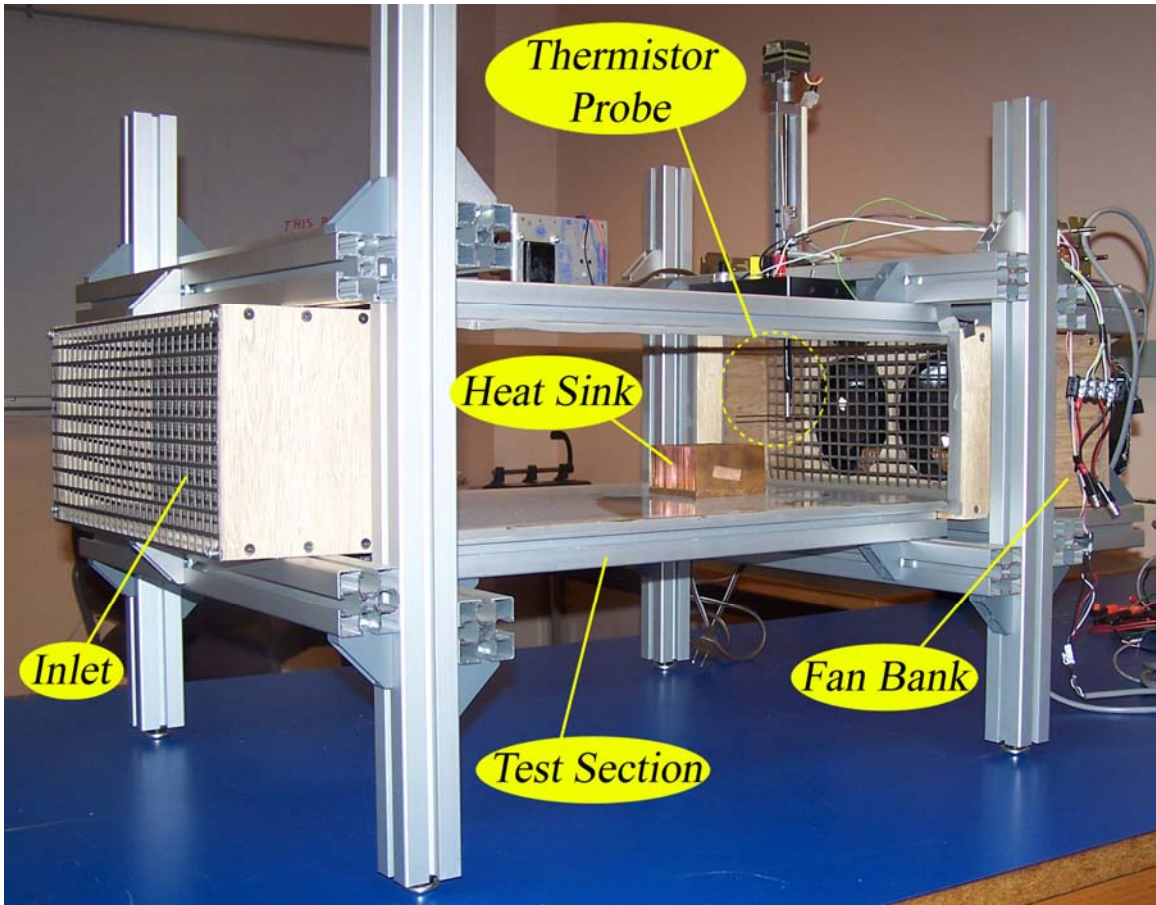
Figure 2.3 Low-Speed Wind Tunnel
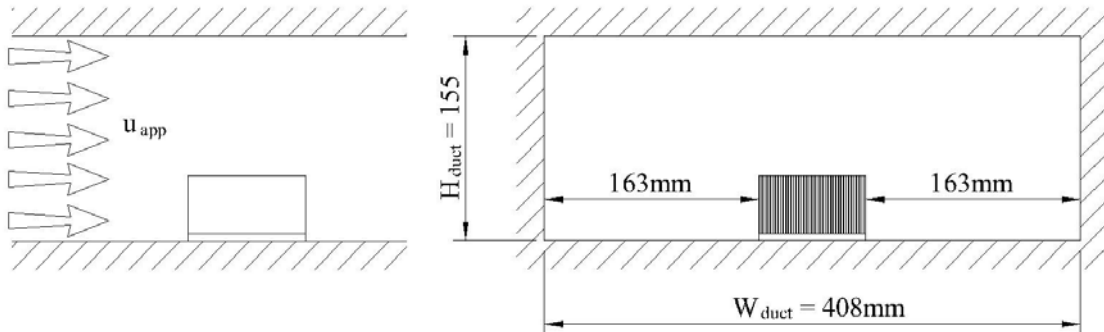
Figure 2.4 Dimensions of the Test Section, Including the Heat Sink
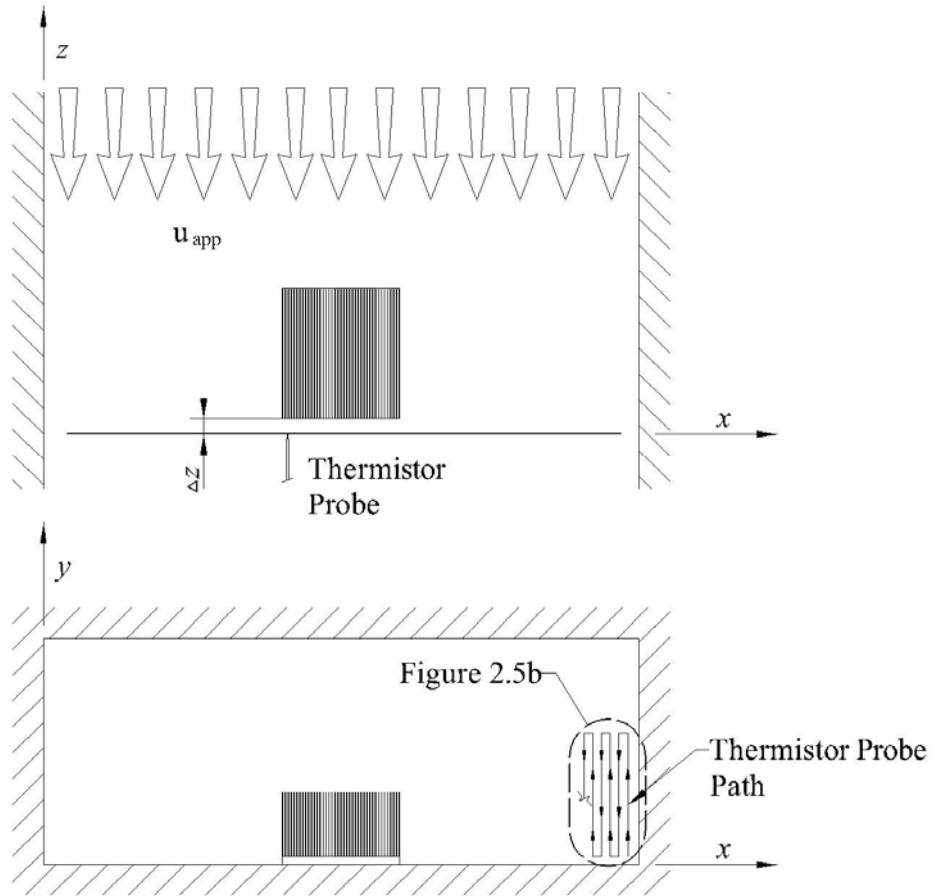
Figure 2.5a Thermistor Velocity Probe Location Relative to the Heat Sink
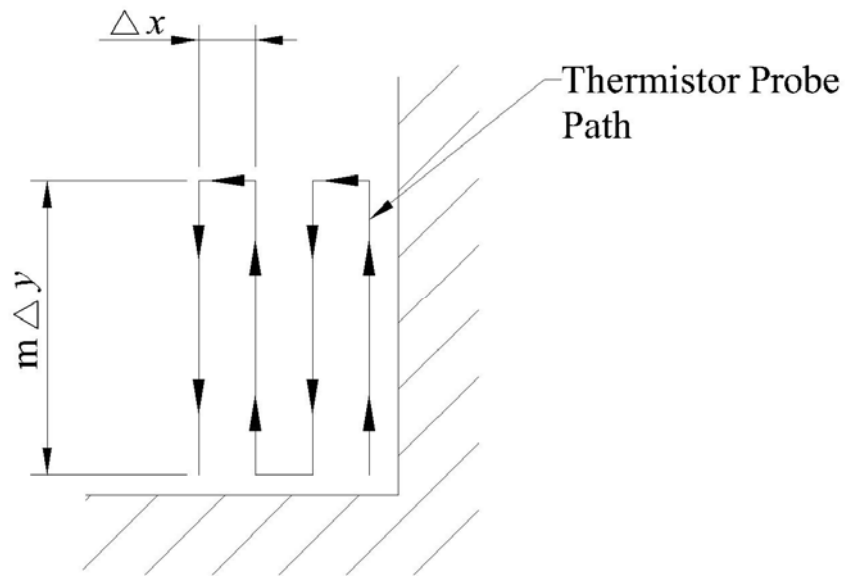
Figure 2.5b Thermistor Velocity Probe Measurement Path
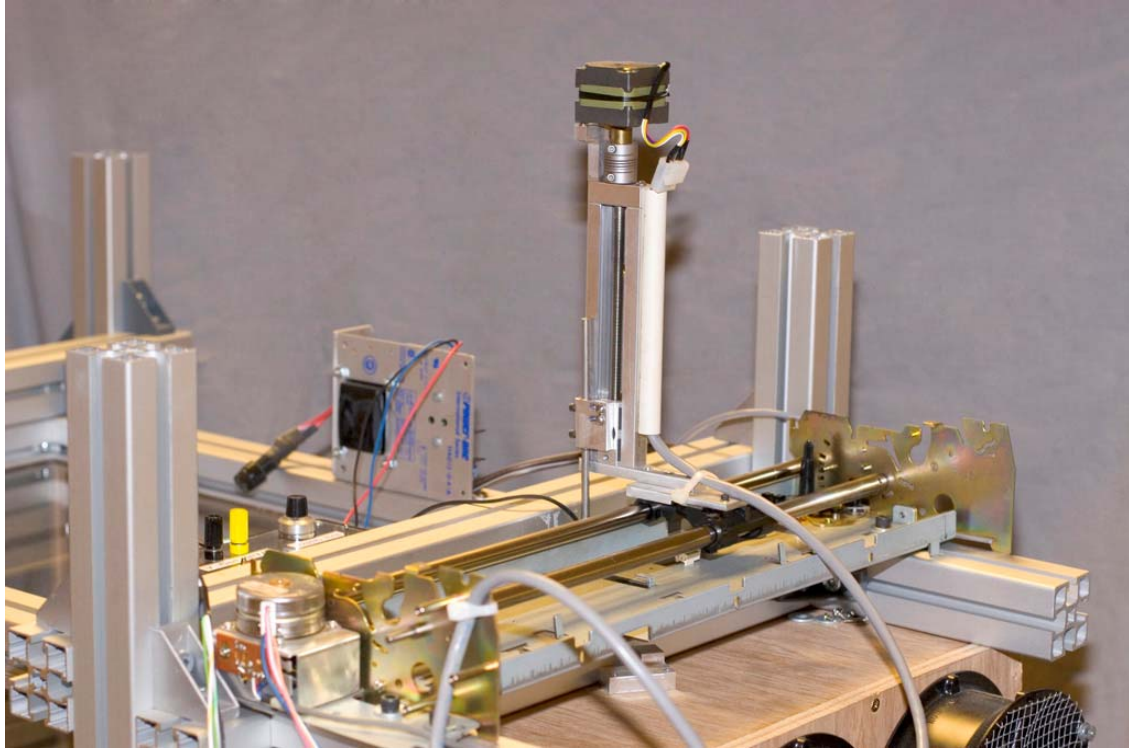
Figure 2.6 *xy*-Traverse
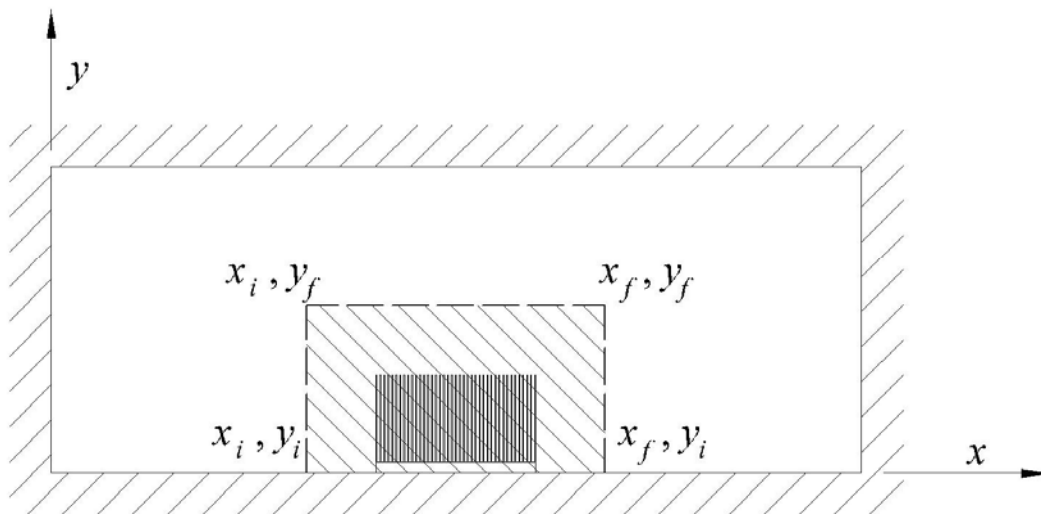
Figure 2.7a High Resolution Survey of the Heat Sink
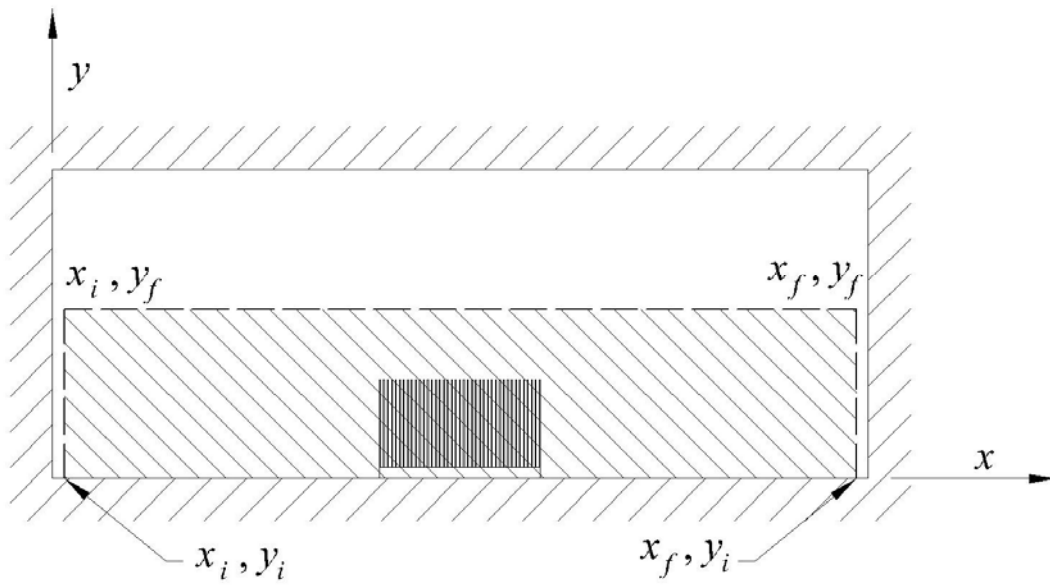
Figure 2.7b Low Resolution Survey of the Lower Tunnel
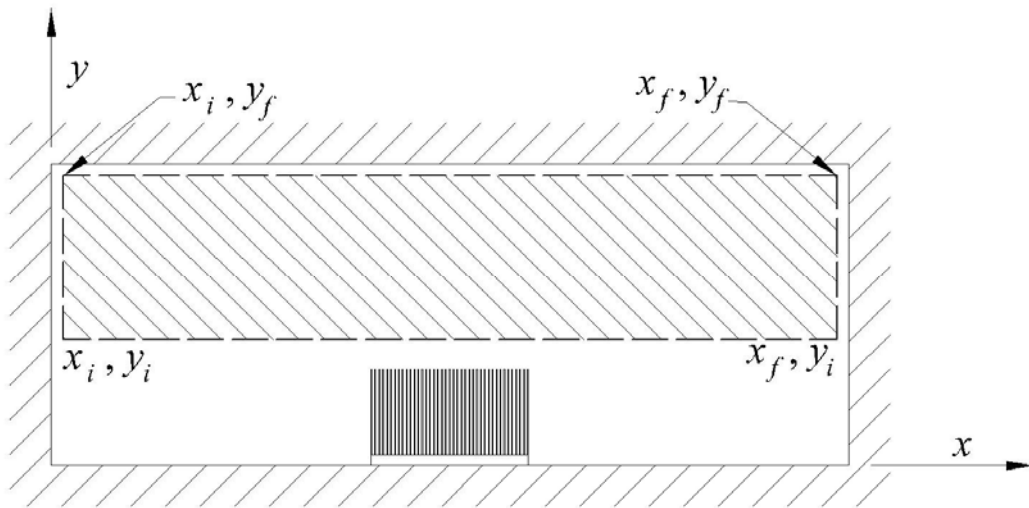
Figure 2.7c Low Resolution Survey of the Upper Tunnel
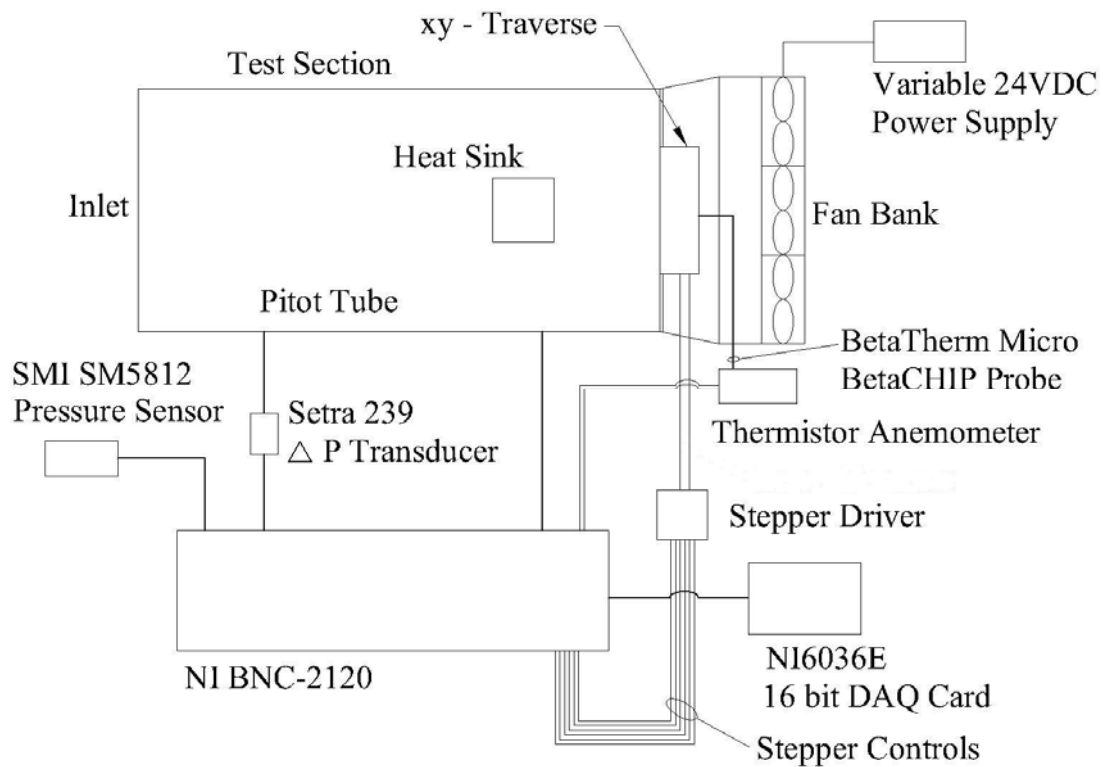
Figure 2.8 Instrumentation and Data Acquisition System Setup

CHAPTER THREE

EXPERIMENTAL RESULTS

Three tests were performed following the experimental methodology outlined in Chapter Two. The first test (t0016) was performed with the thermistor velocity probe located 2 *mm* downstream of the heat sink ($\Delta z = 2 \ mm$, as shown in figure 2.5a). This test was performed in three subsets to capture the high resolution survey of the air velocity near the finned array (t0016a) and two low resolution velocity surveys to capture the lower and upper portions of the wind tunnel (subsets t0016b and t0016c). The second test (t0017) was performed with the thermistor velocity probe located 25 *mm* downstream of the heat sink ($\Delta z = 25 \ mm$, as shown in figure 2.5a). The subsets of the test included the low resolution velocity survey of the upper and lower portions of the duct (subsets t0017a and t0017b) and the high resolution survey of the air velocity near the finned array (t0017c). A third and final test was performed without the heat sink in the wind tunnel (t0019). The subsets included a low resolution velocity survey of both the lower and upper portions of the wind tunnel (subset tests t0019a and t0019b). The purpose of the last test was to measure the air velocity in the absence of the heat sink and compare the results to the first two tests to allow for a check of the continuity equation. For all tests, the fan speed was adjusted by the variable DC power supply until the same reference Pitot-tube velocity was achieved.

The outer corners of the enveloped area tested for each subset (x_i, x_f, y_i, and y_f, as shown in figures 2.7a, b, and c) are provided in table 3.1, in addition to the incremental Δx and Δy movements of the velocity probe (see figure 2.5b). It can be deduced from table 3.1 that as few as 780 points for the low resolution test and up to as many as 24,225 points for the high resolution test were evaluated within their respective surveyed areas. With the large quantity of velocity measurement points taken within the surveyed areas, the tests took as long as an hour-and-one-half to complete for the low resolution tests and

up to as long as ten hours for the high resolution tests. Because of the lengthy duration of the tests, verifying steady state conditions was imperative. Figure 3.1 through Figure 3.7 show the ambient conditions were relatively steady throughout the individual test subsets. The biggest variation occurred for the ambient temperature measurements, where it fluctuated at most ± 1.5 °C. It should be noted, however, that the final downstream velocity results for all tests were normalized to the average Pitot-tube velocity measurement of test t0016a. This, in effect, negated the influence of the small variances seen in the ambient conditions and upstream velocity over the course of individual tests.

In addition to verifying that the tests were performed at steady state conditions, it had to be shown that the nominal upstream velocity was consistent between test subsets. Figure 3.8 through Figure 3.13 illustrate some of the average velocity profiles at different portions of the wind tunnel. At the measurement points where there is overlap between the subsets it is shown that there is relatively good agreement.

For each test, the subsets were combined to provide a velocity map at distance Δz downstream of the finned array. The first test (t0016) provided velocity measurements at $\Delta z = 2 \ mm$ downstream of the heat sink, and its corresponding velocity survey results are shown in figure 3.14. The second test (t0017) provided velocity measurements at $\Delta z = 25 \ mm$ downstream of the array, and its subsequent velocity map is provided in figure 3.15. The differences between the two velocity maps are striking in that the "footprint" of the heat sink is more distinctly visible for the test where the downstream velocity was measured closer to the finned array ($\Delta z = 2 \ mm$). This may be attributed to the fact that for the case where the velocity survey was performed further downstream at $\Delta z = 25 \ mm$, considerable mixing between the flow exiting the heat sink and the bypass flow had occurred.

Ultimately, the purpose of conducting these experiments was to directly measure the flow exiting the heat sink. To determine the amount of flow exiting the finned array, the velocities measured downstream in the projected heat sink cross-sectional area were

numerically integrated over the cross-sectional area of the finned array using the trapezoid rule, as follows:

$$u_{end} = \left(\frac{1}{4A_{array}}\right)\sum_{j=1}^{M-1}\left\{\begin{bmatrix}\sum_{i=1}^{N-1}\left(u_{end,x_ky_{i+1}} + u_{end,x_ky_i}\right)\left(y_{i+1} - y_i\right)\end{bmatrix}_{k=j+1} \\ + \begin{bmatrix}\sum_{i=1}^{N-1}\left(u_{end,x_ky_{i+1}} + u_{end,x_ky_i}\right)\left(y_{i+1} - y_i\right)\end{bmatrix}_{k=j}\right\}\left(x_{j+1} - x_j\right) \tag{3.1}$$

As illustrated in figure 2.4, the distance from the edge of the heat sink to the test section wall was 163 mm; therefore, $x_1 \geq 163\ mm$ in equation (3.1). Furthermore, as shown in figure 2.2, since the heat sink had a width of $W = 82\ mm$, then $x_M \leq (82\ mm + x_1)$ where M was the number of measurement points made in the x-direction across the heat sink cross-sectional area. In a similar fashion, the first point in the y-direction (y_1) was the location just above the wind tunnel floor where the first velocity measurement ($u_{end,xy}$) was made. Given the heat sink had a total height, including the base, of 49 mm, $y_N \leq (49\ mm + y_1)$ where N was the number of measurement points made in the y-direction across the heat sink cross-sectional area. The total summation term on the RHS of equation (3.1) provides a volumetric flow rate of the air exiting the heat sink. To determine the average velocity (u_{end}) of the air exiting the array, this volumetric flow rate was divided by A_{array}, which is equal to the total height of the array, multiplied by its width.

The same process was performed over the projected area of the clearance region to determine the amount of air flow through this particular flow channel and its subsequent average velocity. The clearance region was divided into three rectangular sub-regions so equation (3.1) could be used to calculate the average velocity through the specific flow channel. The A_{array} term in equation (3.1) was replaced with the appropriate cross-sectional area. However, the clearance region cross-sectional area was only divided through after the volumetric flow rates were calculated for all three sub-regions and summed together. For each clearance sub-region, its corresponding M, N, x,

y and $u_{end,xy}$ values were used to calculate its respective volumetric flow rate. These calculations were performed using the compiled FORTRAN open-source code developed by the author and provided in Appendix C.

To validate the results from the two heat sink hydraulic tests (t0016 and t0017), a mass balance was performed using the volumetric flow rates calculated for the bypass clearance region and the heat sink. Assuming incompressible flow, the continuity equation is given by:

$$\dot{V}_{windtunnel} \equiv \dot{V}_{end} + \dot{V}_{clearance} \qquad (3.2)$$

The velocity measurements obtained from the upper tunnel low resolution test without the heat sink (t0019b) were numerically integrated, as was similarly done for the clearance region. From this numerical integration, an upstream approach velocity and corresponding volumetric flow rate of $u_{app} = 4.5\ m/s$ and $\dot{V}_{windtunnel} = 0.28\ m^3/s$ were derived. The results of the velocity numerical integrations are provided in table 3.2. From these values, it was shown the additive array and clearance region flow rates were 2.1 % smaller than the approach flow rate for the $\Delta z = 2\ mm$ test. For the $\Delta z = 25\ mm$ test, the summation of the downstream volumetric flow rates derived from the experimental data was 5.7 % less than the upstream flow rate.

As demonstrated in Chapter One, it is desirable to present bypass in the non-dimensional form of the bypass ratio (*BR*). To determine the bypass ratio, substitute equations (1.4) and (1.5) into equation (1.2) from Chapter One and rearrange the expression as follows:

$$BR = 1 - \frac{u_{end}}{u_{app}} \qquad (3.3)$$

where u_{app} is the upstream velocity, as determined from test t0019. The $\Delta z = 2\ mm$ test provided a bypass ratio of 64 %, while the $\Delta z = 25\ mm$ test provided a substantially smaller bypass ratio of 42 %.

These results were compared to the bypass model developed by Simons et al.

34

(1997). The model consisted of a quadratic equation to calculate the approach velocity
from a predetermined array velocity and corresponding heat sink pressure drop, as well as
the geometry of the duct and the finned array. The model is presented below:

$$u_{app} = \frac{-b + \sqrt{(b^2 - 4ac)}}{2a}$$ (3.4)

$$a = \left(\frac{A_{duct}}{A_{by}}\right)^2$$

$$b = -\left(\frac{2A_{duct}A_f u_f}{A_{by}^2}\right)$$

$$c = -\left[\left(1 - \frac{A_f}{A_{by}}\right)^2 u_f^2 + \frac{2\Delta p}{\rho}\right]$$

The A_f area term and u_f velocity term correspond to the flow channels within the heat
sink. The Δp term in equation (3.3) is the pressure drop across the heat sink, while the
rest of the terms have been defined in previous sections. The pressure drop was
determined from pressure drop measurements performed by Ortega Gutierrez et al.
(2005) for this specific heat sink (Cu 2.0) with $CL = 0$. At an approach velocity of
$u_{app} = 4.5\ m/sec$, as was measured during testing, the Simons model provided an exit
velocity of $u_{end} = 1.4\ m/sec$. The bypass ratio was $BR = 69\ \%$ compared to a bypass
ratio of $BR = 64\ \%$ from the $\Delta z = 2\ mm$ test and, from the $\Delta z = 25\ mm$ test,
$BR = 42\ \%$.

Table 3.1 Boundary Points of the Surveyed Areas and Incremental Movements of the *xy*-Traverse[*]

Test	$\Delta x(mm)$	$\Delta y(mm)$	$x_i(mm)$	$y_i(mm)$	$x_f(mm)$	$y_f(mm)$
t0016a	0.423	0.8	144	1	263.6	69
t0016b	6	6	9	1	399	85
t0016c	6	6	9	76.5	399	148.5
t0017a	6	6	9	69.5	399	141.5
t0017b	6	6	9	1	399	85
t0017c	0.423	0.8	144	1	264.4	69
t0019a	6	6	9	1	399	73
t0019b	6	6	9	67	399	139

Table 3.2 Measured Volumetric Flow Rates, Velocities, and Bypass Ratio[†]

	Clearance Region		*Finned Array*		*Total Duct (Upstream)*		
z	V_{by}	u_{by}	V_{end}	u_{end}	$V_{windtunnel}$	u_{app}	
(mm)	(m³/s)	(m/s)	(m³/s)	(m/s)	(m³/s)	(m/s)	BR
2	0.272	4.7	0.005	1.6	0.277	4.4	64%
25	0.259	4.3	0.008	2.6	0.267	4.2	42%
no array					0.283	4.5	

---

[*]Refer to Figure 2.5 (a and b) and Figure 2.7 (a, b, and c) for explanation of nomenclature.
[†] *BR* is determined using equation (3.3) with the u_{app} measured value from the "no array" test.
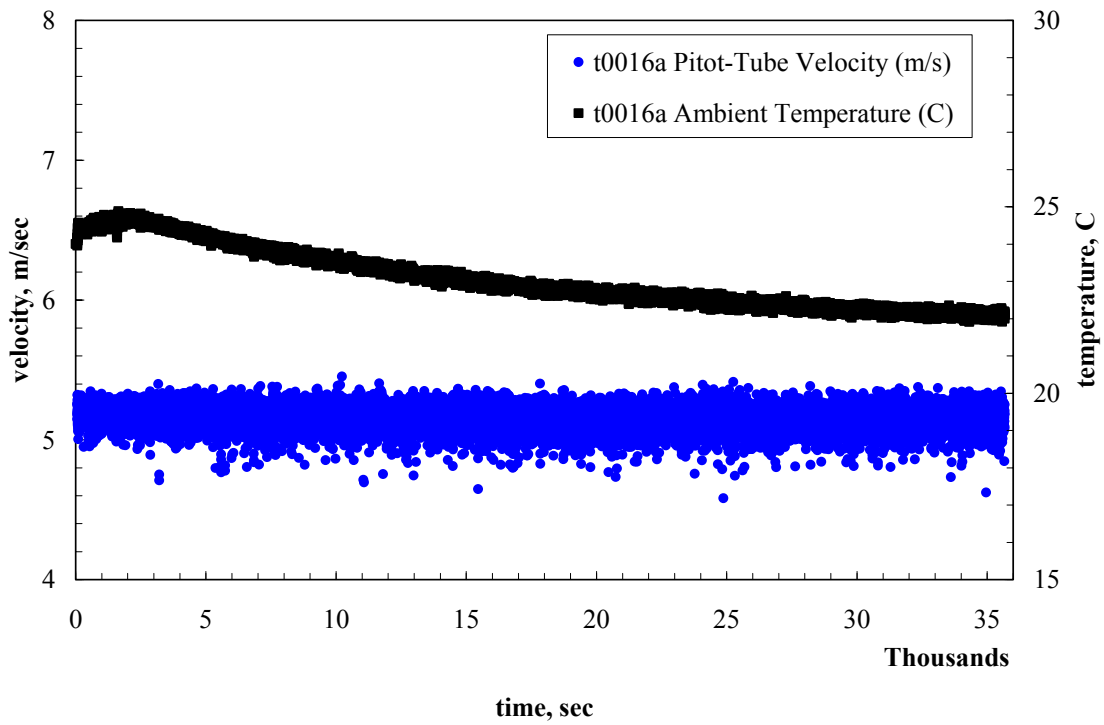
Figure 3.1 Ambient Conditions and Pitot-Tube Velocity Histories (t0016a)
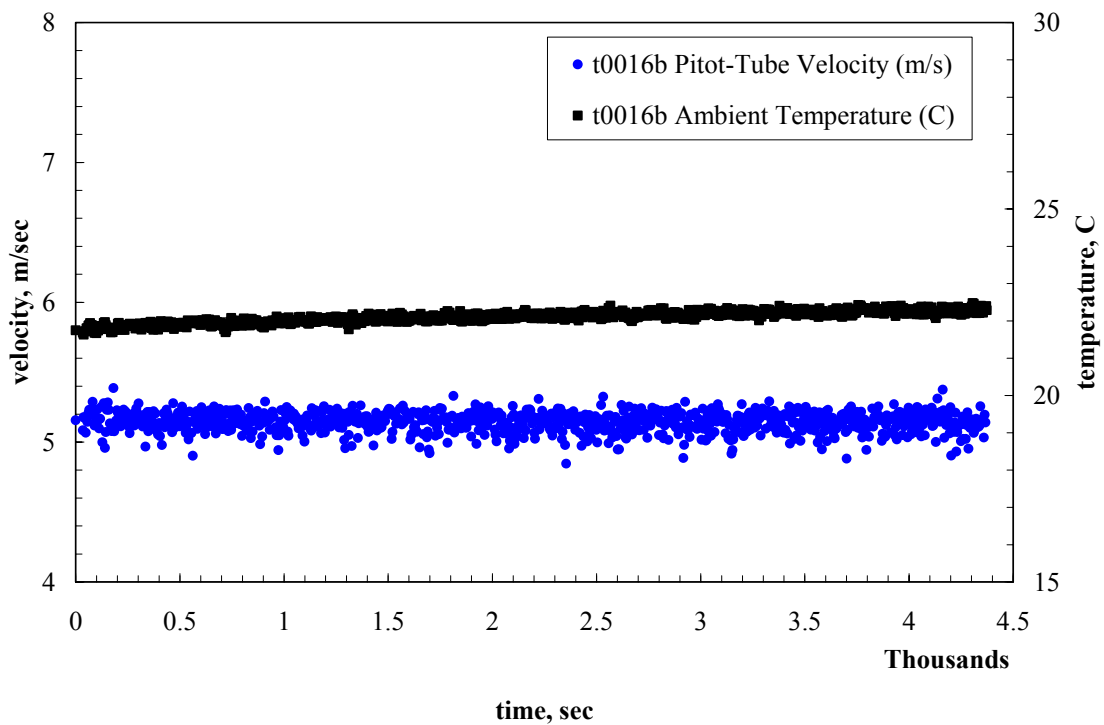
Figure 3.2 Ambient Conditions and Pitot-Tube Velocity Histories (t0016b)

37
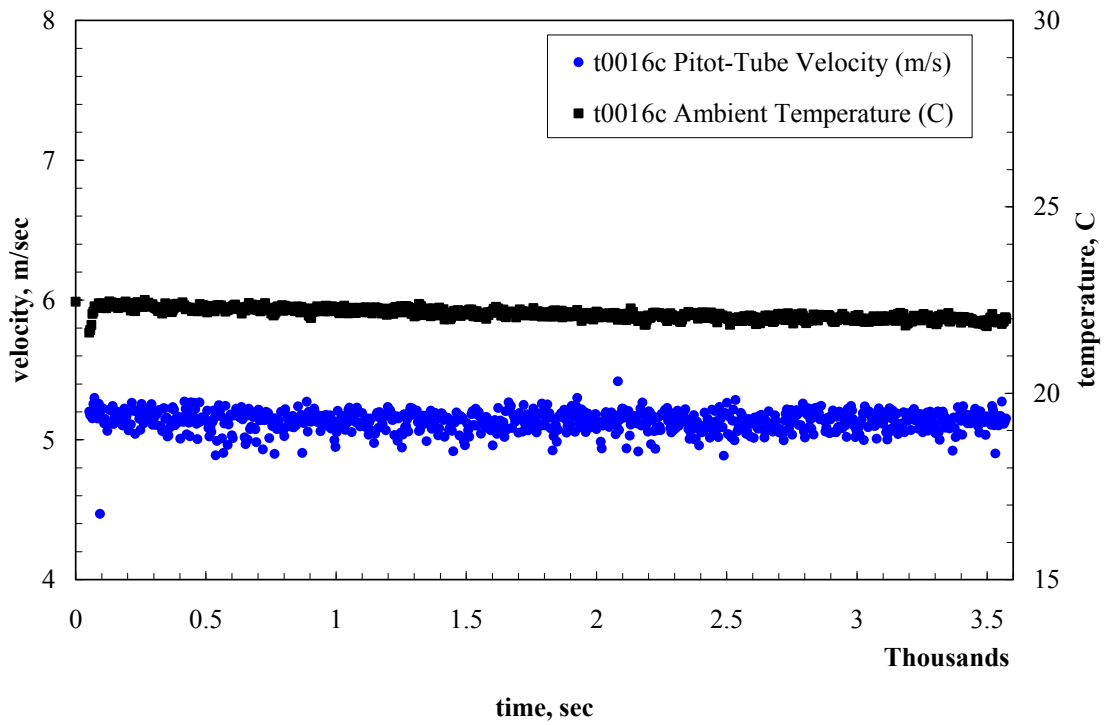
Figure 3.3 Ambient Conditions and Pitot-Tube Velocity Histories (t0016c)
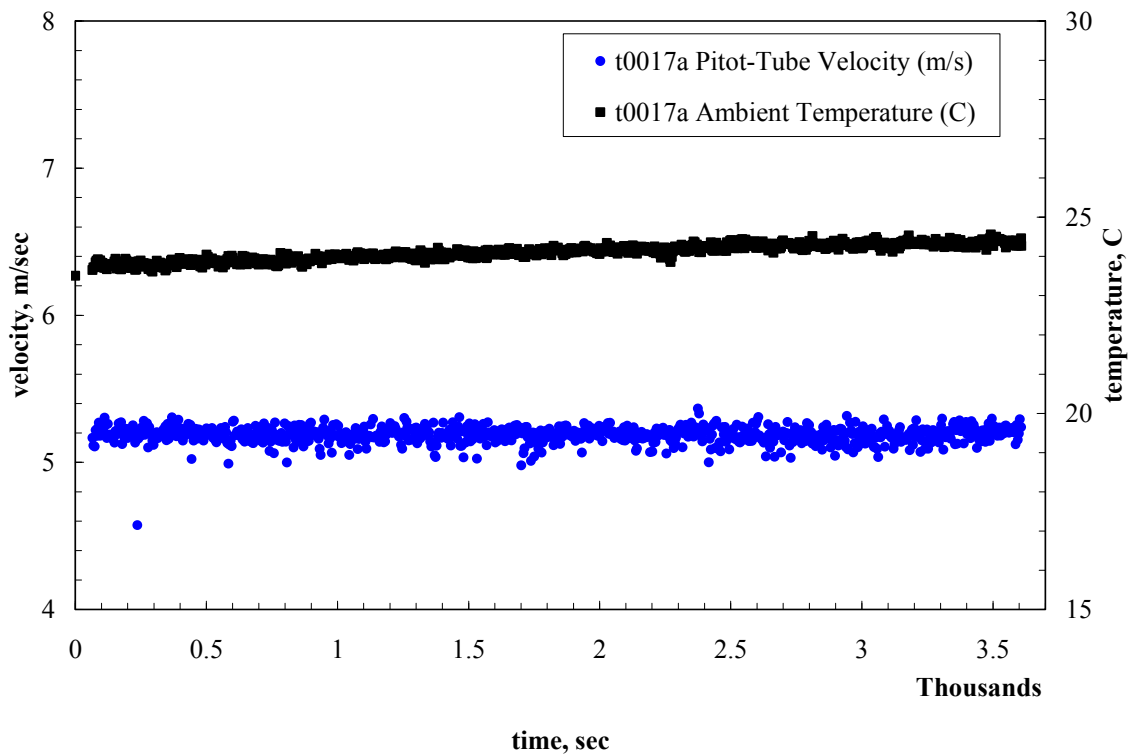
Figure 3.4 Ambient Conditions and Pitot-Tube Velocity Histories (t0017a)
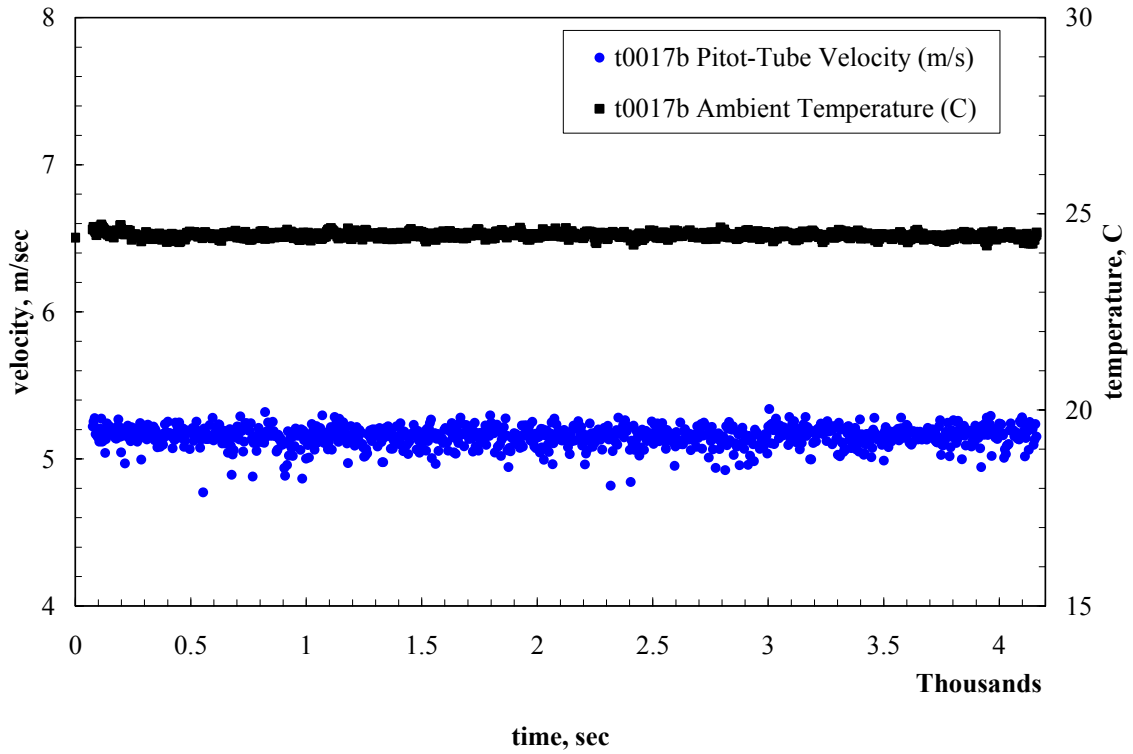
Figure 3.5 Ambient Conditions and Pitot-Tube Velocity Histories (t0017b)
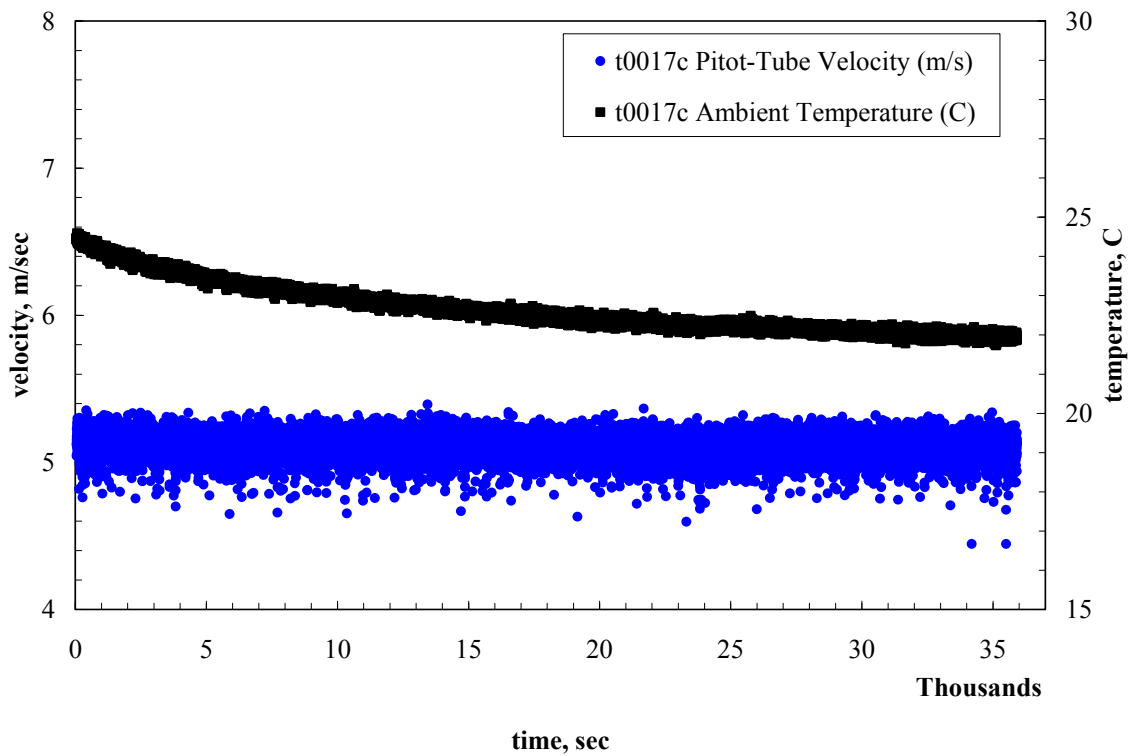
Figure 3.6 Ambient Conditions and Pitot-Tube Velocity Histories (t0017c)
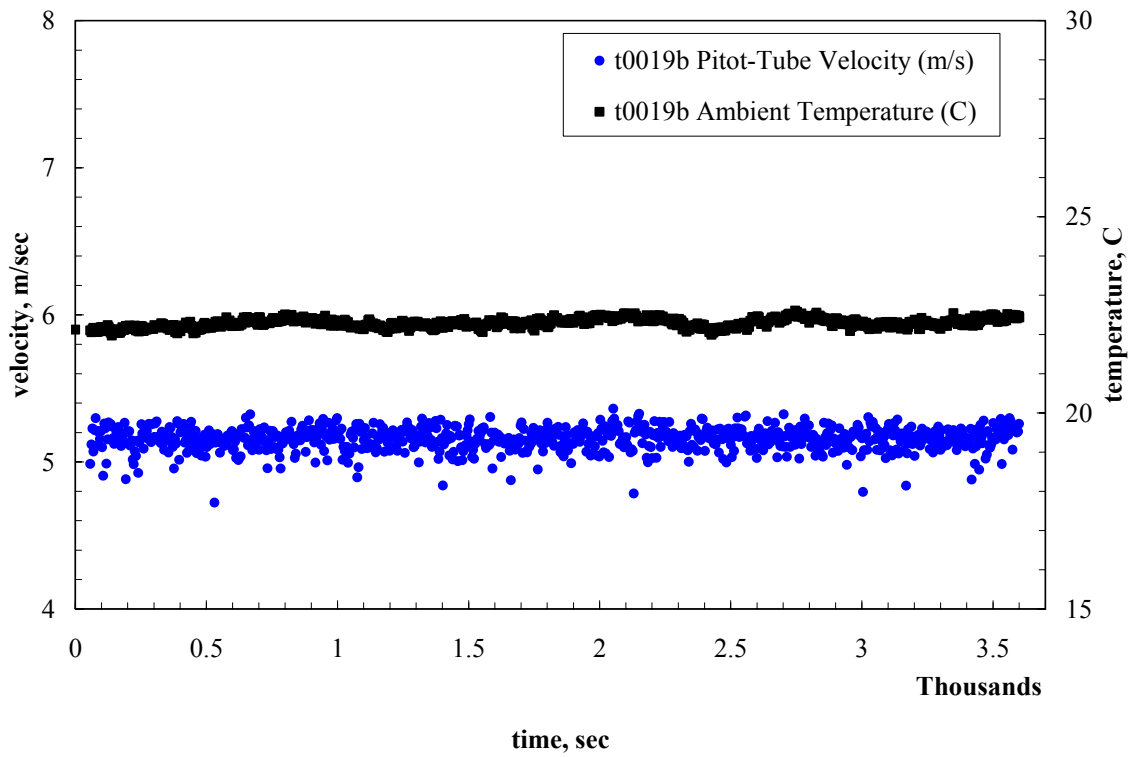
Figure 3.7 Ambient Conditions and Pitot-Tube Velocity Histories (t0019b)
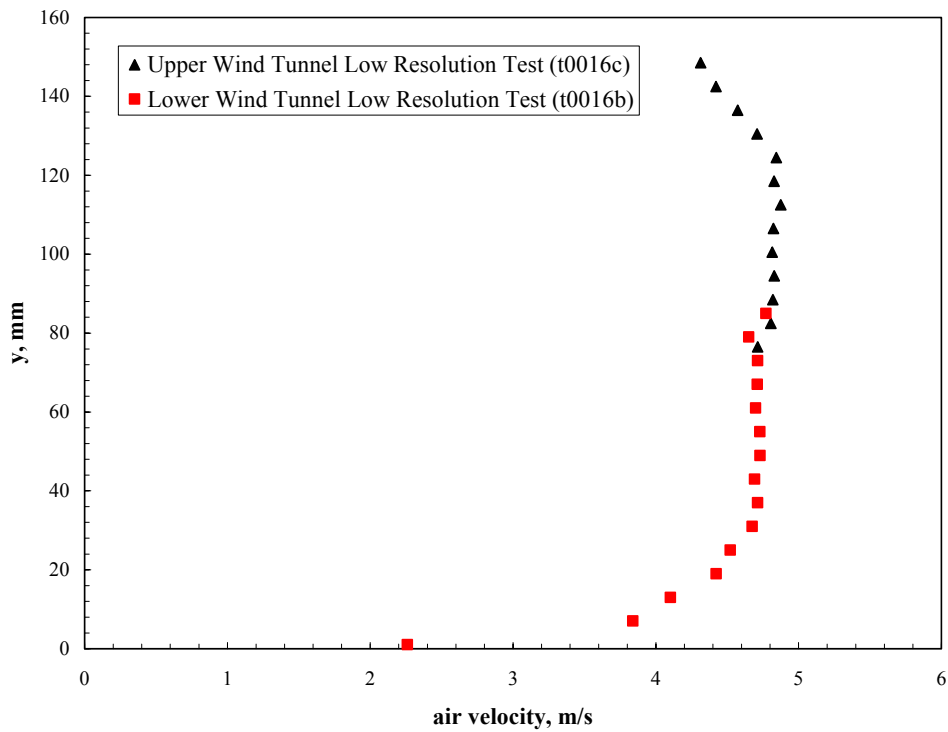
Figure 3.8 Average Velocity Profile at Left Side of Wind Tunnel (t0016)
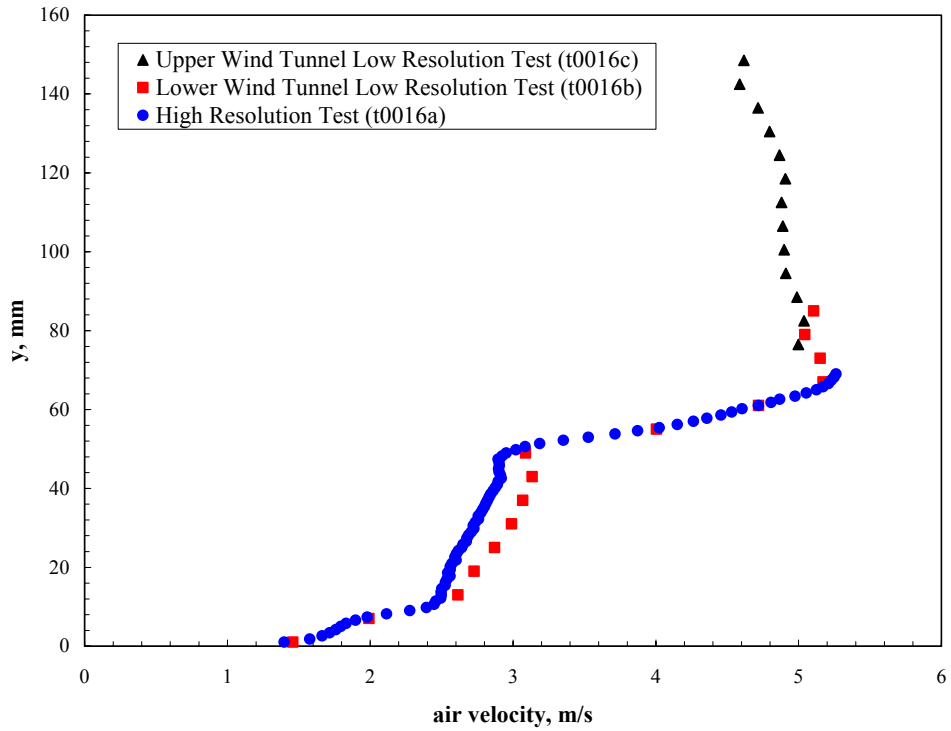
Figure 3.9 Average Velocity Profile at Center of Wind Tunnel (t0016)
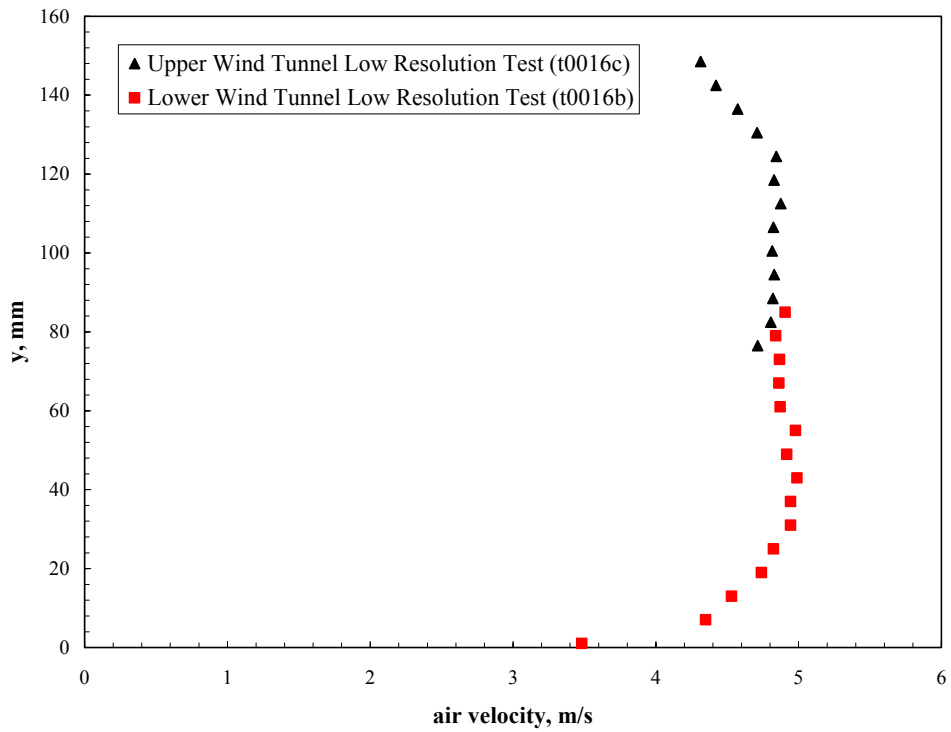
Figure 3.10 Average Velocity Profile at Right Side of Wind Tunnel (t0016)
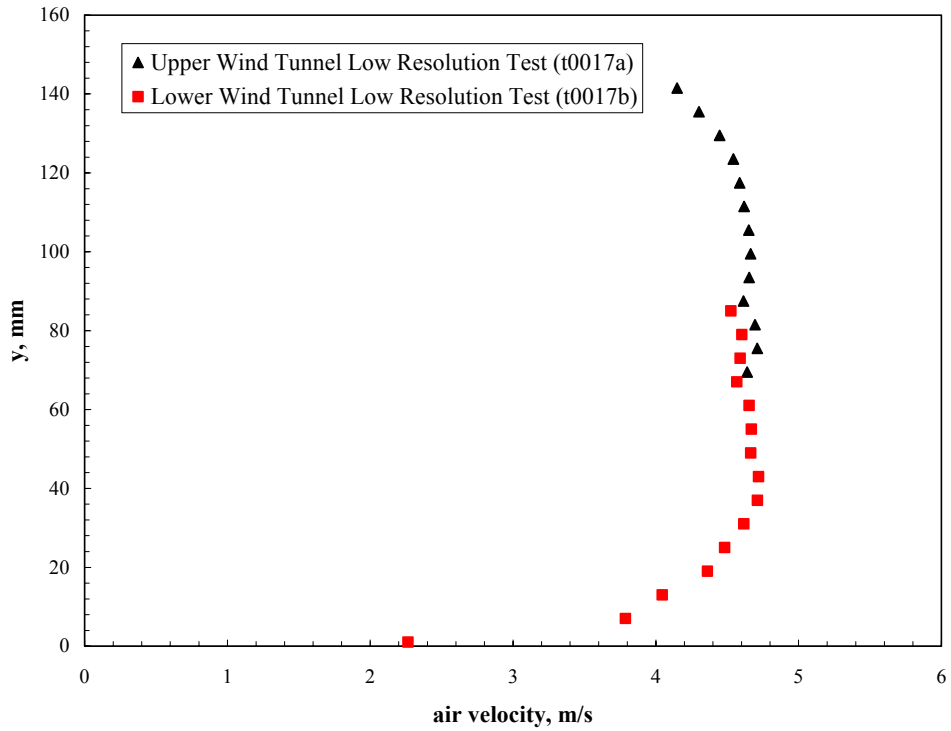
Figure 3.11 Average Velocity Profile at Left Side of Wind Tunnel (t0017)
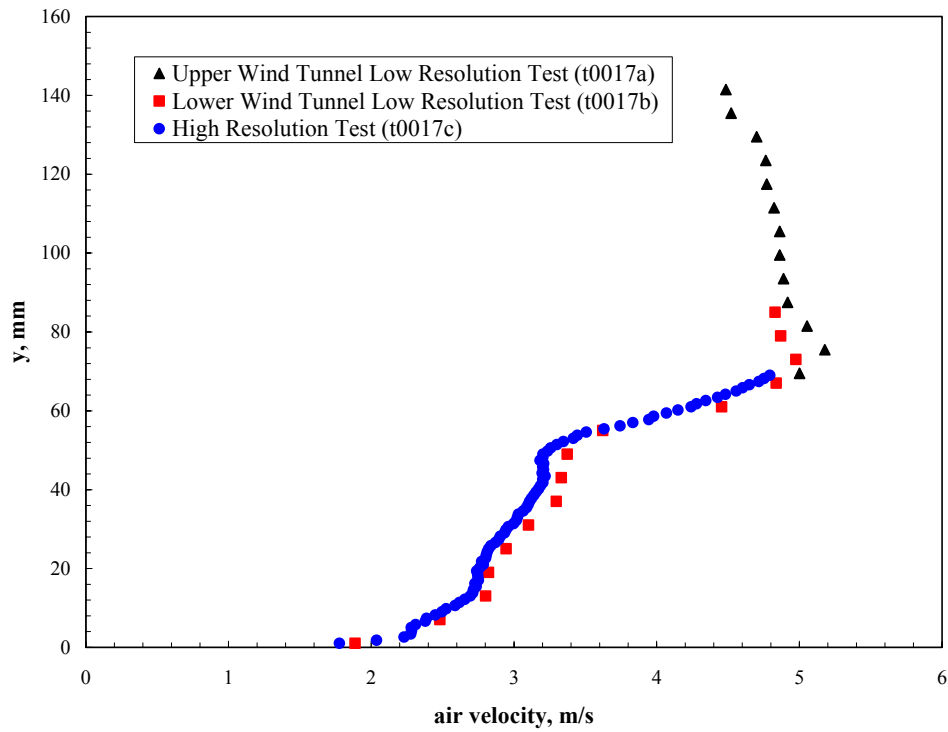
Figure 3.12 Average Velocity Profile at Center of Wind Tunnel (t0017)
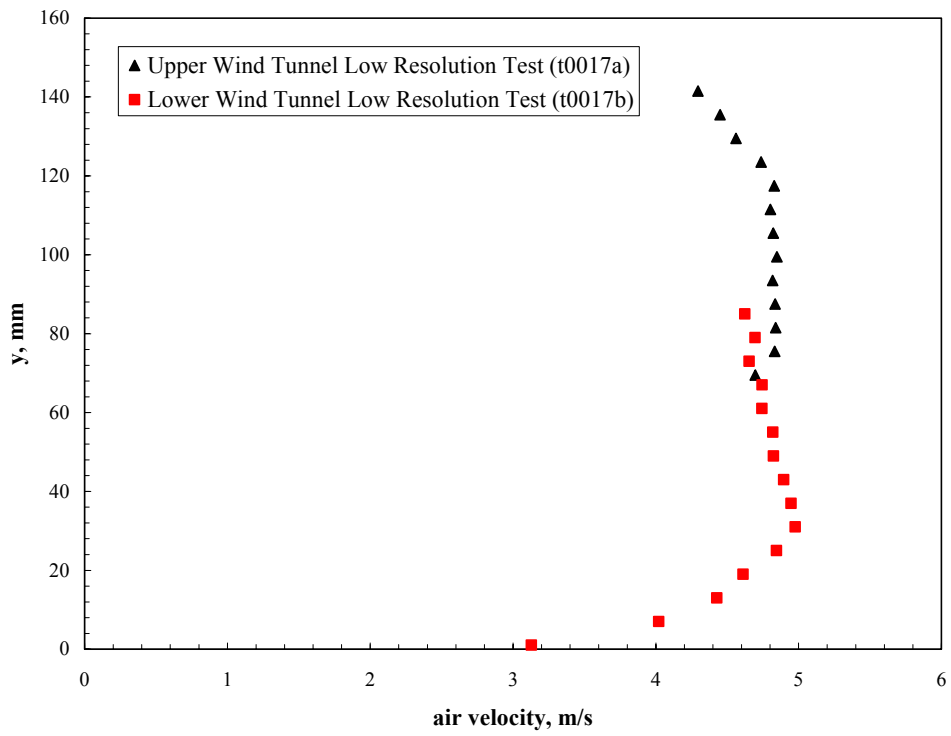
Figure 3.13 Average Velocity Profile at Right Side of Wind Tunnel (t0017)
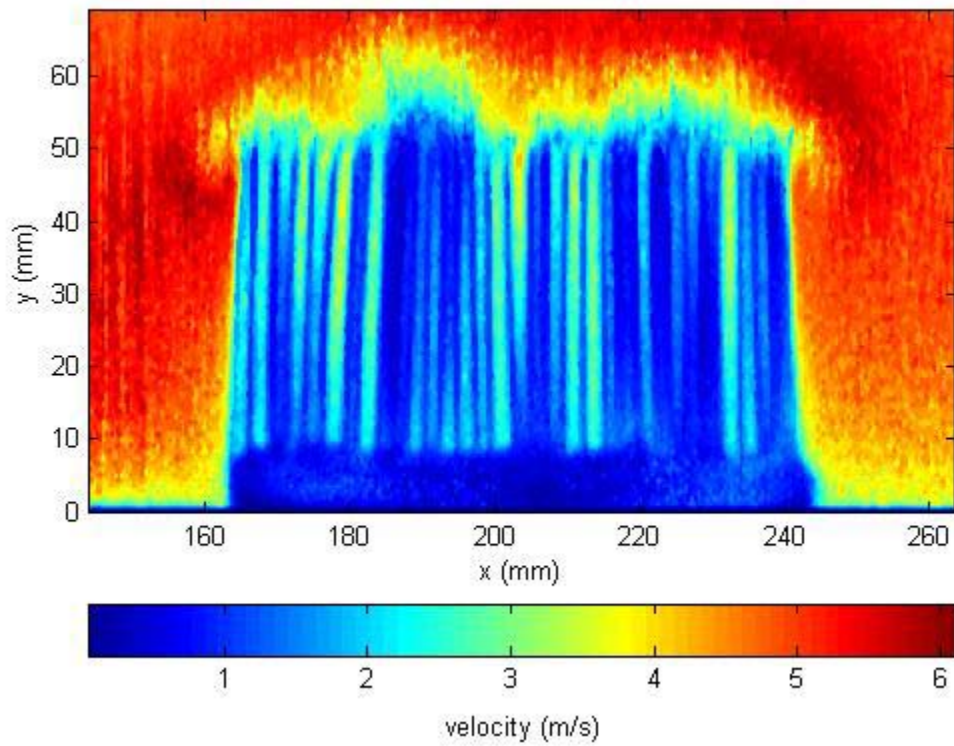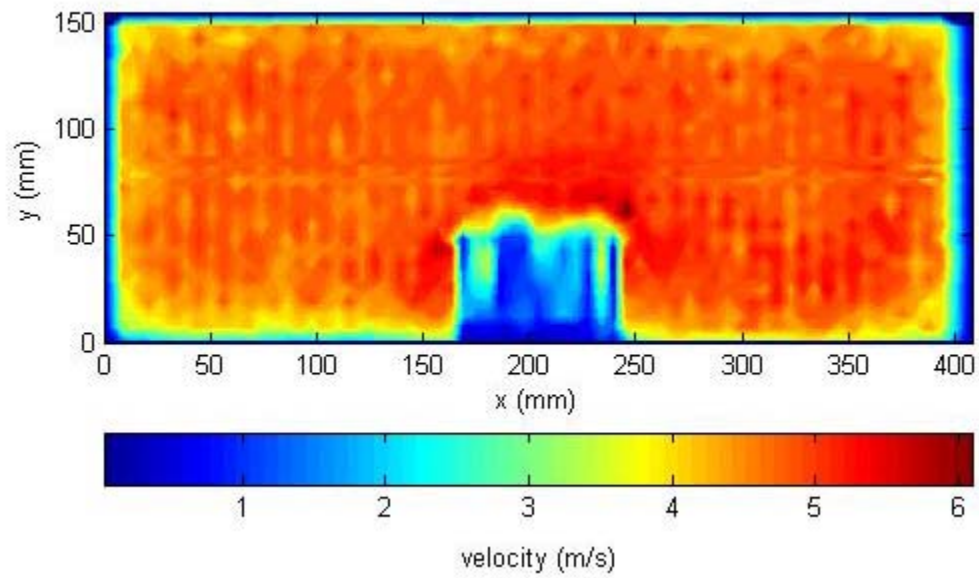
Figure 3.14 Velocity Map 2 *mm* Downstream of the Heat Sink with u$_{app}$=4.5 *m/s* (Test t0016)

44
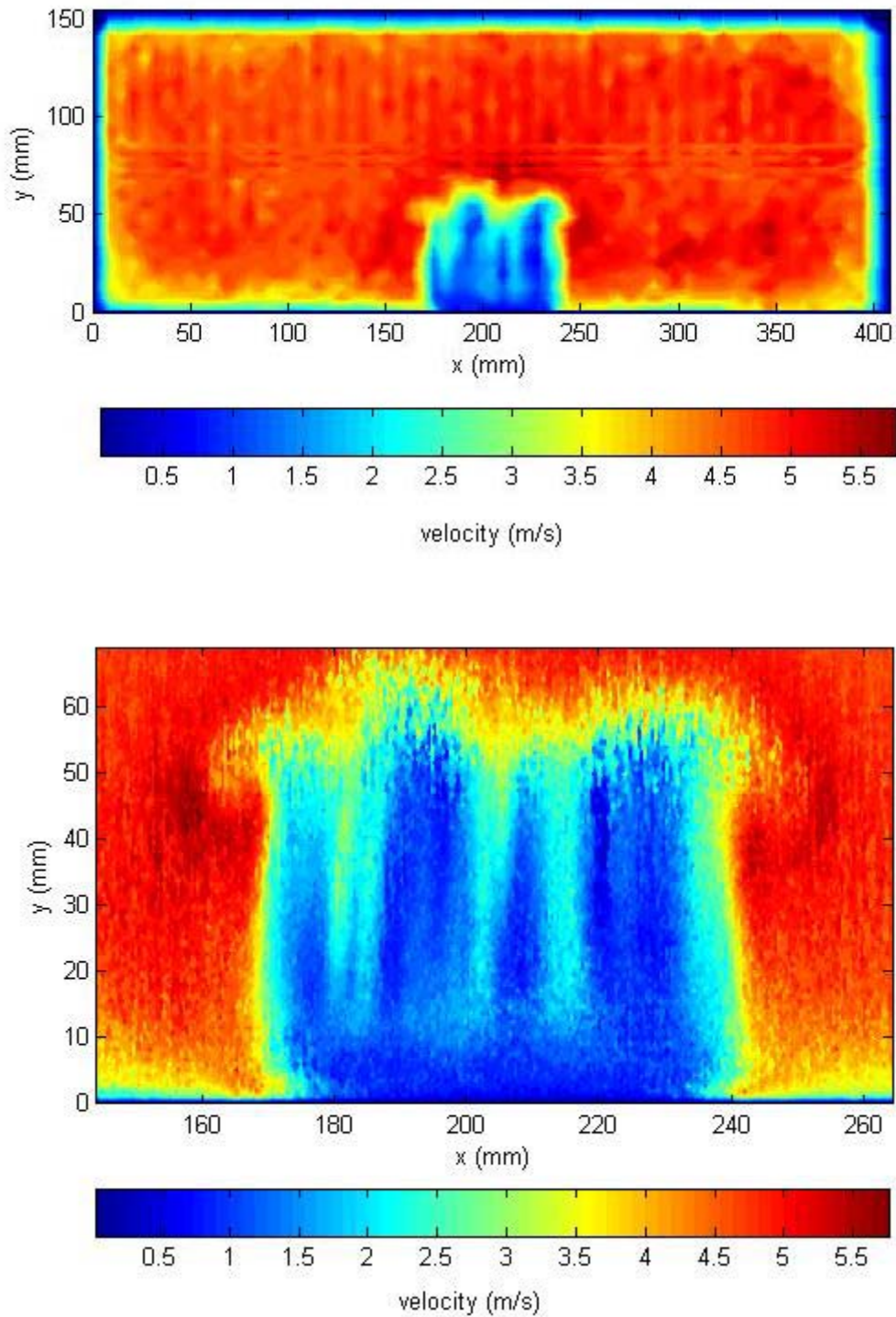
**Figure 3.15 Velocity Map 25 *mm* Downstream of the Heat Sink with u$_{app}$=4.5 *m/s*
(Test t0017)**

CHAPTER FOUR

CONCLUSION AND RECOMMENDATIONS

Three tests were performed for a single, high-density parallel plate heat sink with bypass to directly measure the flow exiting the array. Experiments were conducted using the Electronic Cooling Wind Tunnel in the Fluid Dynamics Lab at Washington State University Tri-Cities which provided for a relatively large clearance ratio ($CL \approx 15$) and low approach velocity speeds ($\leq 5\ m/sec$). Detailed velocity measurements were made with a constant temperature anemometer that utilized a miniature thermistor probe. The tests were automated employing a probe positioning *xy*-traverse with computerized control and data acquisition to provide a high resolution velocity survey of the flow exiting the array.

Two experiments were performed as parametric tests with the velocity probe location downstream of the heat sink (Δz) selected as the varying parameter. In the third test, detailed velocity measurements were performed without the heat sink in the wind tunnel. The purpose of this test was to measure the air velocity in the absence of the array and designate this velocity as the approach velocity (u_{app}) for the parametric tests.

The first test was performed with the thermistor anemometer making detailed spatial velocity measurements at a distance of $\Delta z = 2\ mm$ downstream of the heat sink. The second test was performed with the velocity probe located at a further distance of $\Delta z = 25\ mm$ downstream of the array. The contrast between the two velocity surveys was striking in that the "footprint" of the array was more defined for the test where the downstream velocity was measured closer to the heat sink ($\Delta z = 2\ mm$). This is attributed to the fact that for the case where the velocity survey was performed further downstream at $\Delta z = 25\ mm$, considerable mixing between the clearance region flow regime and the flow exiting the heat sink had occurred.

The velocity measurements from the flow surveys were further reduced by

numerically integrating the results from the parametric tests over the projected area of the array to determine the average flow velocity exiting the heat sink. To determine the approach velocity, the flow measurements made during the test performed without the heat sink were integrated over the area of the wind tunnel. The flow measurements made at the distance $\Delta z = 2\ mm$ downstream of the array provided an average velocity exiting the heat sink of $u_{end} = 1.6\ m/sec$. In contrast, the flow measurements made further downstream at a distance $\Delta z = 25\ mm$ from the downstream side of the heat sink provided an average velocity of $u_{end} = 2.6\ m/sec$, an increase of 63 % compared to the velocity measured closer to the array. This is due to the mixing of the flow from the clearance region with the flow exiting the heat sink further downstream of the array, as previously shown in the velocity surveys.

Using the approach velocity of $u_{app} = 4.5\ m/sec$ obtained from the "no array" test, the bypass ratios were calculated to be $BR = 64\ \%$ and $BR = 42\ \%$ from the $\Delta z = 2\ mm$ and $\Delta z = 25\ mm$ tests. These results were compared to the bypass model developed by Simons et al. (1997) using pressure drop measurements made for this specific heat sink as presented by Ortega Gutierrez et al. (2005). For the same approach velocity of $u_{app} = 4.5\ m/sec$ the model calculated a bypass ratio of $BR = 69\ \%$. The comparison of the bypass ratio calculated using Simons' model with the one obtained experimentally from the $\Delta z = 25\ mm$ test further demonstrates mixing of the clearance region flow regime with the flow exiting the array at this velocity measurement location. The difference in the bypass ratios of the model and the $\Delta z = 2\ mm$ test may be due to the fact that the thermistor anemometer is highly sensitive to the multi-directional flow (see Appendix A) caused by the flow separation directly downstream of the array.

Recommendations for Future Research

It is recommended that more discrete spatial velocity measurements be conducted

at the same flow conditions and using the same experimental arrangement presented here but for several Δz locations varied between $\Delta z = 2\ mm$ and $\Delta z = 25\ mm$. This may allow for a point (Δz) to be determined at which the effects of separation near the downstream face of the array and flow mixing of the clearance region and heat sink regimes further downstream are minimized.

BIBLIOGRAPHY

Coleman, H. W. and Steele, W. G., **Experimentation and Uncertainty Analysis for Engineers**, Second Edition, Wiley-Interscience Publication, 1999.

Culham, J. R. and Muzychka, Y. S., "Optimization of Plate Fin Heat Sinks Using Entropy Generation Minimization," *IEEE Trans. Components and Packaging Technologies*, Vol. 24, No. 2, pgs 159-165, 2001.

Dogruoz, M. B., Ortega, A., and Westphal, R. V., "A Model for Flow Bypass and Tip Leakage in Pin Fin Heat Sinks," *Journal of Electronic Packaging*, Vol. 128, Issue 1, pgs 53-60, March 2006.

Kays, W. M., and London, A. L., **Compact Heat Exchangers**, Third Edition, Krieger Publishing Company, Florida, 1984.

Lee, S., "Optimum Design and Selection of Heat Sinks," *11th IEEE SEMI-THERM Symposium*, pgs. 48-54, 1995.

Muzychka, Y. S. and Yovanovich, M. M., "Modeling Friction Factors in Non-Circular Ducts for Developing Laminar Flow," AIAA 98-2492, *2nd AIAA Theoretical Fluid Mechanics Meeting*, Albuquerque, N.M., 1998.

Ortega, A., Urdaneta, M., and Westphal, R. V., "Experiments and Modeling of the Hydraulic Resistance of In-Line Square Pin Fin Heat Sinks with Top By-Pass Flow," IPACK2003-35268, *2003 International Electronic Packaging Technical Conference and Exhibition*, Maui, Hawaii, July 2003.

Ortega Gutierrez, F. E., Ortega, A., Xu, G.., "Experiments on the Flow and Heat Transfer in Fine Pitch Parallel Plate Heat Sinks with Side Inlet Side Exit Flow," IPACK2005-73228, *2005 International Electronic Packaging Technical Conference and Exhibition*, San Francisco, Ca, July 2005.

Simons, R. E. and Schmidt, R. R., "A Simple Method to Estimate Heat Sink Air Flow Bypass," *Electronics Cooling*, Vol. 3, No. 2, pgs 36-37, 1997.

Simons, R. E., "Estimating the Effect of Flow Bypass On Parallel Plate-Fin Heat Sink Performance," *Electronics Cooling*, Vol. 10, No. 1, pg 6, 2004.

Wirtz, R. A., Chen, W. and Zhou, R., "Effect of Flow Bypass on the Performance of Longitudinal Fin Heat Sinks," *ASME Journal of Electronic Packaging*, Vol. 116, No. 3, pgs 206-211, 1994.

APPENDIX

APPENDIX A

THERMISTOR VELOCITY PROBE DESCRIPTION

The thermistor anemometer was developed by Mr. Donald R. Frame at Washington State University Tri-Cities for this research. A detailed circuit diagram of the velocity anemometer, referred to as a thermistor velocity probe henceforward, is provided in figure A.1. The basic operation of the thermistor velocity probe is that the thermistor is heated electrically while placed in the flow stream. The convective heat transfer rate from the thermistor is given by:

$$Q_{therm} = h_{therm}\left(T_{therm} - T_\infty\right) \tag{A.1}$$

where h_{therm} is the convective heat transfer coefficient, T_{therm} is the temperature of the thermistor, and T_∞ is the free-stream temperature. The convective heat transfer rate can also be expressed in the following form:

$$Q_{therm} = i^2 R_{therm} \tag{A.2}$$

where i is the electrical current supplied to the thermistor and R_{therm} is resistance of the thermistor. Rearranging equation (A.1) and substituting equation (A.2) for Q_{therm}, the convective heat transfer coefficient is provided as follows:

$$h_{therm} = \frac{i^2 R_{therm}}{\left(T_{therm} - T_\infty\right)} \tag{A.3}$$

It was shown in previous calibrations that the convective heat transfer coefficient was a function of the air velocity. It also was demonstrated that the convective heat transfer coefficient and, therefore, the air velocity measurement was sensitive to flow direction. The calibration of the thermistor velocity probe is provided in Appendix B. The calibration was performed with the air flow parallel to the axis of the cylindrical-shaped thermistor probe.

It also should be noted that the thermistor velocity probe had a constant temperature arrangement. As illustrated in figure A.1, this was accomplished with a feedback control circuit varying the current so the temperature of the thermistor remained virtually constant.
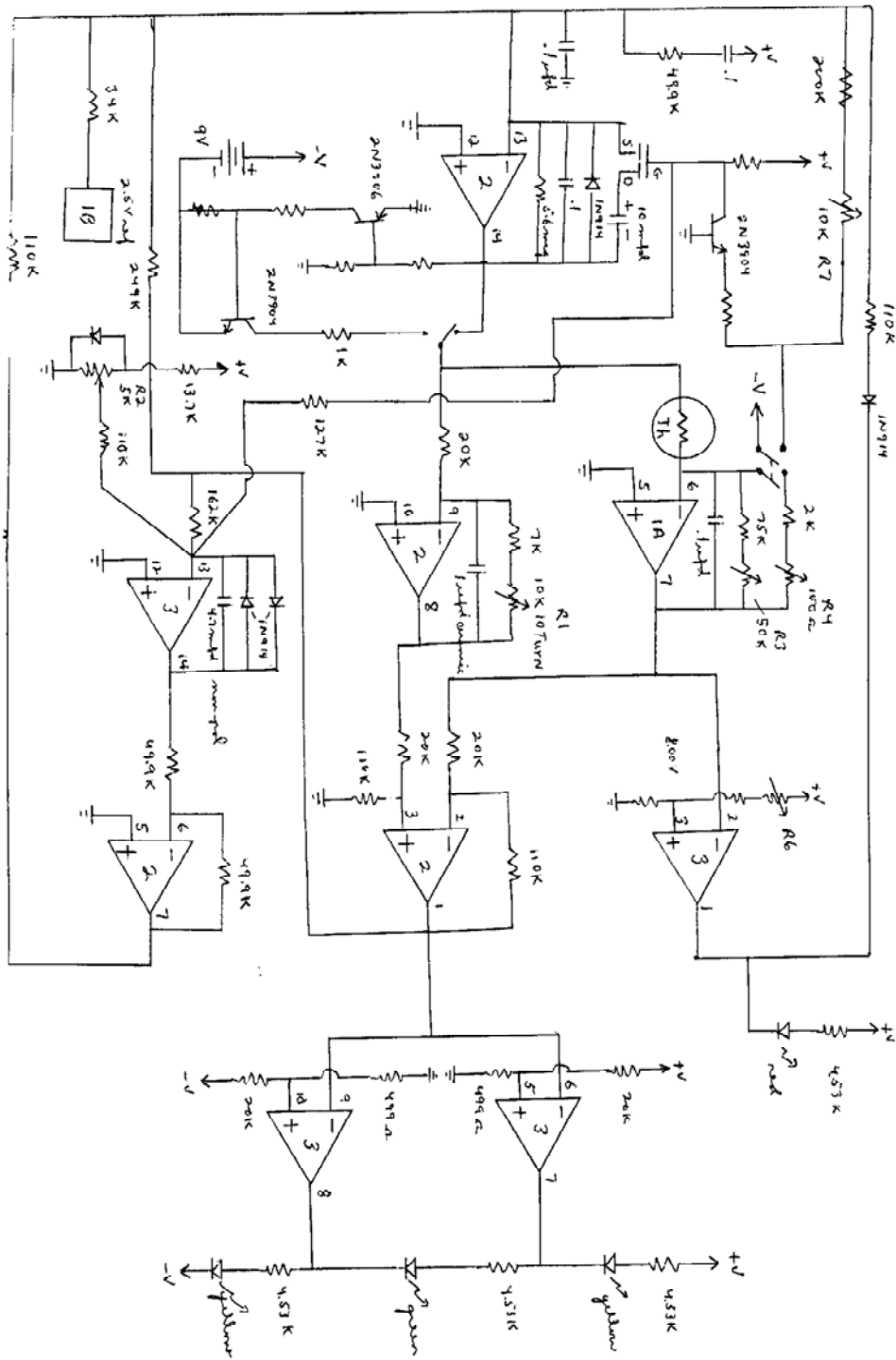
Figure A.1 Thermistor Velocity Probe Circuit Diagram[‡]

[‡]Circuit diagram of the thermistor anemometer is provided courtesy of Mr. Donald R. Frame.

APPENDIX B

INSTRUMENTATION CALIBRATION

The material presented in this appendix expounds on the material presented in Chapter Two within the Uncertainty Analysis subsection (see page 18). The calibration of the SMI SM5812 pressure sensor and the Type-K thermocouple, along with their respective uncertainty analyses, are provided in the following sections. Ultimately, these calibrations were used in the total system calibration of the thermistor velocity probe which is provided in the final subsection of this appendix.

SMI SM5812 Pressure Sensor Calibration and Uncertainty Analysis

The SMI SM5812 pressure sensor was a piezoelectric transducer, which provided a DC voltage output for a corresponding barometric pressure. The equation used to convert the output signal (V_{SMI}) to its corresponding pressure in units of *psia*, as prescribed by the manufacturer, is given by:

$$p_{SMI} = (V_{SMI} - 0.5\,VDC)\frac{15\,psia}{4\,VDC} \tag{B.1}$$

Accounting for the bias uncertainties in the SMI pressure sensor and the analog to digital conversion provided by the NI 6036E 16bit DAQ card (see table 2.1), the overall bias uncertainty contributed by the pressure data reduction is provided below:

$$B_{SMI} = \sqrt{\left(\frac{\partial p_{SMI}}{\partial V_{SMI}}(0.08\,VDC)\right)^2 + \left(\frac{\partial p_{SMI}}{\partial V_{SMI}}(0.00756\,VDC)\right)} \tag{B.2}$$

$$B_{SMI} = \sqrt{\left(\frac{15\,psia}{4\,VDC}\right)^2 \left[(0.08\,VDC)^2 + (0.00756\,VDC)^2\right]}$$

$$B_{SMI} = 0.30\,psia$$

To reduce this bias uncertainty, the SMI pressure sensor was calibrated against an

Airguide Bourdon-tube barometer. The purpose of doing so was to provide an accurate
barometric pressure measurement for the Type-K thermocouple calibration, as described
in the next subsection.

The calibration of the pressure sensor was performed concurrently with the Type-
K thermocouple calibration. The calibration was performed as an overall system
calibration for the SMI pressure sensor and NI 6036E 16-bit DAQ data acquisition chain.
The standard used for the calibration was an Airguide Bourdon-tube barometer. The SMI
pressure sensor measurements, in addition to the corresponding calibration standard
measurements, are provided in table B.1. The resulting linear regression from the
calibration data pairs is provided below:

$$p_{regress} = (8.541 \times 10^{-1})p_{new} + 2.518 \tag{B.3}$$

where p_{new} is the raw pressure measurement provided by the SMI pressure sensor and NI
6036E 16-bit DAQ data acquisition chain.

To determine the uncertainty contribution of $p_{regress}$, the method to determine the
uncertainty for a first order regression as outlined by Coleman et al. (1999) was
employed. The equation for the uncertainty of $p_{regress}$ is given by:

$$\delta p_{regress} = \left[\begin{aligned} & \sum_{i=1}^{N}\left(\frac{\partial p_{regress}}{\partial p_{standard,i}}\right)^2 P_{standard,i}^2 + \sum_{i=1}^{N}\left(\frac{\partial p_{regress}}{\partial p_{SMI,i}}\right)^2 P_{SMI,i}^2 + \ldots \\ & \ldots + \sum_{i=1}^{N}\left(\frac{\partial p_{regress}}{\partial p_{standard,i}}\right)^2 B_{standard,i}^2 + \sum_{i=1}^{N}\left(\frac{\partial p_{regress}}{\partial p_{SMI,i}}\right)^2 B_{SMI,i}^2 + \ldots \\ & \ldots + 2\sum_{i=1}^{N-1}\sum_{k=i+1}^{N}\left(\frac{\partial p_{regress}}{\partial p_{standard,i}}\right)\left(\frac{\partial p_{regress}}{\partial p_{standard,k}}\right)B_{standard,ik} + \ldots \\ & \ldots + 2\sum_{i=1}^{N-1}\sum_{k=i+1}^{N}\left(\frac{\partial p_{regress}}{\partial p_{SMI,i}}\right)\left(\frac{\partial p_{regress}}{\partial p_{SMI,k}}\right)B_{SMI,ik} + \left(\frac{\partial p_{regress}}{\partial p_{new}}\right)^2 B_{new}^2 + \ldots \\ & \ldots + \left(\frac{\partial p_{regress}}{\partial p_{new}}\right)^2 P_{new}^2 \end{aligned} \right]^{1/2} \tag{B.4}$$

where N is the number of data pairs used in the linear regression, and P and B are the
respective random and bias uncertainties. The first six terms on the RHS of equation

(B.4) account for uncertainty from the regression data pairs, while the last two terms

account for the systematic, or bias, and random uncertainty for the new pressure value

(p_{new}). Since the value for p_{new} was measured by the SMI pressure sensor and NI 6036E

16-bit DAQ data acquisition chain during testing, the bias uncertainty (B_{new}) and the

random uncertainty (P_{new}) is equal to B_{SMI} and P_{SMI}. The fifth and sixth term on the

RHS of equation (B.4) account for the correlated bias uncertainties, where B_{ik} is defined

as:

$$B_{ik} = B_i B_k \tag{B.5}$$

Since the calibration history of the Bourdon-tube barometer was unknown, the

bias uncertainty of the standard ($B_{s\tan dard}$) was assumed to be equal to $\pm\,0.1\,cmHg$

($\pm\,0.019\,psia$), which was the least scale division of the barometer. The random

uncertainty of the standard ($P_{s\tan dard}$) was assumed to be equal to $\pm\,0.05\,cmHg$

($\pm\,0.0097\,psia$), which was half of the least scale division of the Bourdon-tube

barometer. The SMI pressure sensor values provided in table B.1 were average values of

several pressure measurements (>100 measurements). Since the corresponding standard

deviations of the average barometric pressure measurements were small (to the third

decimal point), the manufacturer's precision and hysteresis uncertainties were used to

determine the random uncertainty. Accounting for the random uncertainties in the

pressure measurement, as provided in table 2.1, the overall random uncertainty of the

SMI pressure sensor measurement is given by:

$$P_{SMI} = \sqrt{\left(\frac{\partial p_{SMI}}{\partial V_{SMI}}(0.02\,VDC)\right)^2 + \left(\frac{\partial p_{SMI}}{\partial V_{SMI}}(0.004\,VDC)\right)} \tag{B.6}$$

$$P_{SMI} = \sqrt{\left(\frac{15\,psia}{4\,Vdc}\right)^2 \left[(0.02\,VDC)^2 + (0.004\,VDC)^2\right]}$$

$$P_{SMI} = 0.076\,psia$$

These bias and random uncertainties for the standard and the SMI pressure sensor are

provided in table B.1.

The uncertainty associated with the SMI pressure sensor calibration curve was obtained from equation (B.4), in addition to the information provide in table B.1 and is shown as a function of the raw pressure measurement in figure B.1. The second order polynomial:

$$\delta p_{regress} = (1.177)p_{new}^{2} - (3.399 \times 10^{1})p_{new} + (245.466) \tag{B.7}$$

was fit to the uncertainty results and used to express the calibrated pressure uncertainty as a function of the raw pressure measurement.

For a raw pressure measurement of $p_{new} = 14.31\ psia$, the corresponding calibrated pressure measurement as calculated by equation (B.3) is $p_{regress} = 14.74\ psia$. The uncertainty of the calibrated result as calculated by equation (B.7) is $\delta p_{regress} = \pm 0.091 psia$ which is considerably less than the $0.30\ psia$ bias in the raw pressure measurement previously mentioned.

The calibrated regression as calculated by equation (B.3) along with the corresponding uncertainty from equation (B.7), is presented in figure B.2 along with the individual pressure measurements provided in table B.1. Equations (B.3) and (B.7) are accurate for raw barometric pressure measurements (p_{new}) in the range of 14.31 $psia$ to 14.47 $psia$. The uncertainty band encompasses the measured data points with substantial margin.

Type-K Thermocouple Calibration and Uncertainty Analysis

As previously mentioned in Chapter Two, the Type-K thermocouple was used to measure the ambient temperature during the tests. This ambient temperature measurement was used to calculate both the Pitot-tube and thermistor probe velocity measurements. However, the thermistor probe velocity measurements were particularly sensitive to the temperature measurements. Therefore the Type-K thermocouple was calibrated to eliminate or further reduce the $\pm 1.0\,^{\circ}C$ bias of the thermocouple as prescribed by the manufacturer (see table 2.1).

To calibrate the Type-K thermocouple, temperature measurements were made at two known standards-an ice bath and a boiling water bath-at atmospheric conditions. The ice bath calibration was conducted using a mixture of distilled water and ice cubes of distilled water. This mixture was kept insulated by means of a Styrofoam cup and lid with a hole punched into the lid to allow for the thermocouple to be inserted into the ice water mixture. The ice bath standard was presumed to be at $0.0\,^{\circ}C$. A random uncertainty of $\pm\,0.1\,^{\circ}C$ was assumed for spatial temperature differences in the ice bath calibrations. The boiling water bath was conducted with distilled water kept at boiling conditions with an electric hot plate. To determine the temperature of the standard, the calibrated SMI pressure sensor measurements were used in conjunction with the ASME Steam Tables for water at saturated conditions. A random uncertainty of $\pm\,0.2\,^{\circ}C$ was assumed for spatial temperature differences in the boiling water bath. The uncertainty contribution of the analog to digital conversion provided by the NI 6036E 16-bit DAQ was neglected for the Type-K thermocouple calibrations since this was deemed to be minute compared to other uncertainties in the measurements.

The calibration was performed as an overall system calibration for the Type-K thermocouple and NI 6036E 16-bit DAQ data acquisition chain. The thermocouple measurements, along with the corresponding calibration standard measurements are provided in table B.2. The resulting linear regression from the calibration data pairs is provided below:

$$T_{regress} = \left(9.855\times10^{-1}\right)T_{new} + 3.957\times10^{-2} \tag{B.8}$$

where T_{new} is the raw temperature measurement provided by the Type-K thermocouple and NI 6036E 16-bit DAQ data acquisition chain.

To determine the uncertainty contribution of $T_{regress}$, the same method used to determine the uncertainty for $p_{regress}$ in equation (B.4) was employed. The uncertainty for the first order temperature regression as presented by equation (B.8) is as follows:

$$\delta T_{regress} = \left| \begin{array}{l} \sum\limits_{i=1}^{N}\left(\dfrac{\partial T_{regress}}{\partial T_{s\tan dard,i}}\right)^2 P_{s\tan dard,i}^2 + \sum\limits_{i=1}^{N}\left(\dfrac{\partial T_{regress}}{\partial T_{TC,i}}\right)^2 P_{TC,i}^2 + \ldots \\[2ex] \ldots + \sum\limits_{i=1}^{N}\left(\dfrac{\partial T_{regress}}{\partial T_{s\tan dard,i}}\right)^2 B_{s\tan dard,i}^2 + \sum\limits_{i=1}^{N}\left(\dfrac{\partial T_{regress}}{\partial T_{TC,i}}\right)^2 B_{TC,i}^2 + \ldots \\[2ex] \ldots + 2\sum\limits_{i=1}^{N-1}\sum\limits_{k=i+1}^{N}\left(\dfrac{\partial T_{regress}}{\partial T_{s\tan dard,i}}\right)\left(\dfrac{\partial T_{regress}}{\partial T_{s\tan dard,k}}\right) B_{s\tan dard,ik} + \ldots \\[2ex] \ldots + 2\sum\limits_{i=1}^{N-1}\sum\limits_{k=i+1}^{N}\left(\dfrac{\partial T_{regress}}{\partial T_{TC,i}}\right)\left(\dfrac{\partial T_{regress}}{\partial T_{TC,k}}\right) B_{TC,ik} + \left(\dfrac{\partial T_{regress}}{\partial T_{new}}\right)^2 B_{new}^2 + \ldots \\[2ex] \ldots + \left(\dfrac{\partial T_{regress}}{\partial T_{new}}\right)^2 P_{new}^2 \end{array} \right.$$

(B.9)

where N is the number of data pairs used in the linear regression, and P and B are the random and bias uncertainties. The first six terms on the RHS of equation (B.9) account for uncertainty from the regression data pairs, while the last two terms account for the systematic, or bias, and random uncertainty for the new temperature value (T_{new}), which is measured during an actual test. Since the value for T_{new} was measured by the Type-K thermocouple and NI 6036E 16-bit DAQ data acquisition chain during testing, the bias uncertainty B_{new} and the random uncertainty P_{new} is equal to B_{TC} and P_{TC}. The fifth and sixth term on the RHS of equation (B.9) account for the correlated bias uncertainties, where B_{ik} is defined in equation (B.5) from the previous subsection.

For the ice bath calibration, the bias uncertainty of the standard ($B_{s\tan dard}$) was assumed to be negligible compared to other uncertainties in the regression provided in equation (B.9). Therefore, it was set equal to zero. The bias uncertainty of the standard for the boiling water bath was determined from the bias uncertainty of the pressure measurement used to determine the temperature at saturated conditions. The following second order polynomial was developed from the ASME Steam Tables to determine temperature at saturated conditions from barometric pressure measurements:

$$T_{s\tan dard} = \left(-5.436 \times 10^{-2}\right) p_{regress}^2 + 3.509\, p_{regress} + 60.178$$

(B.10)

where $p_{regress}$ is obtained from equation (B.3). To determine the bias uncertainty of the

standard for the boiling water bath calibrations the following equation was used:

$$B_{s\tan dard} = \sqrt{\left(\frac{\partial T_{s\tan dard}}{\partial p_{regress}}\delta p_{regress}\right)^2} \qquad (B.11)$$

$$B_{s\tan dard} = \sqrt{\left(-\left(1.279\times10^{-1}\right)p_{regress}^3 + \left(7.825\right)p_{regress}^2 - \left(145.946\right)p_{regress} + 861.109\right)^2}$$

where $\delta p_{regress}$ is determined from equation (B.7). The random uncertainty for the ice bath and the boiling water bath calibrations were determined to be $P_{s\tan dard} = 0.1\,^\circ C$ and $P_{s\tan dard} = 0.2\,^\circ C$. As previously mentioned, this was due to spatial temperature variations in the water mixture of the baths. The bias uncertainty of the Type-K thermocouple, as obtained from table 2.1, was $B_{TC} = 1.0\,^\circ C$. The individual thermocouple temperature measurements were average values of several temperature measurements made for a single temperature. The random uncertainty of the individual thermocouple temperature measurements (P_{TC}) was determined to be the standard deviation of the average temperature measurements multiplied by the *Student's t* distribution. These uncertainty values, along with the calibration data sets, are provided in table B.2. Since the thermocouple measurements from the test will be used to determine the calibrated temperature as shown in equation (B.8) the random and bias uncertainties P_{new} and B_{new} are equal to the corresponding random and bias uncertainties of the thermocouple.

The uncertainty associated with the Type-K thermocouple calibration curve was obtained from equation (B.9), along with the information provided in table B.2, and is shown as a function of the raw thermocouple temperature measurement in figure B.3. The third order polynomial:

$$\delta T_{regress} = \left[\begin{array}{l}\left(-1.257\times10^{-7}\right)T_{new}^3 + \left(3.936\times10^{-5}\right)T_{new}^2 - \left(2.929\times10^{-4}\right)T_{new} + ...\\ ... + 3.113\times10^{-1}\end{array}\right] \qquad (B.12)$$

was fit to the uncertainty results and used to express the calibrated thermocouple uncertainty as a function of the raw temperature measurement.

For a raw thermocouple temperature measurement of $T_{new} = 22.5\,°C$, the corresponding calibrated temperature value, as calculated by equation (B.8), is $T_{regress} = 22.14\,°C$. The uncertainty of the calibrated result, as calculated by equation (B.12), is $\delta T_{regress} = \pm\, 0.32\,°C$, which is considerably less than the $1.0\,°C$ bias in the raw temperature measurement previously mentioned at the beginning of this subsection.

The calibrated regression, as calculated by equation (B.8), along with the corresponding uncertainty from equation (B.12), is presented in figure B.4a and figure B.4b. Also included in these figures are the individual temperature measurements as provided in table B.2. Equations (B.8) and (B.12) are accurate for raw thermocouple temperature measurements (T_{new}) in the range of $0\,°C$ to $100\,°C$. The uncertainty band encompasses the measured data points with considerable margin.

Thermistor Velocity Probe Calibration and Uncertainty Analysis

The thermistor velocity probe was calibrated against the Pitot-tube in the wind tunnel utilizing the same instrumentation as that which was used during the actual experiments to provide a whole system calibration. During the calibration the Pitot-tube and the thermistor velocity probe were inserted into the instrumentation access slot of the wind tunnel, located between the test section and the exit plenum. They were placed in close proximity to each other to ensure both instruments were measuring the same velocity.

The basic mechanism of velocity measurement provided by the thermistor probe was by means of convective heat transfer. During previous flow calibrations of the thermistor velocity probe, it was shown the convective heat transfer coefficient was proportionate to the velocity. The measured quantities to determine the convective heat transfer coefficient included the heat dissipated by the probe (Q_{therm}), the temperature of the probe (T_{therm}), and the ambient temperature measured by the calibrated Type-K thermocouple (T_{∞}):

$$h_{therm} = \frac{Q_{therm}}{T_{therm} - T_\infty} \tag{B.13}$$

The dissipation is calculated by the following equation:

$$Q_{therm} = i^2 R \tag{B.14}$$

where i is the current supplied to the thermistor and R is the thermistor resistance. As shown in the circuit diagram of the thermistor velocity probe provided in Appendix A, i and R can be determined from the probe voltage outputs V_i and V_{therm} as follows:

$$i = \frac{V_i}{2 k\Omega} \tag{B.15}$$

and

$$R = \frac{V_{therm}\left(1000 \dfrac{\Omega}{k\Omega}\right)}{i} \tag{B.16}$$

$$R = \frac{V_{therm}(2000\ \Omega)}{V_i}$$

substituting equations (B.15) and (B.16) into equation (B.14) provides the following:

$$Q_{therm} = V_i V_{therm}\left(\frac{1}{2}\frac{mW}{VDC^2}\right) \tag{B.17}$$

The thermistor temperature T_{therm} was determined using the thermistor resistance provided by equation (B.16), along with the following correlation:

$$T_{therm} = \begin{bmatrix} (2.956 \times 10^{-23})R^6 - (1.847 \times 10^{-18})R^5 + \ldots \\ \ldots + (4.761 \times 10^{-14})R^4 - (6.582 \times 10^{-10})R^3 + \ldots \\ \ldots + (5.356 \times 10^{-6})R^2 - (2.778 \times 10^{-2})R + (1.044 \times 10^2) \end{bmatrix} \tag{B.18}$$

The thermistor used in the velocity probe was a BetaTHERM 10K3MCD1 micro-BetaCHIP thermistor probe. The correlation presented in equation (B.18) was developed from temperature versus resistance data provided from the micro-BetaCHIP thermistor probe specification sheets. Equation (B.18) is good for the temperature range of $15\,°C$ to $60\,°C$. The ambient temperature (T_∞), provided in equation (B.13), was determined from the calibration regression for the Type-K thermocouple, as shown in equation (B.8)

For the system calibration of the thermistor probe the Pitot-tube velocity measurements provided the calibration standard. The measured quantities for the Pitot-tube velocity measurements included the difference between the total stagnation and static pressure measured by the Pitot-tube (Δh), the barometric pressure (p_∞), and the ambient temperature. These quantities were used to calculate the air velocity as shown below:

$$u = \sqrt{\frac{2\Delta h \gamma_{water}\left(\dfrac{1\,ft^3}{1728\,in^3}\right)R_{air}\left[\left(\dfrac{9\,°F}{5\,°C}T_\infty\right)+491.67\,°F\right]\dfrac{°R}{°F}g_c}{p_\infty}} \tag{B.14}$$

where $\gamma_{water} = 62.3\,lbf/ft^3$ and $R_{air} = 53.35\,ft\cdot lbf/lbm°R$. The measurement of the pressure drop term in equation (B.14) was provided by the Setra 239 differential pressure transducer. To determine this value from the measured results the following data reduction equation was used:

$$\Delta h = \left(V_{setra}-V_0\right)\left(\frac{0.5''\,water}{5\,VDC-V_0}\right) \tag{B.15}$$

where V_{setra} and V_0 are the voltage output signal and the zero voltage reading from the Setra 239 differential transducer. Subsituting equation (B.15) for (Δh) and further reducing equation (B.14) provides the following equation:

$$u = \sqrt{\frac{\left(V_{setra}-V_0\right)\left(T_\infty+273.15\,°C\right)\dfrac{K}{°C}}{\left(5\,VDC-V_0\right)p_\infty}}\left(3.215\,\frac{m\sqrt{psia}}{sec\,\sqrt{K}}\right) \tag{B.16}$$

The Setra 239 differential transducer voltage outputs used in equation (B.16) are raw data signals. The ambient temperature was measured by the calibrated Type-K thermocouple. T_∞ in equation (B.16) was determined by the calibration regression of equation (B.8). Also, the ambient pressure was measured by the calibrated SMI pressure sensor; therefore, p_∞ in equation (B.16) was calculated using the calibration regression presented in equation (B.3).

As previously mentioned, the calibration was performed as an overall system calibration for the thermistor velocity probe against the Pitot-tube velocity measurements within the wind tunnel. The resulting regression from the calibration data pairs is provided below:

$$u_{regress} = \left[8.810 h_{new} - 7.905\sqrt{h_{new}} + 1.247\right]^2 \tag{B.17}$$

where h_{new} is the calculated convective heat transfer coefficient of the velocity probe, as provided by equation (B.13). To determine the uncertainty contribution of $u_{regress}$, the same method used to determine the uncertainty for $p_{regress}$ in equation (B.4) was employed. The uncertainty for the velocity probe calibration regression as presented by equation (B.17) is as follows:

$$
\delta u_{regress} = \left|
\begin{aligned}
& \sum_{i=1}^{N}\left(\frac{\partial u_{regress}}{\partial V_{setra,i}}\right)^2 P_{setra,i}^2 + \sum_{i=1}^{N}\left(\frac{\partial u_{regress}}{\partial V_{0,i}}\right)^2 P_{0,i}^2 + \sum_{i=1}^{N}\left(\frac{\partial u_{regress}}{\partial T_{\infty,i}}\right)^2 P_{T_{\infty},i}^2 \\
& + \sum_{i=1}^{N}\left(\frac{\partial u_{regress}}{\partial T_{therm,i}}\right)^2 P_{therm,i}^2 + \sum_{i=1}^{N}\left(\frac{\partial u_{regress}}{\partial p_{\infty,i}}\right)^2 P_{p_\infty,i}^2 + \sum_{i=1}^{N}\left(\frac{\partial u_{regress}}{\partial V_{setra,i}}\right)^2 B_{setra,i}^2 \\
& + 2\sum_{i=1}^{N-1}\sum_{k=i+1}^{N}\left(\frac{\partial u_{regress}}{\partial V_{setra,i}}\right)\left(\frac{\partial u_{regress}}{\partial V_{setra,k}}\right)B_{setra,ik} + \sum_{i=1}^{N}\left(\frac{\partial u_{regress}}{\partial V_{0,i}}\right)^2 B_{0,i}^2 \\
& + 2\sum_{i=1}^{N-1}\sum_{k=i+1}^{N}\left(\frac{\partial u_{regress}}{\partial V_{0,i}}\right)\left(\frac{\partial u_{regress}}{\partial V_{0,k}}\right)B_{0,ik} + \sum_{i=1}^{N}\left(\frac{\partial u_{regress}}{\partial T_{\infty,i}}\right)^2 B_{T_{\infty},i}^2 \\
& + 2\sum_{i=1}^{N-1}\sum_{k=i+1}^{N}\left(\frac{\partial u_{regress}}{\partial T_{\infty,i}}\right)\left(\frac{\partial u_{regress}}{\partial T_{\infty,k}}\right)B_{T_{\infty},ik} + \sum_{i=1}^{N}\left(\frac{\partial u_{regress}}{\partial T_{therm,i}}\right)^2 B_{therm,i}^2 \\
& + 2\sum_{i=1}^{N-1}\sum_{k=i+1}^{N}\left(\frac{\partial u_{regress}}{\partial T_{therm,i}}\right)\left(\frac{\partial u_{regress}}{\partial T_{therm,k}}\right)B_{therm,ik} + \sum_{i=1}^{N}\left(\frac{\partial u_{regress}}{\partial p_{\infty,i}}\right)^2 B_{p_\infty,i}^2 \\
& + 2\sum_{i=1}^{N-1}\sum_{k=i+1}^{N}\left(\frac{\partial u_{regress}}{\partial p_{\infty,i}}\right)\left(\frac{\partial u_{regress}}{\partial p_{\infty,k}}\right)B_{p_\infty,ik} + \left(\frac{\partial u_{regress}}{\partial T_{\infty,new}}\right)^2 P_{T_{\infty,new}}^2 \\
& + \left(\frac{\partial u_{regress}}{\partial T_{\infty,new}}\right)^2 B_{T_{\infty,new}}^2 + 2\sum_{k=i+1}^{N}\left(\frac{\partial u_{regress}}{\partial T_{\infty,i}}\right)\left(\frac{\partial u_{regress}}{\partial T_{\infty,new}}\right)B_{T_{\infty},inew} \\
& + \left(\frac{\partial u_{regress}}{\partial T_{therm,new}}\right)^2 B_{therm,new}^2 + 2\sum_{k=i+1}^{N}\left(\frac{\partial u_{regress}}{\partial T_{therm,i}}\right)\left(\frac{\partial u_{regress}}{\partial T_{therm,new}}\right)B_{therm,inew} \\
& + \left(\frac{\partial u_{regress}}{\partial T_{therm,new}}\right)^2 P_{therm,new}^2 + 2\sum_{i=1}^{N}\sum_{k=1}^{N}\left(\frac{\partial u_{regress}}{\partial V_{setra,i}}\right)\left(\frac{\partial u_{regress}}{\partial V_{0,k}}\right)B_{setra(i)0(k)}
\end{aligned}
\right|^{1/2} \tag{B.18}
$$

where N is the number of data pairs used in the calibration regression, and P and B are the random and bias uncertainties. The first fifteen terms on the RHS of equation (B.18) account for uncertainty from the regression data pairs. The sixteenth through twenty-first terms account for the systematic and random uncertainty for the new convective heat transfer coefficient value (h_{new}) which is determined from an experimental run. The last term accounts for the correlated uncertainty of two measurements made by the same instrument.

The thermistor probe calibration data, along with their uncertainty values are presented in table B.3. The values for V_{setra} and V_0 are raw data points. However, T_∞ and p_∞ are reduced data points obtained from equations (B.8) and (B.3). The values for Q_{therm} and T_{therm} were calculated using equations (B.17) and (B.18) for measured values V_i and V_{therm}. Since several measurements were made at each velocity point, these values were averages of the measured results. Their random uncertainties were determined to be the standard deviation of the average measurement multiplied by *Student's t* distribution at 95% confidence level. The random uncertainty was not determined for the barometric pressure measurement since its standard deviation was small. Also, both the bias and random uncertainties for the heat dissipation value (Q_{therm}) were neglected since their contribution was deemed negligible to the overall uncertainty. The biased uncertainties for the ambient temperature and pressure measurements were determined from the equations (B.12) and (B.7). The bias uncertainty of the Pitot-tube pressure drop measurement was determined from the manufacturer's specifications for the Setra 239 differential pressure transducer. The bias uncertainty for the thermistor temperature also was determined from the manufacturer's specifications.

The uncertainty associated with the thermistor velocity probe calibration curve, as shown in equation (B.17), was determined by reducing equation (B.18) using the calibration information provided in table B.3. The uncertainty is shown as a function of the measured convective heat transfer coefficient in figure B.5. The sixth order

polynomial:

$$\delta u_{regress} = \begin{bmatrix} \left(-3.520 \times 10^2\right) h_{new}^6 + \left(2.469 \times 10^3\right) h_{new}^5 - \left(6.679 \times 10^3\right) h_{new}^4 \\ + \left(9.188 \times 10^3\right) h_{new}^3 - \left(6.885 \times 10^3\right) h_{new}^2 + \left(2.689 \times 10^3\right) h_{new} \\ - 429.840 \end{bmatrix} \tag{B.19}$$

was fit to the uncertainty results and used to express the calibration uncertainty of the thermistor velocity probe as a function of the convective heat transfer coefficient measurement.

For a velocity probe convective heat transfer coefficient measurement of $h_{new} = 0.96 \; mW/°C$, the corresponding calibrated velocity, as calculated by equation (B.17), is $u_{regress} = 3.84 \; m/sec$. The uncertainty of the calibrated result as calculated by equation (B.19) is $\delta u_{regress} = \pm 0.18 \; m/sec$, or 4.7 %.

The calibrated regression as calculated by equation (B.17), along with the corresponding uncertainty from equation (B.19), is presented in figure B.6 in addition to the individual calibration points as determined from table B.3. The uncertainty band encompasses most of the measured data points within a relatively tight span. Upon visual inspection of figure B.6 the uncertainty analysis is in agreement with the calibration data.

Table B.1 SMI SM5812 Pressure Sensor Calibration and Uncertainty Data

$p_{standard,i}$ (psia)	$B_{standard,i}$ (psia)	$P_{standard,i}$ (psia)	$p_{SMI,i}$ (psia)	$B_{SMI,i}$ (psia)	$P_{SMI,i}$ (psia)
14.73	0.019	0.0097	14.31	0.30	0.076
14.87	0.019	0.0097	14.47	0.30	0.076
14.87	0.019	0.0097	14.47	0.30	0.076
14.88	0.019	0.0097	14.47	0.30	0.076
14.87	0.019	0.0097	14.47	0.30	0.076
14.85	0.019	0.0097	14.44	0.30	0.076

Table B.2 Type-K Thermocouple Calibration and Uncertainty Data

$T_{standard,i}$ (°C)	$p_{regress,i}$ (psia)	$B_{standard,i}$ (°C)	$P_{standard,i}$ (°C)	$T_{TC,i}$ (°C)	$B_{TC,i}$ (°C)	$P_{TC,i}$ (°C)
0.00			0.1	-0.09	1.0	0.09
100.08	14.73	0.37	0.2	101.63	1.0	0.25
100.34	14.87	0.60	0.2	101.79	1.0	0.30
100.36	14.88	0.62	0.2	101.64	1.0	0.28
0.00			0.1	0.01	1.0	0.09

Table B.3 Thermistor Velocity Probe Calibration and Uncertainty Data

$T_{\infty,i}$ (°C)	$B_{T\infty,i}$ (°C)	$P_{T\infty,i}$ (°C)	$p_{\infty,i}$ (psia)	$B_{p\infty,i}$ (psia)	$T_{therm,i}$ (°C)	$B_{therm,i}$ (°C)	$P_{therm,i}$ (°C)	$V_{setra,i}$ (VDC)	$B_{setra,i}$ (VDC)	$P_{setra,i}$ (VDC)	$V_{0,i}$ (VDC)	$P_{0,i}$ (VDC)
22.25	0.32	0.16	14.89	0.07	60.61	0.20	0.08	0.82	0.01	0.03	0.04	0.00
22.49	0.32	0.13	14.89	0.07	60.77	0.20	0.07	0.65	0.01	0.03	0.04	0.00
22.32	0.32	0.12	14.88	0.07	60.65	0.20	0.08	0.58	0.01	0.04	0.04	0.00
22.38	0.32	0.17	14.88	0.07	60.81	0.20	0.08	0.47	0.01	0.02	0.04	0.00
22.43	0.32	0.12	14.88	0.07	60.69	0.20	0.08	0.39	0.01	0.02	0.04	0.00
22.36	0.32	0.13	14.88	0.07	60.87	0.20	0.08	0.30	0.01	0.02	0.04	0.00
22.35	0.32	0.10	14.88	0.07	60.71	0.20	0.09	0.24	0.01	0.01	0.04	0.00
22.35	0.32	0.12	14.88	0.07	60.94	0.20	0.09	0.17	0.01	0.01	0.04	0.00
22.34	0.32	0.08	14.88	0.07	60.78	0.20	0.10	0.12	0.01	0.01	0.04	0.00
22.32	0.32	0.09	14.88	0.07	61.04	0.20	0.08	0.09	0.01	0.00	0.04	0.00
22.35	0.32	0.11	14.88	0.07	60.87	0.20	0.13	0.07	0.01	0.00	0.04	0.00
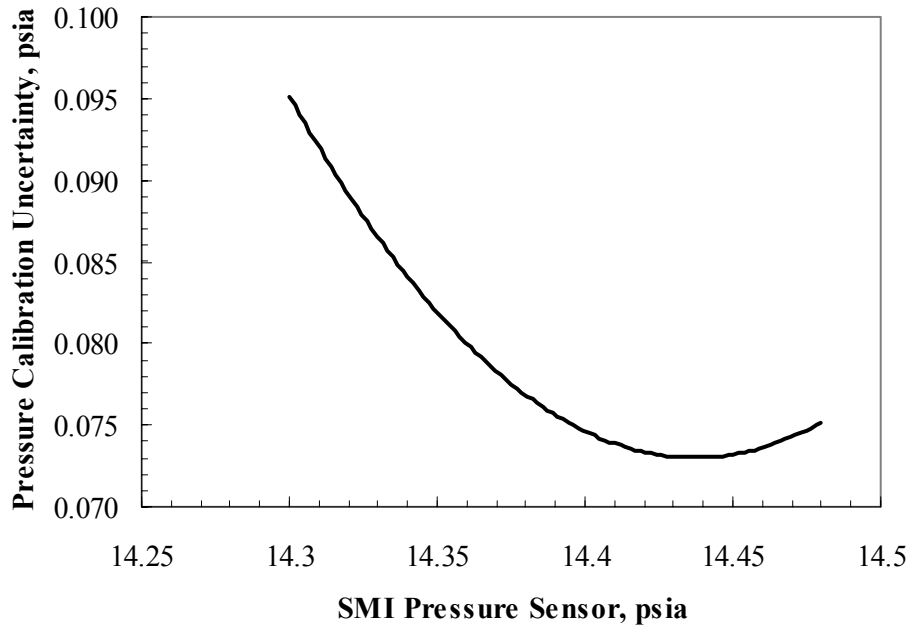
Figure B.1 SMI SM5812 Pressure Sensor Calibration Regression Uncertainty
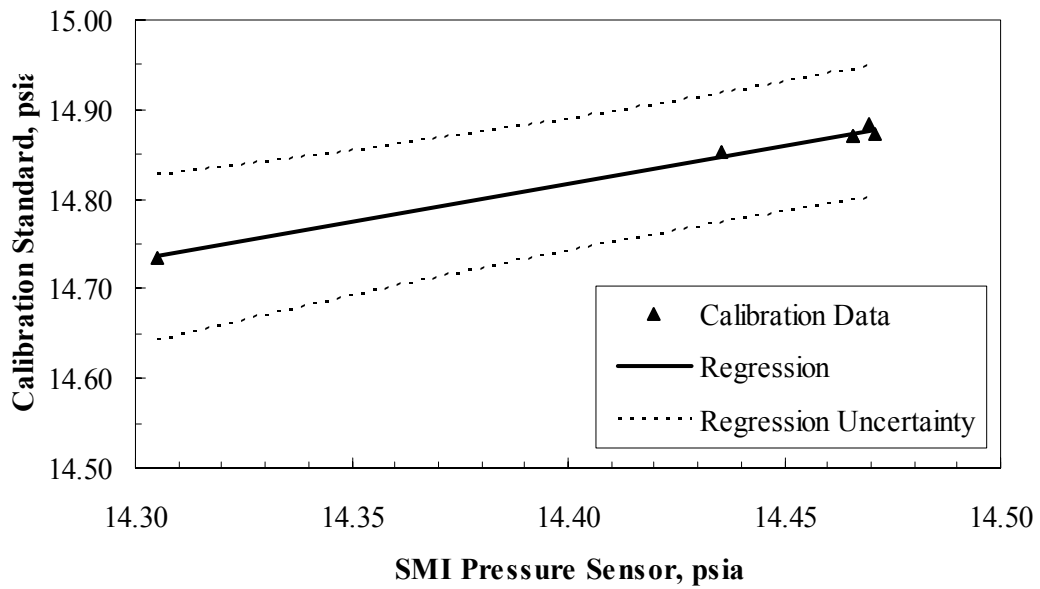
Figure B.2 SMI SM5812 Pressure Sensor Calibration Regression and Uncertainty
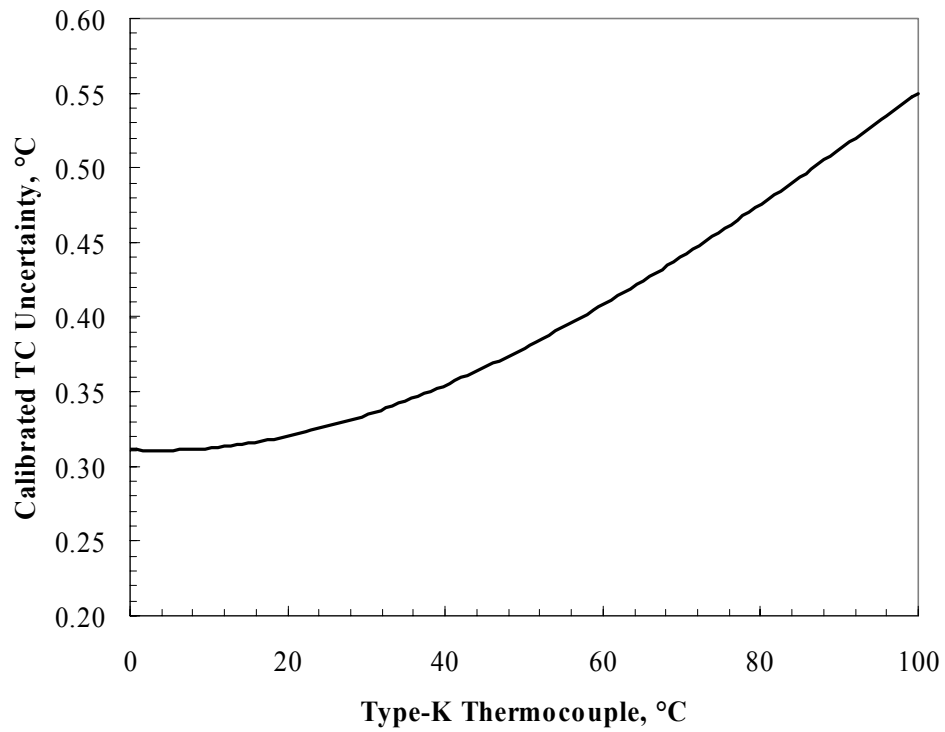
Figure B.3 Type-K Thermocouple Calibration Regression Uncertainty
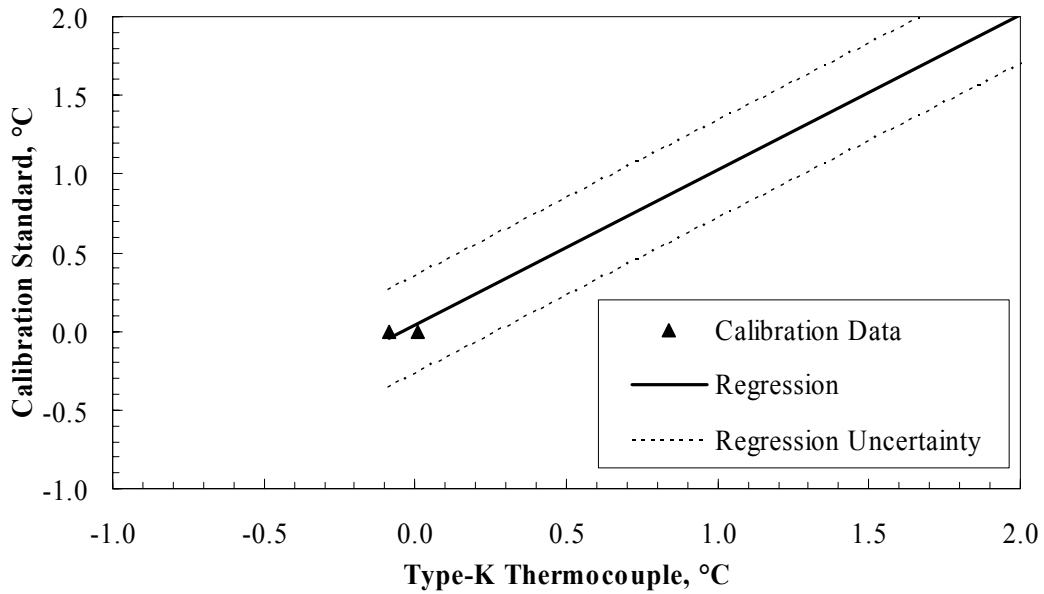
Figure B.4a Type-K Thermocouple Calibration Regression and Uncertainty
(0 °C Calibration Points)
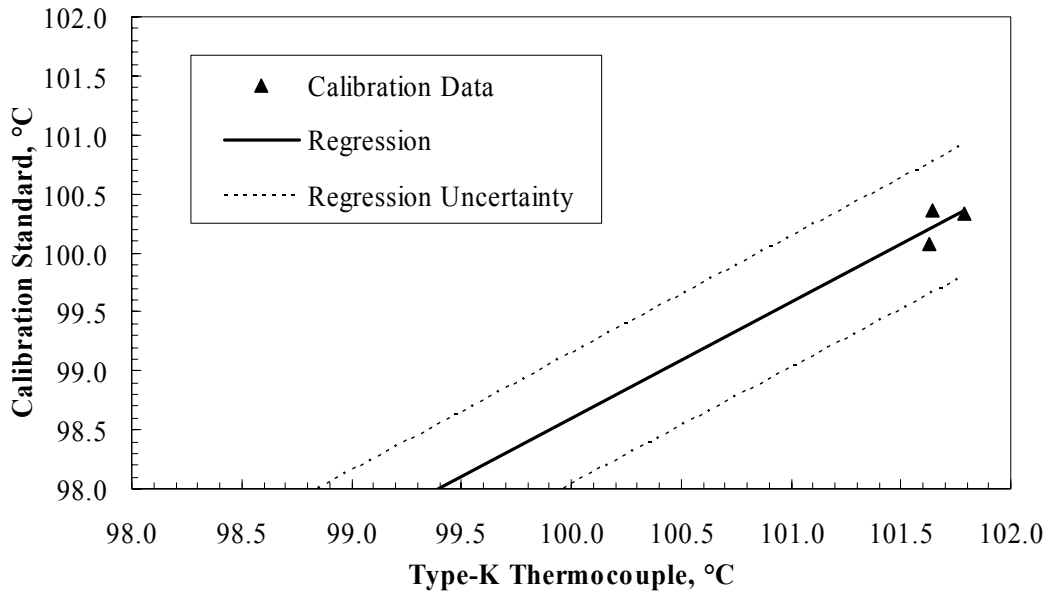
Figure B.4b Type-K Thermocouple Calibration Regression and Uncertainty (100 °C Calibration Points)
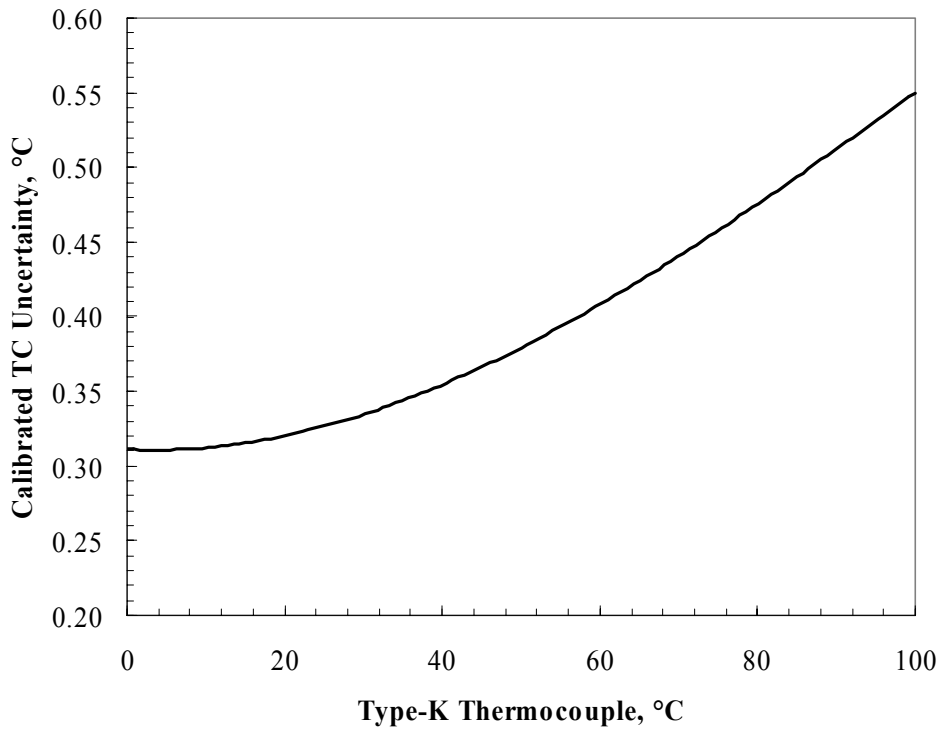
Figure B.5 Thermistor Velocity Probe Calibration Regression Uncertainty
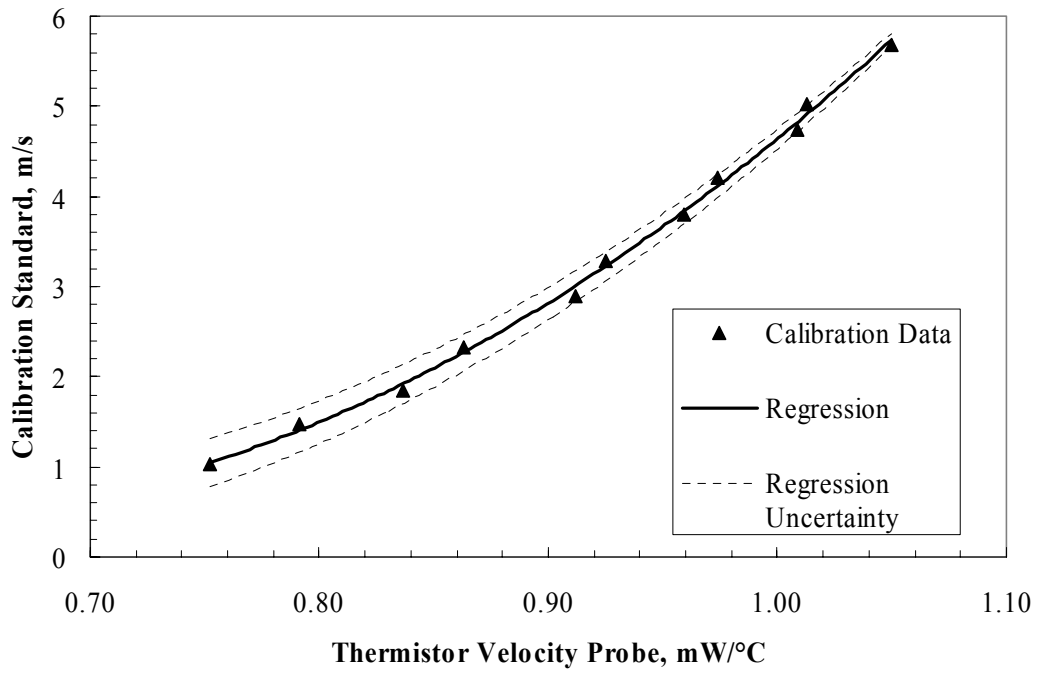
Figure B.6 Thermistor Velocity Probe Calibration Regression and Uncertainty

APPENDIX C

FORTRAN SOURCE CODE FOR DATA REDUCTION

```
*
*==============================================================================
*==============================================================================
*
*              HEAT SINK BYPASS:  DOWNSTREAM DATA REDUCTION
*
*==============================================================================
*==============================================================================
*
*PROGRAM "MAIN" DESCRIPTION ******************************************
*
*==============================================================================

        PROGRAM MAIN

*------------------------------------------------------------------------------
*DEFINE DATA TYPES AND ARRAY DIMENSIONS USED IN THE PROGRAM "MAIN":
*------------------------------------------------------------------------------

*The raw data files have the form of "tXXXXA" where "XXXX" is a unique
*test identifier for a test ran at a specific upstream velocity and
*downstream velocity probe location while "A" is a unique identifier
*for a low or high resolution test and/or wind tunnel region.

        CHARACTER*6 rawdat_uwt_fname, rawdat_lwt_fname, rawdat_hs_fname
        CHARACTER*30 datetimestamp_uwt, datetimestamp_lwt,
     &datetimestamp_hs
        INTEGER ymove_uwt, xmove_uwt, ymove_lwt, xmove_lwt, ymove_hs,
     &xmove_hs
        REAL y0_uwt, x0_uwt, y0_lwt, x0_lwt, y0_hs, x0_hs, t_therm_uwt
        REAL RHO_AIR_UWT(25000), UPT_UWT(25000)
        REAL Y_UWT(25000), X_UWT(25000), UDS_UWT(25000)
        REAL RHO_AIR_LWT(25000), UPT_LWT(25000)
        REAL Y_LWT(25000), X_LWT(25000), UDS_LWT(25000)
        REAL RHO_AIR_HS(25000), UPT_HS(25000)
        REAL Y_HS(25000), X_HS(25000), UDS_HS(25000)
        REAL t_therm_lwt, t_therm_hs
        INTEGER N_UWT, N_RHO_UWT, N_LWT, N_RHO_LWT, N_HS, N_RHO_HS
        REAL AVEUPT_UWT, STDEVUPT_UWT, AVEUPT_LWT, STDEVUPT_LWT
        REAL AVEUPT_HS, STDEVUPT_HS
        REAL AVERHO_UWT, STDEVRHO_UWT, AVERHO_LWT, STDEVRHO_LWT
        REAL AVERHO_HS, STDEVRHO_HS, X1, X2, X3, X4, X5, X6, X7
        REAL Y1, Y2, Y3, Y4, Y5, AVEUPT
        REAL XMAP_UWT(300,100),YMAP_UWT(300,100),UMAP_UWT(300,100)
        INTEGER NROWS_UWT,NCOLS_UWT
        REAL XMAP_LWT(300,100),YMAP_LWT(300,100),UMAP_LWT(300,100)
        INTEGER NROWS_LWT,NCOLS_LWT
        REAL XMAP_HS(300,100),YMAP_HS(300,100),UMAP_HS(300,100)
        INTEGER NROWS_HS,NCOLS_HS
        CHARACTER*12 FILENAME
        REAL XMAP_WT(300,100),YMAP_WT(300,100),UMAP_WT(300,100)
        REAL XMAPHS(300,100), YMAPHS(300,100), UMAPHS(300,100)
        INTEGER I,J
        REAL UINT(100), INC
*------------------------------------------------------------------------------
*READ "TEST.DAT" FILE INPUTS:
*------------------------------------------------------------------------------

        OPEN(1,FILE='TEST.DAT')
   10   FORMAT(A)

*Read the filename for the Upper Wind Tunnel (UWT) test from "TEST.DAT."
```

```
        READ(1,10) rawdat_uwt_fname

*Read the filename for the lower wind tunnel (LWT) test from "TEST.DAT."

        READ(1,10) rawdat_lwt_fname

*Read the filename for the high res Heat Sink (HS) test from "TEST.DAT."

        READ(1,10) rawdat_hs_fname

*Read the number of movements the velocity probe undergoes in the "y"
*direction for the UWT test from "TEST.DAT."

        READ(1,*) ymove_uwt
*        write(6,*) ymove_uwt
*Read the number of movements the velocity probe undergoes in the "x"
*direction for the UWT test from "TEST.DAT."

        READ(1,*) xmove_uwt
*        write(6,*) xmove_uwt
*Read the origin of the velocity probe in the "y" direction for the UWT
*test from "TEST.DAT" (in mm).

        READ(1,*) y0_uwt

*Read the origin of the velocity probe in the "x" direction for the UWT
*test from "TEST.DAT" (in mm).

        READ(1,*) x0_uwt

*Read the number of movements the velocity probe undergoes in the "y"
*direction for the LWT test from "TEST.DAT."

        READ(1,*) ymove_lwt

*Read the number of movements the velocity probe undergoes in the "x"
*direction for the LWT test from "TEST.DAT."

        READ(1,*) xmove_lwt

*Read the origin of the velocity probe in the "y" direction for the LWT
*test from "TEST.DAT" (in mm).

        READ(1,*) y0_lwt

*Read the origin of the velocity probe in the "x" direction for the LWT
*test from "TEST.DAT" (in mm).

        READ(1,*) x0_lwt

*Read the number of movements the velocity probe undergoes in the "y"
*direction for the HS test from "TEST.DAT."

        READ(1,*) ymove_hs

*Read the number of movements the velocity probe undergoes in the "x"
*direction for the HS test from "TEST.DAT."

        READ(1,*) xmove_hs

*Read the origin of the velocity probe in the "y" direction for the HS
*test from "TEST.DAT" (in mm).
```

```
        READ(1,*) y0_hs

*Read the origin of the velocity probe in the "x" direction for the HS
*test from "TEST.DAT" (in mm).

        READ(1,*) x0_hs

        READ(1,*) X1
        X2=x0_hs
        READ(1,*) X3
        READ(1,*) X4
        READ(1,*) X5
        READ(1,*) X7
        READ(1,*) Y1
        READ(1,*) Y2
        READ(1,*) Y3
        READ(1,*) Y5
        READ(1,*) AVEUPT

*Close data file "TEST.DAT."

        CLOSE(1)


*-------------------------------------------------------------------------
*CREATE DATA HISTORY FILES ("TXXXXA_HISTORY"):
*-------------------------------------------------------------------------


        CALL HISTORY(rawdat_uwt_fname,datetimestamp_uwt,xmove_uwt,
     &ymove_uwt, t_therm_uwt, RHO_AIR_UWT, y0_uwt, x0_uwt, UPT_UWT,
     &Y_UWT, X_UWT, UDS_UWT, N_UWT, N_RHO_UWT)
        CALL AVE(UPT_UWT,N_UWT,AVEUPT_UWT)
        CALL STDEV(UPT_UWT,N_UWT,AVEUPT_UWT,STDEVUPT_UWT)
        CALL AVE(RHO_AIR_UWT,N_RHO_UWT,AVERHO_UWT)
        CALL STDEV(RHO_AIR_UWT,N_RHO_UWT,AVERHO_UWT,STDEVRHO_UWT)
        CALL HISTORY(rawdat_lwt_fname,datetimestamp_lwt,xmove_lwt,
     &ymove_lwt, t_therm_lwt, RHO_AIR_LWT, y0_lwt, x0_lwt, UPT_LWT,
     &Y_LWT, X_LWT, UDS_LWT, N_LWT, N_RHO_LWT)
        CALL AVE(UPT_LWT,N_LWT,AVEUPT_LWT)
        CALL STDEV(UPT_LWT,N_LWT,AVEUPT_LWT,STDEVUPT_LWT)
        CALL AVE(RHO_AIR_LWT,N_RHO_LWT,AVERHO_LWT)
        CALL STDEV(RHO_AIR_LWT,N_RHO_LWT,AVERHO_LWT,STDEVRHO_LWT)
        CALL HISTORY(rawdat_hs_fname,datetimestamp_hs,xmove_hs,
     &ymove_hs, t_therm_hs, RHO_AIR_HS, y0_hs, x0_hs, UPT_HS,
     &Y_HS, X_HS, UDS_HS, N_HS, N_RHO_HS)
        CALL AVE(UPT_HS,N_HS,AVEUPT_HS)
        CALL STDEV(UPT_HS,N_HS,AVEUPT_HS,STDEVUPT_HS)
        CALL AVE(RHO_AIR_HS,N_RHO_HS,AVERHO_HS)
        CALL STDEV(RHO_AIR_HS,N_RHO_HS,AVERHO_HS,STDEVRHO_HS)
        CALL MAP(X_HS,Y_HS,UDS_HS,UPT_HS,AVEUPT,XMAP_HS,YMAP_HS,
     &UMAP_HS,NROWS_HS,NCOLS_HS,xmove_hs,ymove_hs)
        X6=XMAP_HS(NROWS_HS,1)
        FILENAME='UPRO_HS_HS'
        CALL AVEPROF(XMAP_HS,YMAP_HS,UMAP_HS,X2,X6,FILENAME,
     &NROWS_HS,NCOLS_HS)

*NO SLIP CONDITIONS (U=0) AT THE WIND TUNNEL FLOOR.

        OPEN(1,FILE='XMAP_HS')
        OPEN(2,FILE='YMAP_HS')
        OPEN(3,FILE='UMAP_HS')
        DO 30 I=1, NROWS_HS
          XMAPHS(I,1)=XMAP_HS(I,1)
```

```
            YMAPHS(I,1)=0
            UMAPHS(I,1)=0
            DO 20 J=1, NCOLS_HS+1
               XMAPHS(I,J+1)=XMAP_HS(I,J)
               YMAPHS(I,J+1)=YMAP_HS(I,J)
               UMAPHS(I,J+1)=UMAP_HS(I,J)
   20       CONTINUE
   40       FORMAT(100F6.1)
   50       FORMAT(100F6.1)
   60       FORMAT(100F6.3)
            WRITE(1,40)  (XMAPHS(I,J), J=1, NCOLS_HS+1)
            WRITE(2,50)  (YMAPHS(I,J), J=1, NCOLS_HS+1)
            WRITE(3,60)  (UMAPHS(I,J), J=1, NCOLS_HS+1)
   30       CONTINUE
            Y4=YMAPHS(1,NCOLS_HS+1)
            CLOSE(1)
            CLOSE(2)
            CLOSE(3)

            CALL MAP(X_UWT,Y_UWT,UDS_UWT,UPT_UWT,AVEUPT,XMAP_UWT,YMAP_UWT,
      &UMAP_UWT,NROWS_UWT,NCOLS_UWT,xmove_uwt,ymove_uwt)
            FILENAME='UPRO_UWT_LS'
            CALL AVEPROF(XMAP_UWT,YMAP_UWT,UMAP_UWT,X1,X2,FILENAME,
      &NROWS_UWT,NCOLS_UWT)
            FILENAME='UPRO_UWT_HS'
            CALL AVEPROF(XMAP_UWT,YMAP_UWT,UMAP_UWT,X2,X6,FILENAME,
      &NROWS_UWT,NCOLS_UWT)
            FILENAME='UPRO_UWT_RS'
            CALL AVEPROF(XMAP_UWT,YMAP_UWT,UMAP_UWT,X6,X7,FILENAME,
      &NROWS_UWT,NCOLS_UWT)
            CALL MAP(X_LWT,Y_LWT,UDS_LWT,UPT_LWT,AVEUPT,XMAP_LWT,YMAP_LWT,
      &UMAP_LWT,NROWS_LWT,NCOLS_LWT,xmove_lwt,ymove_lwt)
            FILENAME='UPRO_LWT_LS'
            CALL AVEPROF(XMAP_LWT,YMAP_LWT,UMAP_LWT,X1,X2,FILENAME,
      &NROWS_LWT,NCOLS_LWT)
            FILENAME='UPRO_LWT_HS'
            CALL AVEPROF(XMAP_LWT,YMAP_LWT,UMAP_LWT,X2,X6,FILENAME,
      &NROWS_LWT,NCOLS_LWT)
            FILENAME='UPRO_LWT_RS'
            CALL AVEPROF(XMAP_LWT,YMAP_LWT,UMAP_LWT,X6,X7,FILENAME,
      &NROWS_LWT,NCOLS_LWT)
            CALL WTMAP(XMAP_UWT,YMAP_UWT,UMAP_UWT,NCOLS_UWT,
      &XMAP_LWT,YMAP_LWT,UMAP_LWT,NROWS_LWT,NCOLS_LWT,XMAP_WT,YMAP_WT,
      &UMAP_WT,Y5,X7)

*FIND 'X2' AND 'X6.'  THESE POINTS ARE THE POINTS FARTHEST AWAY FROM THE
*HEATSINK IN THE X DIRECTION IN THE 'XMAPHS' ARRAY THAT MATCHES CLOSEST
*TO A 'X' POINT IN THE 'XMAP_WT' ARRAY.  THESE POINTS WILL BE USED TO
*DEFINE 'REGIONS' FOR NUMERICAL INTEGRATION OF THE VELOCITY MAP TO
*DETERMINE AVERAGE BYPASS AND HEAT SINK VELOCITY.

*FIND 'X2' FOR 'XMAP_WT.'

            I2WT=1
   70       IF(XMAP_WT(I2WT,1).LT.XMAPHS(1,1)) THEN
              I2WT=I2WT+1
              GO TO 70
            ENDIF
            X2WT=XMAP_WT(I2WT,1)
            WRITE(6,*) I2WT
            WRITE(6,*) X2WT

*FIND 'X2' FOR 'XMAPHS.'
```

```
      I2HS=1
  80  IF(XMAPHS(I2HS,1).LT.X2WT) THEN
        I2HS=I2HS+1
        GO TO 80
      ENDIF
      X2HS=XMAPHS(I2HS,1)
      WRITE(6,*) I2HS
      WRITE(6,*) X2HS


*FIND 'X3' FOR 'XMAPHS.'

      I3HS=1
  81  IF(XMAPHS(I3HS,1).LT.X3) THEN
        I3HS=I3HS+1
        GO TO 81
      ENDIF
      X3HS=XMAPHS(I3HS,1)
      WRITE(6,*) I3HS
      WRITE(6,*) X3HS

*FIND 'X4' FOR 'XMAP_HS.'

      I4HS=1
  82  IF(XMAPHS(I4HS,1).LT.X4) THEN
        I4HS=I4HS+1
        GO TO 82
      ENDIF
      I4HS=I4HS-1
      X4HS=XMAPHS(I4HS,1)
      WRITE(6,*) I4HS
      WRITE(6,*) X4HS

*FIND 'X5' FOR 'XMAP_HS.'

      I5HS=1
  83  IF(XMAPHS(I5HS,1).LT.X5) THEN
        I5HS=I5HS+1
        GO TO 83
      ENDIF
      I5HS=I5HS-1
      X5HS=XMAPHS(I5HS,1)
      WRITE(6,*) I5HS
      WRITE(6,*) X5HS

*FIND 'X6' FOR 'XMAP_WT.'

      I6WT=1
  90  IF(XMAP_WT(I6WT,1).LT.XMAPHS(NROWS_HS,1)) THEN
        I6WT=I6WT+1
        GO TO 90
      ENDIF
      I6WT=I6WT-1
      X6WT=XMAP_WT(I6WT,1)
      WRITE(6,*) I6WT
      WRITE(6,*) X6WT

*FIND 'X6' FOR 'XMAPHS.'

      I6HS=1
 100  IF(XMAPHS(I6HS,1).LT.X6WT) THEN
        I6HS=I6HS+1
```

```
            GO TO 100
         ENDIF
         I6HS=I6HS-1
         X6HS=XMAPHS(I6HS,1)
         WRITE(6,*) I6HS
         WRITE(6,*) X6HS


*FIND 'X7' FOR 'XMAPWT.'

         I7WT=NROWS_LWT+2
         X7WT=XMAP_WT(I7WT,1)
         WRITE(6,*) I7WT
         WRITE(6,*) X7WT


*FIND 'Y' VALUES SIMILARLY AS ABOVE.


*FIND 'Y2' FOR 'YMAPHS.'

         J2HS=1
  105    IF(YMAPHS(1,J2HS).LT.Y2) THEN
            J2HS=J2HS+1
            GO TO 105
         ENDIF
         Y2HS=YMAPHS(1,J2HS)
         WRITE(6,*) J2HS
         WRITE(6,*) Y2HS


*FIND 'Y3' FOR 'YMAPHS.'

         J3HS=1
  108    IF(YMAPHS(1,J3HS).LT.Y3) THEN
            J3HS=J3HS+1
            GO TO 108
         ENDIF
         Y3HS=YMAPHS(1,J3HS)
         WRITE(6,*) J3HS
         WRITE(6,*) Y3HS


*FIND 'Y4' FOR 'YMAP_WT.'

         J4WT=1
  110    IF(YMAP_WT(1,J4WT).LT.YMAPHS(1,NCOLS_HS+1)) THEN
            J4WT=J4WT+1
            GO TO 110
         ENDIF
         J4WT=J4WT-1
         Y4WT=YMAP_WT(2,J4WT)
         WRITE(6,*) J4WT
         WRITE(6,*) Y4WT


*FIND Y4 FOR 'YMAPHS.'

         J4HS=1
  120    IF(YMAPHS(1,J4HS).LT.Y4WT) THEN
            J4HS=J4HS+1
            GO TO 120
         ENDIF
         J4HS=J4HS-1
         Y4HS=YMAPHS(2,J4HS)
         WRITE(6,*) J4HS
         WRITE(6,*) Y4HS


*FIND 'Y5' FOR 'YMAP_WT.'
```

```
        J5WT=NCOLS_LWT+NCOLS_UWT+2
        Y5WT=YMAP_WT(1,J5WT)
        WRITE(6,*) J5WT
        WRITE(6,*) Y5WT

*NUMERICALY INTEGRATE OVER REGION I USING TRAPEZOID RULE TO CALCULATE
*VOLUMETRIC FLOW IN REGION I.

        FLOW=0
        DO 140 I=1,I2WT
          INC=0
          DO 130 J=2,J5WT
            DELY=(YMAP_WT(I,J)-YMAP_WT(I,J-1))*0.001
            INC=((UMAP_WT(I,J)+UMAP_WT(I,J-1))*0.5*DELY)+INC
  130     CONTINUE
          UINT(I)=INC
          IF(I.GT.1) THEN
            DELX=(XMAP_WT(I,1)-XMAP_WT(I-1,1))*0.001
            FLOW=((UINT(I)+UINT(I-1))*0.5*DELX)+FLOW
          ENDIF
  140   CONTINUE
        FLOWI=FLOW
        WRITE(6,*) FLOWI
        AREAI=(Y5-Y1)*(X2WT-X1)*0.001*0.001
        WRITE(6,*) AREAI
        VELOCITYI=FLOWI/AREAI
        WRITE(6,*) VELOCITYI

*NUMERICALY INTEGRATE OVER REGION II USING TRAPEZOID RULE TO CALCULATE
*VOLUMETRIC FLOW IN REGION II.

        FLOW=0
        DO 160 I=I2WT,I6WT
          INC=0
          DO 150 J=J4WT+1,J5WT
            DELY=(YMAP_WT(I,J)-YMAP_WT(I,J-1))*0.001
            INC=((UMAP_WT(I,J)+UMAP_WT(I,J-1))*0.5*DELY)+INC
  150     CONTINUE
          UINT(I)=INC
          IF(I.GT.1) THEN
            DELX=(XMAP_WT(I,1)-XMAP_WT(I-1,1))*0.001
            FLOW=((UINT(I)+UINT(I-1))*0.5*DELX)+FLOW
          ENDIF
  160   CONTINUE
        FLOWII=FLOW
        WRITE(6,*) FLOWII
        AREAII=(Y5-Y4WT)*(X6WT-X2WT)*0.001*0.001
        WRITE(6,*) AREAII
        VELOCITYII=FLOWII/AREAII
        WRITE(6,*) VELOCITYII

*NUMERICALY INTEGRATE OVER REGION III USING TRAPEZOID RULE TO CALCULATE
*VOLUMETRIC FLOW IN REGION III.

        FLOW=0
        DO 180 I=I6WT,I7WT
          INC=0
          DO 170 J=2,J5WT
            DELY=(YMAP_WT(I,J)-YMAP_WT(I,J-1))*0.001
            INC=((UMAP_WT(I,J)+UMAP_WT(I,J-1))*0.5*DELY)+INC
  170     CONTINUE
          UINT(I)=INC
```

```fortran
            IF(I.GT.1) THEN
               DELX=(XMAP_WT(I,1)-XMAP_WT(I-1,1))*0.001
               FLOW=((UINT(I)+UINT(I-1))*0.5*DELX)+FLOW
            ENDIF
  180     CONTINUE
          FLOWIII=FLOW
          WRITE(6,*) FLOWIII
          AREAIII=(Y5-Y1)*(X7-X6WT)*0.001*0.001
          WRITE(6,*) AREAIII
          VELOCITYIII=FLOWIII/AREAIII
          WRITE(6,*) VELOCITYIII

*NUMERICALY INTEGRATE OVER REGION IV USING TRAPEZOID RULE TO CALCULATE
*VOLUMETRIC FLOW IN REGION IV.

          FLOW=0
          DO 200 I=I2HS,I3HS
            INC=0
            DO 190 J=2,J4HS
              DELY=(YMAP_HS(I,J)-YMAP_HS(I,J-1))*0.001
              INC=((UMAP_HS(I,J)+UMAP_HS(I,J-1))*0.5*DELY)+INC
  190       CONTINUE
            UINT(I)=INC
            IF(I.GT.1) THEN
               DELX=(XMAP_HS(I,1)-XMAP_HS(I-1,1))*0.001
               FLOW=((UINT(I)+UINT(I-1))*0.5*DELX)+FLOW
            ENDIF
  200     CONTINUE
          FLOWIV=FLOW
          WRITE(6,*) FLOWIV
          AREAIV=(Y4HS-Y1)*(X3HS-X2HS)*0.001*0.001
          WRITE(6,*) AREAIV
          VELOCITYIV=FLOWIV/AREAIV
          WRITE(6,*) VELOCITYIV

*NUMERICALY INTEGRATE OVER REGION V USING TRAPEZOID RULE TO CALCULATE
*VOLUMETRIC FLOW IN REGION V.

          FLOW=0
          DO 220 I=I2HS,I6HS
            INC=0
            DO 210 J=J3HS+1,J4HS
              DELY=(YMAP_HS(I,J)-YMAP_HS(I,J-1))*0.001
              INC=((UMAP_HS(I,J)+UMAP_HS(I,J-1))*0.5*DELY)+INC
  210       CONTINUE
            UINT(I)=INC
            IF(I.GT.1) THEN
               DELX=(XMAP_HS(I,1)-XMAP_HS(I-1,1))*0.001
               FLOW=((UINT(I)+UINT(I-1))*0.5*DELX)+FLOW
            ENDIF
  220     CONTINUE
          FLOWV=FLOW
          WRITE(6,*) FLOWV
          AREAV=(Y4HS-Y3HS)*(X6HS-X2HS)*0.001*0.001
          WRITE(6,*) AREAV
          VELOCITYV=FLOWV/AREAV
          WRITE(6,*) VELOCITYV

*NUMERICALY INTEGRATE OVER REGION VI USING TRAPEZOID RULE TO CALCULATE
*VOLUMETRIC FLOW IN REGION VI.

          FLOW=0
          DO 240 I=I4HS,I6HS
```

```
              INC=0
              DO 230 J=J2HS+1,J4HS
                DELY=(YMAP_HS(I,J)-YMAP_HS(I,J-1))*0.001
                INC=((UMAP_HS(I,J)+UMAP_HS(I,J-1))*0.5*DELY)+INC
  230         CONTINUE
              UINT(I)=INC
              IF(I.GT.1) THEN
                DELX=(XMAP_HS(I,1)-XMAP_HS(I-1,1))*0.001
                FLOW=((UINT(I)+UINT(I-1))*0.5*DELX)+FLOW
              ENDIF
  240       CONTINUE
            FLOWVI=FLOW
            WRITE(6,*) FLOWVI
            AREAVI=(Y4HS-Y2HS)*(X6HS-X4HS)*0.001*0.001
            WRITE(6,*) AREAVI
            VELOCITYVI=FLOWVI/AREAVI
            WRITE(6,*) VELOCITYVI

*NUMERICALY INTEGRATE OVER REGION VII USING TRAPEZOID RULE TO CALCULATE
*VOLUMETRIC FLOW IN REGION VII.

            FLOW=0
            DO 260 I=I5HS,I6HS
              INC=0
              DO 250 J=2,J2HS
                DELY=(YMAP_HS(I,J)-YMAP_HS(I,J-1))*0.001
                INC=((UMAP_HS(I,J)+UMAP_HS(I,J-1))*0.5*DELY)+INC
  250         CONTINUE
              UINT(I)=INC
              IF(I.GT.1) THEN
                DELX=(XMAP_HS(I,1)-XMAP_HS(I-1,1))*0.001
                FLOW=((UINT(I)+UINT(I-1))*0.5*DELX)+FLOW
              ENDIF
  260       CONTINUE
            FLOWVII=FLOW
            WRITE(6,*) FLOWVII
            AREAVII=(Y2HS-Y1)*(X6HS-X5HS)*0.001*0.001
            WRITE(6,*) AREAVII
            VELOCITYVII=FLOWVII/AREAVII
            WRITE(6,*) VELOCITYVII

            BP_FLOW=FLOWI+FLOWII+FLOWIII+FLOWIV+FLOWV+FLOWVI+FLOWVII
            BP_AREA_FLOW=AREAI+AREAII+AREAIII+AREAIV+AREAV+AREAVI+AREAVII
            BP_AREA=(((X3-X1)*(Y5-Y1))+((X4-X3)*(Y5-Y3))+((X7-X4)*(Y5-Y2))+
   &((X7-X5)*(Y2-Y1)))*0.001*0.001
            UBP=BP_FLOW/BP_AREA_FLOW

  261       FORMAT(5X,F5.3)
  262       FORMAT(5X,F5.4)
  263       FORMAT(5X,F5.3)

            WRITE(6,261) BP_FLOW
            WRITE(6,262) BP_AREA_FLOW
            WRITE(6,262) BP_AREA
            WRITE(6,263) UBP

*NUMERICALY INTEGRATE OVER REGION VIII USING TRAPEZOID RULE TO CALCULATE
*VOLUMETRIC FLOW IN REGION VIII.

            FLOW=0
            DO 280 I=I3HS,I4HS
              INC=0
              DO 270 J=J2HS+1,J3HS
```

81

```
                  DELY=(YMAP_HS(I,J)-YMAP_HS(I,J-1))*0.001
                  INC=((UMAP_HS(I,J)+UMAP_HS(I,J-1))*0.5*DELY)+INC
  270      CONTINUE
           UINT(I)=INC
           IF(I.GT.1) THEN
              DELX=(XMAP_HS(I,1)-XMAP_HS(I-1,1))*0.001
              FLOW=((UINT(I)+UINT(I-1))*0.5*DELX)+FLOW
           ENDIF
  280      CONTINUE
           FLOWVIII=FLOW
           WRITE(6,*) FLOWVIII
           AREAVIII=(Y3HS-Y2HS)*(X4HS-X3HS)*0.001*0.001
           WRITE(6,*) AREAVIII
           VELOCITYVIII=FLOWVIII/AREAVIII
           WRITE(6,*) VELOCITYVIII

*NUMERICALY INTEGRATE OVER REGION IX USING TRAPEZOID RULE TO CALCULATE
*VOLUMETRIC FLOW IN REGION IX.

           FLOW=0
           DO 300 I=I3HS,I5HS
             INC=0
             DO 290 J=2,J2HS
                DELY=(YMAP_HS(I,J)-YMAP_HS(I,J-1))*0.001
                INC=((UMAP_HS(I,J)+UMAP_HS(I,J-1))*0.5*DELY)+INC
  290      CONTINUE
           UINT(I)=INC
           IF(I.GT.1) THEN
              DELX=(XMAP_HS(I,1)-XMAP_HS(I-1,1))*0.001
              FLOW=((UINT(I)+UINT(I-1))*0.5*DELX)+FLOW
           ENDIF
  300      CONTINUE
           FLOWIX=FLOW
           WRITE(6,*) FLOWIX
           AREAIX=(Y2HS-Y1)*(X5HS-X4HS)*0.001*0.001
           WRITE(6,*) AREAIX
           VELOCITYIX=FLOWIX/AREAIX
           WRITE(6,*) VELOCITYIX

           HS_FLOW=FLOWVIII+FLOWIX
           HS_AREA_FLOW=AREAVIII+AREAIX
           HS_AREA=(((X4-X3)*(Y3-Y2))+((X5-X3)*(Y2-Y1)))*0.001*0.001
           UHS=HS_FLOW/HS_AREA_FLOW

           WRITE(6,261) HS_FLOW
           WRITE(6,262) HS_AREA_FLOW
           WRITE(6,262) HS_AREA
           WRITE(6,263) UHS

           OPEN(2,FILE='DS_OUTPUT.DAT')
           WRITE(2,*) 'UWT TEST NUMBER:  ', rawdat_uwt_fname
           WRITE(2,*) 'RAW DATA FILE TIME STAMP:  ', datetimestamp_uwt
  400      FORMAT(A38,F5.3,A5,F5.3,A6)
           WRITE(2,400) 'AVERAGE PITOT TUBE VELOCITY READING:  ',
      &AVEUPT_UWT, ' +/- ', 2*STDEVUPT_UWT, ' (M/S)'
  401      FORMAT(A30,F6.4,A5,F7.5,A11)
           WRITE(2,401) 'AVERAGE AIR DENSITY READING:  ',
      &AVERHO_UWT, ' +/- ', 2*STDEVRHO_UWT, ' (LBM/FT3)'
           WRITE(2,*) '=================================================
      &=================='
           WRITE(2,*) 'LWT TEST NUMBER:  ', rawdat_lwt_fname
           WRITE(2,*) 'RAW DATA FILE TIME STAMP:  ', datetimestamp_lwt
           WRITE(2,400) 'AVERAGE PITOT TUBE VELOCITY READING:  ',
```

```
      &AVEUPT_LWT, ' +/- ', 2*STDEVUPT_LWT, ' (M/S)'
          WRITE(2,401) 'AVERAGE AIR DENSITY READING:  ',
      &AVERHO_LWT, ' +/- ', 2*STDEVRHO_LWT, ' (LBM/FT3)'
          WRITE(2,*) '=================================================
      &=================='
          WRITE(2,*) 'HEAT SINK TEST NUMBER:  ', rawdat_hs_fname
          WRITE(2,*) 'RAW DATA FILE TIME STAMP:  ', datetimestamp_hs
          WRITE(2,400) 'AVERAGE PITOT TUBE VELOCITY READING:  ',
      &AVEUPT_HS, ' +/- ', 2*STDEVUPT_HS, ' (M/S)'
          WRITE(2,401) 'AVERAGE AIR DENSITY READING:  ',
      &AVERHO_HS, ' +/- ', 2*STDEVRHO_HS, ' (LBM/FT3)'
          WRITE(2,*) '=================================================
      &=================='
  402   FORMAT(A37,F6.4,A6)
          WRITE(2,402) 'HEAT SINK FLOW CROSS-SECTIONAL AREA:  ',
      & HS_AREA_FLOW, ' (M^2)'
*  403
*          WRITE(2,402) 'ACTUAL HEAT SINK CROSS-SECTIONAL AREA:  ', HS_AREA,
      &' (M^2)'
  404   FORMAT(A32,F5.3,A8)
          WRITE(2,404) 'HEAT SINK VOLUMETRIC FLOW RATE:  ', HS_FLOW,
      &' (M^3/S)'
  405   FORMAT(A39,F5.3,A6)
          WRITE(2,405) 'AVERAGE HEAT SINK DOWNSTREAM VELOCITY:  ', UHS,
      &' (M/S)'
          WRITE(2,*) '=================================================
      &=================='
  406   FORMAT(A34,F6.4,A6)
          WRITE(2,406) 'BYPASS FLOW CROSS-SECTIONAL AREA:  ',
      & BP_AREA_FLOW, ' (M^2)'
*  403
*          WRITE(2,402) 'ACTUAL HEAT SINK CROSS-SECTIONAL AREA:  ', HS_AREA,
      &' (M^2)'
  408   FORMAT(A29,F5.3,A8)
          WRITE(2,408) 'BYPASS VOLUMETRIC FLOW RATE:  ', BP_FLOW,
      &' (M^3/S)'
  409   FORMAT(A36,F5.3,A6)
          WRITE(2,409) 'AVERAGE BYPASS DOWNSTREAM VELOCITY:  ', UBP,
      &' (M/S)'
          CLOSE(2)


          END
*==============================================================================
*
*SUBROUTINE "HISTORY" HISTORY DESCRIPTION********************************
*
*==============================================================================

       SUBROUTINE HISTORY(FILENAME,DATETIMESTAMP,XMOVES,YMOVES, T_TH,
      &RHO_AIR, Y0, X0, UPT, Y, X, UDS, N, NRHO)

          CHARACTER*6 FILENAME
          CHARACTER*30 DATETIMESTAMP
          INTEGER XMOVES, YMOVES, I, ROWS
          REAL TIMEF, TIME, TIME0, T, M_TCCAL, B_TCCAL, VDC_TO_PSIA, V
          REAL BP_CAL, P, M_BPCAL, B_BPCAL, C_TO_R, RHOF, RAIR, VPT0
          REAL VI, VTH, VPT, VBP, REHU, T_AIR, P_BP, RHO_AIR(25000)
          REAL RESISTANCE, T_VP, A, B, C, D, E, F, G, T_TH, RES, R, LINEID
          REAL UPT(25000), PPTF, PPT, RHO_H2O, RHO, UPTF, TH
          REAL YMOVE, XMOVE, YSTEP, XSTEP, X0, Y0, RESHOT, Q, HCOEF
          REAL UVP, AA, BB, CC, UDS(25000), YF, XF, QTH, TC, HCOEFF
          REAL Y(25000), X(25000)
```

83

```
      INTEGER N, NRHO

*INITIALIZE INDICIES TO ONE.

      DATA JRHO,J /1,0/
*-----------------------------------------------------------------------
*DEFINE A FUNCTION THAT TAKES TIME IN MILLISECONDS AND SUBTRACTS TIME
*(IN MILLISECONDS) AT ZERO AND CONVERTS THAT VALUE FROM MILLISECONDS TO
*SECONDS.

      TIMEF(TIME,TIME0)=(TIME-TIME0)*0.001

*-----------------------------------------------------------------------
*DEFINE A FUNCTION THAT TAKES THE RAW TEMPERATURE VALUE AND CONVERTS IT
*TO ITS CALIBRATED VALUE.

      T_CAL(T)=(M_TCCAL*T)+B_TCCAL

*-----------------------------------------------------------------------
*DEFINE A FUNCTION THAT CONVERTS THE RAW BAROMETRIC PRESSURE READING (IN
*VOLTS DC) AND CONVERTS IT TO ABSOLUTE PRESSURE IN UNITS OF PSIA.

      VDC_TO_PSIA(V)=(V-0.5)*3.75

*-----------------------------------------------------------------------
*DEFINE A FUNCTION THAT TAKES THE RAW BAROMETRIC PRESSURE (IN PSIA) AND
*CONVERTS IT TO ITS CALIBRATED VALUE.

      BP_CAL(P)=(M_BPCAL*P)+B_BPCAL

*-----------------------------------------------------------------------
*DEFINE A FUNCTION THAT CONVERTS THE TEMPERATURE FROM DEGREES CELSIUS TO
*RANKINE.

      C_TO_R(T)=(((9.0/5.0)*T)+32)+459.67

*-----------------------------------------------------------------------
*DEFINE A FUNCTION THAT CALCULATES AIR DENSITY (IN LB/FT^3) USING IDEAL
*GAS LAW.  THE FUNCTION TAKES AS VARIABLES THE BAROMETRIC PRESSURE (IN
*PSIA) AND TEMPERATURE (IN RANKINE).

      RHOF(P,T)=(P*144)/(RAIR*T)

*-----------------------------------------------------------------------
*DEFINE THE FUNCTIONS USED TO CALCULATE THE AIR TEMPERATURE MEASURED BY
*THE THERMISTOR (VELOCITY PROBE).  THE FIRST FUNCTION CALCULATES THE
*THERMISOR RESISTANCE (OHMS) FROM THE THERMISTOR VOLTAGE READING (VDC).
*THE SECOND FUNCTION CALCULATES THE TEMPERATURE (C) FROM THIS RESISTANCE
*(OHMS) VALUE USING A POLYNOMIAL FIT OF THE VENDOR DATA.

      RESISTANCE(V)=V*10000
      T_VP(R)=(A*(R**6))+(B*(R**5))+(C*(R**4))+(D*(R**3))+(E*(R**2))+
     &(F*R)+G

*-----------------------------------------------------------------------
*DEFINE THE FUNCTIONS THAT CALCULATE THE PITOT TUBE VELOCITY.

      PPTF(VPT0,VPT)=(((0.5*VPT)/(5-VPT0))-((0.5*VPT0)/(5-VPT0)))*
     &(RHO_H2O/12)
      UPTF(P,RHO)=(((2*32.174*P)/RHO)**0.5)*0.3048

*-----------------------------------------------------------------------
*DEFINE THE FUNCTIONS THAT CALCULATE THE X AND Y COORDINATE IN MM.
```

```
          YF(YSTEP)=(YSTEP*0.02)+Y0
          XF(XSTEP)=(XSTEP*0.4225)+(0.0078)+X0


*----------------------------------------------------------------------
*DEFINE THE FUNCTION THAT CALCULATES THE HEAT DISIPATION OF THE VELOCITY
*PROBE IN UNITS OF MILLIWATTS.  IT IS A FUNCTION OF "VI" (VDC) AND "VTH"
*(VDC).

          Q(VI,VTH)=ABS(VI)*ABS(VTH)*0.5


*----------------------------------------------------------------------
*DEFINE THE FUNCTION THAT CALCULATES THE RESISTANCE (OHMS) OF THE THERM-
*ISTOR (VELOCITY PROBE) IN "VELOCITY" MODE.  IT IS A FUNCTION OF "VI"
*AND "VTH" (BOTH IN UNITS VDC).

          RESHOT(VI,VTH)=(ABS(VTH)/ABS(VI))*2000


*----------------------------------------------------------------------
*DEFINE THE FUNCTION THAT CALCULATES THE CONVECTIVE HEAT TRANSFER COEFF.
*(MILLIWATTS/(DEG_C)) AS A FUNCTION OF THE HEAT DISSIPATED AND THE TEMP-
*ERATURE DIFFERENTIAL.

          HCOEF(QTH,TH,TC)=QTH/(TH-TC)


*----------------------------------------------------------------------
*DEFINE THE FUNCTION THAT CALCULATES THE AIR VELOCITY MEASURED BY THE
*VELOCITY PROBE (M/S).  IT IS A 2ND DEGREE POLYNOMIAL WITH THE VARIABLE
*SET AS THE HEAT TRANSFER COEFFICIENT (MILLIWATTS/(DEG_C)).

          UVP(HCOEFF)=((AA*HCOEFF)+(BB*(HCOEFF**0.5)))+CC)**2


*----------------------------------------------------------------------
*DEFINE VARIABLES:
*================
*
*CALIBRATION DATA FOR THERMOCOUPLE TEMPERATURE MEASUREMENT IN DEGREES C
*(SLOPE AND INTERCEPT).

          B_TCCAL=0.039571
          M_TCCAL=0.985506

*CALIBRATION DATA FOR THE BAROMETRIC PRESSURE MEASUREMENT IN PSIA (SLOPE
*AND INTERCEPT).

          B_BPCAL=2.517747
          M_BPCAL=0.854111

*POLYNOMIAL COEFFICIENTS FOR RESISTANCE TO TEMPERATURE CONVERSION FOR
*THE VELOCITY PROBE.

          A=2.9557E-23
          B=-1.8467E-18
          C=4.7610E-14
          D=-6.5819E-10
          E=5.3561E-6
          F=-2.7780E-2
          G=1.0437E2

*GAS CONSTANT FOR AIR (LBF*FT/(LBM*R)).

          RAIR=53.5
```

85

```
        RHO_H2O=62.3

        AA=8.810413
        BB=-7.904538
        CC=1.247277

*-----------------------------------------------------------------------

*OPEN INPUT FILE "TXXXXA."

        OPEN(1,FILE=FILENAME)

*OPEN OUTPUT FILE "TXXXXA_HISTORY."

        OPEN(2,FILE=FILENAME//'_HISTORY')

*FORMAT FOR OUTPUT FILE "TXXXXA_HISTORY".

  100   FORMAT(A)
  110   FORMAT(T5,F9.3,T17,F6.3,T26,F7.4,T36,F8.6)
  120   FORMAT(T5,F9.3,T17,F6.3,T26,F7.4,T36,F8.6,T47,F6.4)
  130   FORMAT(T5,F9.3,T17,F6.3,T36,F8.6,T47,F6.4)

*CREATE COLUMN HEADERS FOR OUTPUT FILE "TXXXXA_HISTORY."

        WRITE(2,*) '      TIME      TMP      BARO       RHO       UPT '
        WRITE(2,*) '     (SEC)    (DEG C)   (PSIA)   (LB/FT^3)   (M/S)'
        WRITE(2,*) '   ========  =======  ========  =========  =======
     &'

*READ THE DATE/TIME STAMP FROM THE FIRST LINE (ROW) OF DATA IN "TXXXXA."

        READ(1,100) DATETIMESTAMP

*NUMBER OF ROWS IN THE RAW DATA FILE EXCLUDING THE DATE/TIME STAMP ROW.

        ROWS=((XMOVES+1)*(YMOVES+2))+1

*READ FIRST LINE OF DATA (ZERO READINGS).

        READ(1,*) TIME, LINEID, VI, VTH, VPT, T, VBP, REHU

*SET INITIAL TIME TO 0 SECONDS.

        TIME0=TIME
        TIME=TIMEF(TIME,TIME0)

*CALCULATE THE TEMPERATURE OF THE AIR IN DEGREES CELSIUS.

        T_AIR=T_CAL(T)

*CALCULATE THE TEMPERATURE OF THE AIR USING THE THERMISTOR (VELOCITY
*PROBE) MEASUREMENT.

        RES=RESISTANCE(ABS(VTH))
        T_TH=T_VP(RES)

*CALCULATE THE BAROMETRIC PRESSURE IN PSIA.

        P_BP=BP_CAL(VDC_TO_PSIA(VBP))

*CALCULATE THE DENSITY OF THE AIR IN LBM/FT^3.
```

```
          JRHO=1
          J=0
          RHO_AIR(JRHO)=RHOF(P_BP,C_TO_R(T_AIR))

*WRITE THE TIME, AIR TEMPERATURE, BAROMETRIC PRESSURE, AND AIR DENSITY
*TO THE OUTPUT FILE "TXXXA_HISTORY."

          VPT0=VPT

          WRITE(2,110) TIME, T_AIR, P_BP, RHO_AIR(JRHO)

          DO 140 I=1, ROWS-1
            READ(1,*) TIME, LINEID

            BACKSPACE(1)
            IF(LINEID.EQ.999999.) THEN
              READ(1,*) TIME, LINEID, VI, VTH, VPT, T, VBP, REHU
              JRHO=JRHO+1
              TIME=TIMEF(TIME,TIME0)
              T_AIR=T_CAL(T)
              P_BP=BP_CAL(VDC_TO_PSIA(VBP))
              RHO_AIR(JRHO)=RHOF(P_BP,C_TO_R(T_AIR))
              WRITE(2,110) TIME, T_AIR, P_BP, RHO_AIR(JRHO)
              ELSE
              READ(1,*) TIME, YMOVE, XMOVE, YSTEP, XSTEP, VI, VTH, VPT,
     &T
              TIME=TIMEF(TIME,TIME0)
              JRHO=JRHO+1
              T_AIR=T_CAL(T)
              P_BP=BP_CAL(VDC_TO_PSIA(VBP))
              RHO_AIR(JRHO)=RHOF(P_BP,C_TO_R(T_AIR))
              PPT=PPTF(VPT0,VPT)
              J=J+1
              UPT(J)=UPTF(PPT,RHO_AIR(JRHO))
              Y(J)=YF(YSTEP)
              IF (XSTEP.EQ.0) THEN
                X(J)=X0
                ELSE
                X(J)=XF(XSTEP)
              ENDIF
              UDS(J)=UVP(HCOEF(Q(VI,VTH),T_VP(RESHOT(VI,VTH)),T_AIR))
              WRITE(2,130) TIME, T_AIR, RHO_AIR(JRHO), UPT(J)
            ENDIF
  140     CONTINUE
          N=J
          NRHO=JRHO

          CLOSE(1)
          CLOSE(2)
          RETURN
          END

*=========================================================================
*
*SUBROUTINE "AVE" AVERAGE DESCRIPTION*****************************
*
*=========================================================================

        SUBROUTINE AVE(X,N,MU)

          REAL X(25000), SUM, MU
          INTEGER N, I
```

```
        SUM=0
        DO 200 I=1, N
          SUM=SUM+X(I)
  200   CONTINUE
        MU=SUM/N

        RETURN
        END


*========================================================================
*
*SUBROUTINE "STDEV" STANDARD DEVIATION DESCRIPTION**********************
*
*========================================================================

        SUBROUTINE STDEV(X,N,MU,SIGMA)

        REAL X(25000), SUM, MU, SIGMA
        INTEGER N, I

        SUM=0
        DO 300 I=1, N
          SUM=((X(I)-MU)**2)+SUM
  300   CONTINUE
        SIGMA=(SUM/N)**0.5

        RETURN
        END


*========================================================================
*
*SUBROUTINE "MAP" MAP DESCRIPTION*********************
*
*========================================================================

        SUBROUTINE MAP(X,Y,UDS,UPT,AVEUPT,XMAP,YMAP,UMAP,NROWS,NCOLS,
     &XMOVE,YMOVE)

        REAL X(25000),Y(25000),UDS(25000),UPT(25000)
        REAL AVEUPT
        REAL XMAP(300,100),YMAP(300,100),UMAP(300,100)
        INTEGER NROWS,NCOLS,XMOVE,YMOVE,I,J,K,MININD
        REAL MIN,XTMP,YTMP,UDSTMP,UPTTMP

        NROWS=XMOVE+1
        NCOLS=YMOVE+1
        DO 420 I=1, NROWS
          DO 410 J=1, NCOLS-1
            MININD=J+((I-1)*NCOLS)
            MIN=Y(MININD)
            DO 400 K=J+1, NCOLS
              IF(Y(K+((I-1)*NCOLS)).LT.MIN) THEN
                MININD=K+((I-1)*NCOLS)
                MIN=Y(MININD)
              ENDIF
  400       CONTINUE
            IF(MIN.LT.Y(J+((I-1)*NCOLS))) THEN
              YTMP=Y(J+((I-1)*NCOLS))
              YMAP(I,J)=Y(MININD)
              Y(MININD)=YTMP
              XTMP=X(J+((I-1)*NCOLS))
              XMAP(I,J)=X(MININD)
              X(MININD)=XTMP
```

```
            UDSTMP=UDS(J+((I-1)*NCOLS))
            UPTTMP=UPT(J+((I-1)*NCOLS))
            UMAP(I,J)=UDS(MININD)*UPT(MININD)/AVEUPT
            UDS(MININD)=UDSTMP
            UPT(MININD)=UPTTMP
            ELSE
            YMAP(I,J)=Y(J+((I-1)*NCOLS))
            XMAP(I,J)=X(J+((I-1)*NCOLS))
            UMAP(I,J)=UDS(J+((I-1)*NCOLS))*UPT(J+((I-1)*NCOLS))/AVEUPT
            ENDIF
  410     CONTINUE
          YMAP(I,NCOLS)=Y(NCOLS+((I-1)*NCOLS))
          XMAP(I,NCOLS)=X(NCOLS+((I-1)*NCOLS))
          UMAP(I,NCOLS)=UDS(NCOLS+((I-1)*NCOLS))*UPT(NCOLS+((I-1)*NCOLS
     &))/AVEUPT
  420     CONTINUE
          RETURN
          END

*========================================================================
*
*SUBROUTINE "AVEPROF" AVERAGE PROFILE DESCRIPTION**********************
*
*========================================================================

          SUBROUTINE AVEPROF(XMAP,YMAP,UMAP,X0,XN,FILENAME,NROWS,NCOLS)

          REAL XMAP(300,100),YMAP(300,100),UMAP(300,100)
          INTEGER NROWS,NCOLS,I,J,NPNTS(100)
          REAL X0,XN,SUM(100),UAVE(100),Y(100)
          CHARACTER*12 FILENAME

          OPEN(1,FILE=FILENAME)

          DO 510 J=1, NCOLS
            SUM(J)=0
            NPNTS(J)=0
            DO 500 I=1, NROWS
              IF(XMAP(I,J).GE.X0) THEN
                IF(XMAP(I,J).LE.XN) THEN
                  SUM(J)=UMAP(I,J)+SUM(J)
                  NPNTS(J)=NPNTS(J)+1
                  Y(J)=YMAP(I,J)
                  ENDIF
                ENDIF
  500       CONTINUE
          UAVE(J)=SUM(J)/NPNTS(J)
          WRITE(1,*)UAVE(J),Y(J)
  510     CONTINUE
          CLOSE(1)
          RETURN
          END

*========================================================================

          SUBROUTINE WTMAP(XMAPU,YMAPU,UMAPU,NCOLSU,XMAPL,YMAPL,
     &UMAPL,NROWSL,NCOLSL,XMAP,YMAP,UMAP,YFINAL,XFINAL)

          REAL XMAP(300,100),YMAP(300,100),UMAP(300,100)
          REAL XMAPU(300,100),YMAPU(300,100),UMAPU(300,100)
          REAL XMAPL(300,100),YMAPL(300,100),UMAPL(300,100)
          REAL YFINAL,XFINAL
          INTEGER NCOLSU,NROWSL,NCOLSL,I,J,K,N
```

```
        REAL MIN, XTMP, YTMP, UTMP
        INTEGER MININD

        OPEN(1,FILE='XMAP_WT')
        OPEN(2,FILE='YMAP_WT')
        OPEN(3,FILE='UMAP_WT')

*NO SLIP CONDITIONS (U=0) AT LS WALL.

        XMAP(1,1)=0
        YMAP(1,1)=0
        UMAP(1,1)=0
        DO 600 J=1, NCOLSL
          XMAP(1,J+1)=0
          YMAP(1,J+1)=YMAPL(1,J)
          UMAP(1,J+1)=0
  600   CONTINUE
        DO 610 J=1, NCOLSU
          XMAP(1,J+NCOLSL+1)=0
          YMAP(1,J+NCOLSL+1)=YMAPU(1,J)
          UMAP(1,J+NCOLSL+1)=0
  610   CONTINUE
        XMAP(1,NCOLSU+NCOLSL+2)=0
        YMAP(1,NCOLSU+NCOLSL+2)=YFINAL
        UMAP(1,NCOLSU+NCOLSL+2)=0

*MIDDLE PORTION OF WINDTUNNEL.

        DO 640 I=1, NROWSL

*NO SLIP CONDITIONS (U=0) AT FLOOR.

          XMAP(I+1,1)=XMAPL(I,1)
          YMAP(I+1,1)=0
          UMAP(I+1,1)=0

          DO 620 J=1, NCOLSL
            XMAP(I+1,J+1)=XMAPL(I,J)
            YMAP(I+1,J+1)=YMAPL(I,J)
            UMAP(I+1,J+1)=UMAPL(I,J)
  620     CONTINUE
          DO 630 J=1, NCOLSU
            XMAP(I+1,J+NCOLSL+1)=XMAPU(I,J)
            YMAP(I+1,J+NCOLSL+1)=YMAPU(I,J)
            UMAP(I+1,J+NCOLSL+1)=UMAPU(I,J)
  630     CONTINUE

*NO SLIP CONDITIONS (U=0) AT CEILING.

          XMAP(I+1,NCOLSU+NCOLSL+2)=XMAPU(I,NCOLSU)
          YMAP(I+1,NCOLSU+NCOLSL+2)=YFINAL
          UMAP(I+1,NCOLSU+NCOLSL+2)=0

  640   CONTINUE

*NO SLIP CONDITIONS (U=0) AT RS WALL.

        XMAP(NROWSL+2,1)=XFINAL
        YMAP(NROWSL+2,1)=0
        UMAP(NROWSL+2,1)=0
        DO 650 J=1, NCOLSL
          XMAP(NROWSL+2,J+1)=XFINAL
          YMAP(NROWSL+2,J+1)=YMAPL(1,J)
```

```
            UMAP(NROWSL+2,J+1)=0
   650    CONTINUE
          DO 660 J=1, NCOLSU
            XMAP(NROWSL+2,J+NCOLSL+1)=XFINAL
            YMAP(NROWSL+2,J+NCOLSL+1)=YMAPU(1,J)
            UMAP(NROWSL+2,J+NCOLSL+1)=0
   660    CONTINUE
          XMAP(NROWSL+2,NCOLSU+NCOLSL+2)=XFINAL
          YMAP(NROWSL+2,NCOLSU+NCOLSL+2)=YFINAL
          UMAP(NROWSL+2,NCOLSU+NCOLSL+2)=0

*SORT IN ASCENDING ORDER IN THE Y DIRECTION.

          N=NCOLSU+NCOLSL+2
          DO 690 I=1, NROWSL+2
            DO 680 J=1, N-1
              MININD=J
              MIN=YMAP(I,MININD)
              DO 670 K=J+1, N
                IF(YMAP(I,K).LT.MIN) THEN
                  MININD=K
                  MIN=YMAP(I,MININD)
                ENDIF
   670        CONTINUE
              IF(MIN.LT.YMAP(I,J)) THEN
                YTMP=YMAP(I,J)
                YMAP(I,J)=YMAP(I,MININD)
                YMAP(I,MININD)=YTMP
                XTMP=XMAP(I,J)
                XMAP(I,J)=XMAP(I,MININD)
                XMAP(I,MININD)=XTMP
                UTMP=UMAP(I,J)
                UMAP(I,J)=UMAP(I,MININD)
                UMAP(I,MININD)=UTMP
              ELSE
              ENDIF
   680      CONTINUE
   681      FORMAT(100F6.1)
   682      FORMAT(100F6.1)
   683      FORMAT(100F6.3)


            WRITE(1,681) (XMAP(I,K), K=1,N)
            WRITE(2,682) (YMAP(I,K), K=1,N)
            WRITE(3,683) (UMAP(I,K), K=1,N)
   690    CONTINUE

          CLOSE(1)
          CLOSE(2)
          CLOSE(3)
          RETURN
          END

*=======================================================================
```